ScienceInnovation
INTERNATIONAL SCIENTIFIC JOURNAL

ISSN:
2181-3337

INTERNATIONAL SCIENTIFIC JOURNAL

SCIENCE AND INNOVATION

VOLUME 5 / ISSUE 6

A:
CHEMISTRY
TECHNIQUE
ECONOMICS
PHYSICS AND
MATHEMATICS

JUNE 2026

International Scientific Journal
SCIENCE AND INNOVATION
Series A
Volume 5 Issue 6
June 2026

Tashkent 2026

ISSN: 2181-3337

International Scientific Journal SCIENCE AND INNOVATION. Series A volume 5 issue 6 – 132 p.

The collection contains scientific articles accepted for issue 6 for 2026 of the international scientific journal "Science and Innovation".

In this scientific journal, in the form of scientific articles, the results of scientific research conducted by professors and teachers of the Republic of Uzbekistan and international higher educational institutions, independent researchers, doctoral students, undergraduates were published. In addition to higher educational institutions, the journal also includes scientific articles by employees working in other research institutes, production organizations and enterprises of our region and republic.

The materials of the journal can be used by professors, teachers, independent researchers, doctoral students, undergraduates, students, teachers of lyceums and schools, scientists and everyone who is interested in science.

This issue of the journal is indexed in the international scientific databases Index Copernicus, eLibrary.ru, OpenAire, EuroPub, ZENODO and Google Scholar.

All articles were placed in the electronic scientific database of the journal (scientists.uz).

© Science and Innovation

© Authors

Editorial team			
Baxtiyor Rustamov	Chief Editor	**Gulirano Raxmatullayeva**	Deputy Chief Editor
Mahliyo Sotivoldiyeva	Reception Manager	**Feruza Ollomurodova**	Reception Manager
Farangiz Sagdullayeva	Technical Editor	**Dilnoza Narzullayeva**	Manager
Zulayxo Xakimova	Editor	**Sevara O'rinboyeva**	Manager
Kozim Ergashov	Editor	**Humoyun Qodirov**	Technical Editor
Feruzabonu Mannonova	Translator	**Mansur Suyunqulov**	Technical Editor
Jahongir Bekmuradov	Translator	**Samandar Rasulov**	Motion Designer
Asila Xaydaralieva	Editor	**Zafarbek Madaminov**	Motion Designer

Scientific editorial board	
Khayrulla Pulatov	Doctor of Chemical Sciences, Professor, Vice-Rector for Scientific Affairs and Innovations of Tashkent Institute of Chemical Technology, Tashkent, Uzbekistan.
Salim Otakulov	Doctor of Physical and Mathematical Sciences, Professor of the Department of Higher Mathematics of Jizzakh Polytechnic Institute, Jizzakh, Uzbekistan.
Shavkat Abdullayev	Doctor of Chemical Sciences, Professor of the Department of "Organic Chemistry" of Namangan State University, Namangan, Uzbekistan.
Erkin Imamov	Doctor of Physical and Mathematical Sciences, Professor of Tashkent University of Information Technologies, Tashkent, Uzbekistan.
Karimberdi Onarqulov	Doctor of Physical and Mathematical Sciences, Head of the Department of Physics of Fergana State University, professor, Fergana, Uzbekistan.
Amin Jarrah	PhD, Associate Professor of Computer Engineering at Yarmouk University, Irbid, Jordan.
Fakhriddin Pirlepesov	PhD, Computational Physicist, St Jude Children's Research Hospital, Radiation Oncology Department, Memphis, Tennessee, USA.
Borisyuk Petr	Doctor of Physical and Mathematical Sciences, Head of the Department of the Institute of Laser and Plasma Technologies, National Research Nuclear University MEPhI, Associate Professor, Moscow, Russia.
Mirdjalil Yunusov	Doctor of technical sciences, Scientific secretary of Tashkent Institute of Chemical Technology, professor, The owner of the Order of "Labour Fame", Tashkent, Uzbekistan.
Toyir Safarov	Doctor of technical sciences, Vice-Rector for Academic Affairs of Tashkent Institute of Chemical Technology, Professor, Tashkent, Uzbekistan.
Dilshod Ruziyev	Doctor of Philosophy in Technical Sciences, Associate Professor, Deputy director of professional training and retraining at the Institute for the Development of Professional Education.
Baxtiyor Sabirov	Doctor of technical sciences, Head of the department "Non-metallic and technogenic minerals" of the Navoi branch of the Academy of Sciences of the Republic of Uzbekistan, Senior researcher, Navoi, Uzbekistan.
Munovar Abdurakhmanova	Candidate of Economical Sciences, associate professor, Head of the Department of Organization of the Scientific and Educational Process of the Scientific Research Institute of Physics of Semiconductors and Microelectronics at UzNU, Deputy Director for the integration of the educational process with scientific activities, Tashkent, Uzbekistan.
Abdukakhkhor Khadjimuratov	Doctor of economic sciences, Associate Professor of the Department of "Social Sciences" of Fergana Public Health Medical Institute, Fergana, Uzbekistan.
Shoira Musayeva	Candidate of Economics, Professor of the Samarkand Institute of Economics and Service, Samarkand, Uzbekistan.
Ikhtiyor Kamolov	Candidate of technical sciences, Dean of the Faculty of Physical and Technological Education of the Navoi State University, Professor of the Department of Physics and Astronomy, Navoi, Uzbekistan.
Mirkozimjon Nishonov	Candidate of technical sciences, Professor of Fergana State University
Khaydar Rasulov	Candidate of Physical and Mathematical Sciences, Associate Professor of Bukhara State University, Bukhara, Uzbekistan.
Akramjon Karimov	Candidate of Physical and Mathematical Sciences, Professor of Tashkent State Law University, Tashkent, Uzbekistan.
Azizjon Kurbanov	Candidate of Physical and Mathematical Sciences, Head of the department of "Physics" of Andijan State University, Andijan, Uzbekistan.
Dilfuza Makhmudova	Doctor of Pedagogical Sciences, Head of the Department of Methods of Teaching Mathematics of Chirchik State Pedagogical University, Chirchik, Uzbekistan.
Dilorom Karimova	Candidate of Chemical Sciences, Professor of Navoi State University, Navoi, Uzbekistan.
Madinakhon Muydinova	Doctor of Philosophy on Physical and Mathematical Sciences, Head of the Department of Methods of Teaching Informatics and Exact Sciences at Pedagogical Institute of Andijan State University, Andijan, Uzbekistan.
Ilxom Usmonov	Candidate of Technical Sciences, Professor of the Samarkand State Institute of Architecture and Construction, Samarkand, Uzbekistan.
Nodira Saidaxmedova	Doctor of Economic Sciences, Professor of UZNPU named after Nizami, Tashkent, Uzbekistan.
Umar Babakhodjayev	Candidate of Physical and Mathematical Sciences, Associate Professor of Namangan State University, Namangan, Uzbekistan.
Dilshod Eshmuradov	Candidate of Technical Sciences, Associate Professor, Head of Department, Tashkent University of Information Technologies, Tashkent, Uzbekistan.

SURFACE-WAVE PROPAGATION IN ELASTIC ANISOTROPIC MEDIA AND ITS MATHEMATICAL MODELS: THEORY, COMPUTATION, AND INVERSION

A.E. Xolmurodov[1], M.A. Quzratov[2]
Karshi State University, Doctor of Physical and Mathematical Sciences, Professor[1]
Karshi State University, Doctoral Student[2]
https://doi.org/10.5281/zenodo.20625194

Abstract. *Surface waves (Rayleigh and Love) recorded near the free surface are exceptionally sensitive to directional stiffness contrasts in real rocks and engineered solids. We develop a coherent theoretical and computational framework for surface-wave propagation in elastic anisotropic media. The approach (i) builds on the Stroh first-order formalism and the Barnett-Lothe surface-impedance method to derive energy-consistent secular equations for Rayleigh-type waves in TI/TTI/orthorhombic symmetries; (ii) introduces two observable indices-the azimuthal dispersion index and the Rayleigh ellipticity index* $E(\theta)$*-and a complementary anisotropic energy-flux factor that together provide robust constraints for inversion; (iii) details high-accuracy discretizations via the spectral-element method (SEM) and high-order SBP-SAT finite differences, including PML absorbing layers; and (iv) presents a weak-anisotropy analysis that clarifies how Thomsen-style parameters affect phase velocity, polarization and the occurrence of zero-group-velocity (ZGV) points. We further derive implicit Fréchet sensitivity expressions of the Rayleigh phase velocity with respect to elastic constants and outline a multi-azimuth, multi-observable inversion strategy. The framework is applicable to site response, geotechnical characterization, nondestructive evaluation and crystal acoustics.*

Keywords: *elastic anisotropy, Stroh formalism, Barnett-Lothe surface impedance, Rayleigh/Love waves, Thomsen parameters, spectral elements, SBP-SAT, dispersion, ellipticity, ZGV, inversion.*

Introduction. Surface waves dominate the energy recorded at shallow depths and thus encode the mechanical fingerprint of near-surface structures. In many geologic and engineered solids, anisotropy arises from layering, preferred microcrack orientation, texture, or crystallinity. This directional stiffness breaks the isotropic assumption, leading to azimuth-dependent phase velocities, polarization changes and mode coupling between Rayleigh- and Love-type waves. Modeling surface waves without anisotropy risks biased velocity estimates, mislocated ZGV points and incorrect thickness/stiffness trade-offs in inversion.

Contributions. We present:

A compact Stroh-Barnett-Lothe derivation of the Rayleigh secular equation for general symmetries with physically admissible (decaying) vertical wavenumbers;

Original observables for field practice- $J(\theta)$ (azimuthal dispersion), (Rayleigh ellipticity) and (normalized surface energy flux)-designed to stabilize inversions;

Computation protocols for SEM and SBP-SAT with PML, including resolution/CFL guidelines tailored to dispersion-sensitive surface waves;

A weak-anisotropy analysis that links Thomsen-style parameters to measurable azimuthal signatures; and

Sensitivity formulas and a joint inversion recipe combining phase velocity, ellipticity and ZGV constraints.

Materials and Methods

Governing Equations and Boundary Conditions

Linear anisotropic elasticity. Let $\mathbf{u}(\mathbf{x},\mathbf{t})$ be the displacement field, $\boldsymbol{\varepsilon}(\mathbf{u}) = \frac{\mathbf{1}}{\mathbf{2}}(\boldsymbol{\nabla}\mathbf{u} + \boldsymbol{\nabla}\mathbf{u}\top)$the strain tensor and the fourth-order stiffness tensor satisfying the medium's symmetry (e.g., TI/TTI/orthorhombic).

Dinamika tenglamasi $\rho\ddot{u}\text{-}\nabla\cdot\sigma\text{=}f$ (1)

Free-surface and interface conditions. On the traction-free boundary Γ_{fs}. Across internal interfaces, continuity of displacements and tractions holds. In layered anisotropic structures, decoupling may occur (supporting Love waves), but in general anisotropy couples and components; careful enforcement of interface conditions is essential to avoid spurious modes.

Stroh formulation. Writing the elastodynamic equations in the Stroh first-order form yields a eigenproblem. For a horizontal wavenumber vectov $\mathbf{k} = (\mathbf{k}\cos\boldsymbol{\theta}, \mathbf{k}\sin\boldsymbol{\theta}, \mathbf{0})$and time-harmonic dependence $\mathbf{exp}\lceil \mathbf{i}(\mathbf{k}\cdot\mathbf{x} - \boldsymbol{\omega}\mathbf{t})\rceil$, one seeks vertical eigenvalues with (decay with depth) and associated eigenvectors collected into block matrices $\mathbf{A}, \mathbf{B}$. Physical admissibility (no upward energy growth) dictates selecting only the decaying set.

Surface impedance and the secular equation

The surface-impedance matrix relates surface tractions to surface velocities. For a homogeneous half-space, Rayleigh waves satisfy the secular condition

$$\mathcal{S}_R(\omega, k; m) \equiv \det Z(\omega, k; m) = 0 \quad (2)$$

where collects elastic constants and density. This equation implicitly defines the phase velocity as a function of azimuth θ and symmetry class. In layered media, one combines layerwise impedances via propagator or global-impedance techniques to obtain the overall secular condition. Love waves arise when SH motion decouples; otherwise Rayleigh-Love coupling may occur.

Correct root selection and stability

Spurious roots are eliminated by enforcing (i) $\mathrm{Im}(s_j) > 0$for all depth-decaying partial modes and (ii) non-radiation at depth (no energy inflow from infinity). These constraints ensure the secular determinant represents a physically realizable surface mode.

Weak-Anisotropy Analysis (TI/TTI) and Azimuthal Effects

For a TI skeleton with symmetry axis not necessarily vertical (TTI), azimuthal variations become explicit. In the weak-anisotropy regime, the Rayleigh phase velocity perturbation admits a first-order representation

$$\frac{c_R(\theta) - c_{R,0}}{c_{R,0}} \approx B_1\,\epsilon\cos^2\theta + B_2\,\delta\sin^2\theta + B_3\,\gamma\sin^2(2\theta) \quad (3)$$

Where is the isotropic reference and coefficients B_i depend on near-surface stiffness depth trends. This expression clarifies which anisotropy components control azimuthal dispersion.

Rayleigh ellipticity. Particle motion near the free surface is retrograde elliptical in isotropy; anisotropy modifies the ellipse's aspect ratio and tilt. We define

$$E(\theta) = \frac{b(\theta)}{a(\theta)} \quad (4)$$

the ratio of minor to major axes of the polarization ellipse. Changes in provide constraints independent of helping to break parameter trade-offs.

Layered Anisotropic Media, Mode Coupling and ZGV Points

In layered TI/TTI/orthorhombic stacks, assembling layer impedances yields dispersion curves with potential mode crossings. Zero-group-velocity (ZGV) points appear when $\frac{\partial\omega}{\partial k}=0$, often near resonant trapping. ZGV frequencies are extremely diagnostic of thin compliant layers and greatly aid inversion by anchoring the model at distinct spectral landmarks.

Original indicators for measurement and inversion

We introduce three practical, dimensionless observables:

Azimuthal dispersion index

$$J(\theta)=\frac{c_R(\theta)-\overline{c_R}}{\overline{c_R}},\quad \overline{c_R}=\frac{1}{\pi}\int_0^{\pi} c_R(\theta)\,d\theta \qquad (5)$$

which normalizes phase-velocity deviations and suppresses acquisition bias.

Rayleigh ellipticity index

$$E(\theta)=\frac{b(\theta)}{a(\theta)} \qquad (6)$$

directly measurable from three-component surface records; it is sensitive to symmetry axis orientation and layering.

Anisotropic energy-flux factor

$$A_F(\theta)=\frac{\|\langle S\rangle(\theta)\|}{\overline{\|\langle S\rangle\|}} \qquad (7)$$

where is the time-averaged Poynting (energy-flux) vector at the surface. Together, add complementary information beyond c_R alone and stabilize anisotropic inversions.

Sensitivity Kernels and Inversion Strategy

Let the secular condition be with $c=\omega/k$. By implicit differentiation,

$$\frac{\partial c}{\partial m_i}=-\frac{\partial S/\partial m_i}{\partial S/\partial c} \qquad (8)$$

For layered media, depth-dependent kernels are computed with adjoint fields, enabling gradient-based or Bayesian inversion. We recommend a multi-objective functional that jointly fits:

$$\Phi=\Phi_c[c_R(\theta,f)]+\lambda_E\,\Phi_E[E(\theta,f)]+\lambda_{ZGV}\,\Phi_{ZGV}(f^*) \qquad (9)$$

with weights Including $E(\theta)$and ZGV frequencies reduces trade-offs among c_{ij}, density and layer thicknesses. Priors enforce physical stability (positive definiteness of and smoothness (e.g., TV or constraints on depth trends).

Numerical Discretization: SEM and SBP-SAT with PML

SEM is well suited to complex free-surface topography. Accuracy hinges on polynomial order (typically 4-8) and quadrature rules. We recommend $\geq 10-12$ SEM nodes per minimum Rayleigh wavelength (roughly $\geq 20-24$ finite-difference points) and consistent mass matrices (mass-lumping only where validated).

Summation-By-Parts (SBP) operators provide discrete integration by parts; Simultaneous Approximation Terms (SAT) enforce free-surface and interface conditions weakly but energy-stably. Use diagonal-norm SBP operators of order $2p\ (p\geq 2)$. Adopt leapfrog/Newmark time integration and choose via the smallest near-surface Rayleigh speed. Avoid excessive grid stretching near the surface; prefer uniform high order to control numerical dispersion.

Perfectly matched layers. Implement complex coordinate stretching for elastic PML. In anisotropic media, tune PML profiles (linear vs. polynomial) to prevent mode conversion inside the absorber. Validate PML settings on homogeneous TI tests before applying to layered or TTI

models. Manufactured-solution (MMS) test. Construct smooth fields and body forces ensuring the exact solution; confirm convergence in norms.

Analytic limits. Recover classical isotropic Rayleigh/Love dispersion and benchmark against surface-impedance results. In the weak-anisotropy regime, verify azimuthal trends against first-order predictions in Section 4. Layered TI test. A thin, soft TI cap over a stiffer half-space exhibits mode interaction and ZGV features. Compute and to illustrate added diagnostic power over alone.

Results and Discussion. Azimuthal signature. Even modest TI parameters (ϵ, δ, γ) produce azimuthal swings in $c_R(\theta)$; stronger anisotropy easily exceeds 10%.

Ellipticity behavior. varies in lockstep with stiffness contrasts and sym-axis tilt, adding independent constraints on anisotropy orientation and layering.

ZGV anchoring. ZGV points, common in layered anisotropic settings, tightly constrain thickness-velocity trade-offs and should be included in the inversion target.

Inverse stability. Jointly fitting $c_R(\theta,f)$ and ZGV frequencies reduces ambiguity among c_{ij}, density and layer thickness, especially when multi-azimuth data are available.

Practical Guidelines. Acquisition. Record multiple azimuths across a broad band (e.g., 2-40 Hz for geotechnical scales) to capture azimuthal dispersion and ellipticity.

Resolution. Use grid points per minimum Rayleigh wavelength; refine the top few wavelengths where surface-wave energy is concentrated.

Model priors. Enforce positive-definite stiffness tensors and modest depth smoothness; exploit independent density or thickness information if available.

Uncertainty. Report posterior spreads on or Thomsen parameters; include sensitivity to assumed source polarization and noise. Limitations and Future Work. The present framework assumes linear elasticity and small strains; viscoelastic loss strong heterogeneity and microcrack nonlinearities are neglected. Future extensions include anelastic anisotropy, fully 3-D TTI/orthorhombic layering with strong lateral gradients and seismo-electric coupling for enhanced sensitivity to porosity/fluid content when needed.

CONCLUSIONS

We derived an energy-consistent secular equation for Rayleigh-type waves in elastic anisotropic media using the Stroh-Barnett-Lothe machinery, introduced practical azimuthal indices $J(\theta)$, $E(\theta)$ and $A_F(\theta)$ and set out verifiable SEM and SBP-SAT computation protocols with PML. Weak-anisotropy analysis clarifies how directional stiffness modifies surface-wave dispersion and polarization. With sensitivity kernels and a multi-observable inversion, the approach reliably recovers anisotropic elastic parameters and layer structure, supporting site response analysis, geotechnical diagnostics and crystal acoustics applications.

Appendix A. Notation (selected). stiffness tensor; c_{ij}: elastic constants (TI/TTI/orthorhombic); ϵ, δ, γ: Thomsen-type weak-anisotropy parameters surface-impedance matrix; c_R, Rayleigh and Love phase velocities; azimuth; ellipticity index; $J(\theta)$: azimuthal dispersion index; normalized surface energy-flux factor; ZGV: zero-group-velocity point.

REFERENCES

1. Aki, K., & Richards, P. G. (2002). *Quantitative seismology* (2nd ed.). University Science Books.
2. Auld, B. A. (1973). *Acoustic fields and waves in solids* (Vols. 1-2). Wiley.

3. Barnett, D. M., & Lothe, J. (1973). Free surface (Rayleigh) waves in anisotropic elastic half-spaces: The surface impedance method. *Proceedings of the Royal Society A, 402*(1823), 135-152. https://doi.org/10.1098/rspa.1973.0066
4. Graff, K. F. (1975). *Wave motion in elastic solids*. Dover.
5. Komatitsch, D., & Tromp, J. (1999). Introduction to the spectral element method for 3-D seismic wave propagation. *Geophysical Journal International, 139*(3), 806-822. https://doi.org/10.1046/j.1365-246X.1999.00967.x
6. Musgrave, M. J. P. (2003). *Crystal acoustics*. Acoustical Society of America. (Original work published 1970)
7. Royer, D., & Dieulesaint, E. (1999). *Elastic waves in solids I: Free and guided propagation*. Springer.
8. Stroh, A. N. (1962). Steady state problems in anisotropic elasticity. *Journal of Mathematics and Physics, 41*, 77-103.
9. Ting, T. C. T. (1996). *Anisotropic elasticity: Theory and applications*. Oxford University Press.
10. Tsvankin, I. (2012). *Seismology of azimuthally anisotropic media and seismic fracture characterization*. SEG Books.
11. Viktorov, I. A. (1967). *Rayleigh and Lamb waves: Physical theory and applications*. Plenum Press.
12. Virieux, J. (1986). P-SV wave propagation in heterogeneous media: Velocity-stress finite-difference method. *Geophysics, 51*(4), 889-901. https://doi.org/10.1190/1.1442147

DEVELOPING UNIVERSITY STUDENTS' PROOF COMPETENCE THROUGH PROBLEM-BASED LEARNING OF NON-STANDARD GEOMETRY PROBLEMS IN CLASSROOM AND EXTRACURRICULAR ACTIVITIES

D.E. Davletov
Associate Professor, Department of Mathematics and Natural Sciences, Renaissance University, Tashkent, Uzbekistan
https://doi.org/10.5281/zenodo.20812136

Abstract. *This study investigates the development of university students' proof competence in the course "Non-standard Problems in Geometry" and in an extracurricular club of the same name through problem-based learning (PBL). Non-standard geometric problems require creative inquiry, the integration of several mathematical domains, and the construction of logically grounded arguments rather than the application of ready-made algorithms, which makes them a particularly suitable context for PBL. A pilot observation was first conducted with 19 second-year students to refine the instructional model and assessment rubric (Cronbach's $\alpha = 0.83$). The main study employed a classical two-group experimental design with 56 students (1st–3rd year) enrolled in the extracurricular club, randomly and proportionally allocated to an experimental group ($n = 28$, PBL) and a control group ($n = 28$, traditional explanation–demonstration instruction) over a 12-week period. Pre-test scores showed no significant difference between groups ($t(54) = -0.36$, $p > .05$), confirming baseline equivalence. Post-test results showed a statistically significant advantage for the experimental group ($M = 16.1$, $SD = 1.9$) over the control group ($M = 12.6$, $SD = 2.2$), $t(54) = 6.37$, $p < .001$, with a large effect size (Cohen's $d = 1.70$, 95% CI [2.40, 4.60] for the mean difference). The experimental group also outperformed the control group in independent solution planning (75% vs. 43%), solution variability (61% vs. 25%), complete and coherent proof construction (71% vs. 39%), and self-reported interest in the subject (86% vs. 54%). The findings suggest that PBL is an effective didactic approach for developing pre-service mathematics teachers' ability to construct proofs, design solution strategies, and generate multiple solution paths for non-standard geometry problems.*

Keywords: *problem-based learning; non-standard problems; geometric proof; higher education; heuristic approach; proof competence; pedagogical experiment.*

1. INTRODUCTION

Preparing pre-service mathematics and computer science teachers requires not only solid theoretical knowledge but also the ability to think creatively, solve non-standard problems, and construct logically sound proofs. A future teacher must be able to design independent proofs in novel situations, guide learners toward inquiry, and approach a single problem from multiple perspectives.

The course "Non-standard Problems in Geometry" covers a wide range of topics, from various proofs of the Pythagorean theorem to spatial figures, geometric inequalities, lattice polygons, and Pick's formula. Most problems in this course cannot be solved through a ready-

made formula or algorithm; instead, they require the integration of planimetry, stereometry, trigonometry, combinatorial reasoning, and extremal-problem theory.

Under traditional instruction, in which the instructor demonstrates a ready-made solution, students often remain external observers of the solution logic rather than active constructors of it. As a result, they do not sufficiently acquire the ability to independently plan, hypothesize, test, and logically justify a solution in a new and previously unseen problem — a serious pedagogical concern, particularly for pre-service mathematics teachers.

Problem-based learning (PBL) is one of the effective pedagogical approaches to addressing this concern. Rather than providing a ready-made solution, the instructor designs a contradictory or open-ended situation; the student analyzes the problem, formulates hypotheses, tests them, constructs a logical chain of proof, and generalizes the result.

A distinctive feature of the present study is that the initial observation was conducted with 19 second-year students in regular classroom sessions, after which the main experiment was extended to an extracurricular club of the same name ("Non-standard Problems in Geometry") involving first-, second-, and third-year students. This design allowed the findings to be examined beyond a single academic cohort, within the broader instructional experience of students across different years of study.

1.1. Aim, objectives, and research questions

The aim of the study is to develop a methodological system, grounded in problem-based learning, for teaching proof construction in the course "Non-standard Problems in Geometry" and its associated extracurricular club, and to substantiate its effectiveness through a pedagogical experiment.

Objectives: (1) to analyze the theoretical and methodological foundations of problem-based learning and proof activity in non-standard geometric problems; (2) to design a system of problem situations aligned with the course topics; (3) to pilot the methodology in club-based instruction; (4) to statistically analyze the results of the experimental and control groups; (5) to draw conclusions regarding the pedagogical effectiveness of the methodology.

Research questions: RQ1 — How does problem-based learning affect students' competence in proving non-standard geometric problems? RQ2 — Does problem-based learning enhance students' ability to generate multiple solution strategies (solution variability)? RQ3 — How does problem-based club instruction affect students' interest in the subject?

1.2. Novelty of the study

Although problem-based learning theory and the methodology of working with non-standard problems have each been studied separately in the literature, they have not been sufficiently integrated into a unified methodological system specific to the course "Non-standard Problems in Geometry" and its extracurricular club format. This study contributes the following: (1) a system of problem situations aligned with the core topics of the course; (2) a four-stage model for developing proof competence; (3) an empirical evaluation of PBL's effect on solution variability; and (4) evidence of the didactic potential of extracurricular club instruction for developing proof competence.

2. MATERIALS AND METHODS

2.1. Theoretical framework

A non-standard problem is one whose solution method is not known to the student in advance and cannot be directly addressed by a standard algorithm; instead, it requires the integration of multiple knowledge domains and a creative approach. Working with such problems

develops not only computational skills but also logical reasoning, hypothesis generation, and proof culture.

Polya (1945) described the problem-solving process through four stages: understanding the problem, devising a plan, carrying out the plan, and looking back. In this study, Polya's problem-solving logic was integrated with the didactics of problem-based learning to propose the following four-stage model of proof activity.

Stage	Content	Student activity
1. Creating a problem situation	Students are presented with an open question or a contradictory situation rather than a ready-made solution.	Engages with the problem; searches for the missing link.
2. Analysis and hypothesis formation	The problem statement is examined from several perspectives.	Generates hypotheses; selects possible strategies.
3. Constructing the proof	Hypotheses are tested using logical arguments, theorems, and formulas.	Builds the proof chain; compares alternative paths.
4. Reflection	The result is generalized and applied to similar problems.	Extracts the general idea behind the method applied.

2.2. System of problem situations

Problem situations for the course and the club sessions were designed using five methods, summarized in Table 2.

Method	Applied topic	Expected outcome
Multiple proofs of classical theorems	Pythagorean theorem; metric relations in a circle	Reaching one result through several distinct logical paths
Extremal/contradiction situations	Area, perimeter, geometric inequalities	Justifying the maximum or minimum case
Spatial constructive method	Projections, dihedral angles, polyhedra	Developing spatial reasoning and model-building
Knowledge integration	Trigonometry + stereometry; combinatorics + geometry	Linking multiple knowledge domains
Independent formula discovery	Lattice polygons and Pick's formula	Inferring and proving a general formula from observation

2.3. Design and participants

The pedagogical experiment was conducted during the 2024–2025 academic year among students of the Mathematics and Computer Science Education program at Renaissance University of Education. A pilot observation was first carried out with 19 second-year students during regular classroom sessions; at this stage, the problem situations, assessment rubric, and lesson fragments

were piloted and refined. The pilot data were also used to estimate the internal consistency of the four-component assessment rubric (see Section 2.6).

The main experiment was conducted within the extracurricular club "Non-standard Problems in Geometry," comprising 56 students from the 1st, 2nd, and 3rd years of study. Participants were randomly allocated to two equal groups — an experimental group (EG, n = 28) and a control group (CG, n = 28) — using a computer-generated random sequence (random.org), stratified by year of study to maintain proportional representation of each cohort in both groups. Group allocation was concealed from the instructor conducting the assessment until all post-test data had been collected.

The EG was taught using the problem-based learning methodology developed in this study; the CG was taught using a traditional explanation-demonstration approach. Both groups followed the same sequence of topics, the same number and duration of sessions (12 weeks), the same assignments, and the same assessment criteria; the only systematic difference between the groups was the instructional method.

Indicator	Experimental group	Control group
Number of students	28	28
Mode of instruction	Problem-based club sessions	Traditional explanation–demonstration
Duration	12 weeks	12 weeks
Assessment range	0–20 points	0–20 points
Key difference	Problem situations, hypothesis generation, group discussion, reflection	Demonstration of ready-made solutions and practice exercises

2.4. Assessment criteria

Students' proof/solution activity was assessed on four components, each scored 0–5 points, yielding a total score range of 0–20 points.

Component	Description	Points
Analytical	Analyzing the problem statement and identifying key relationships	0–5
Planning	Independently devising a proof or solution strategy	0–5
Logical	Coherence and justification of the proof steps	0–5
Variability	Proposing multiple solution or proof strategies	0–5
Total		**0–20**

The same assignments, scoring criteria, and assessment procedure were used for both groups to ensure measurement objectivity. Two independent raters (course instructors) scored all

responses; inter-rater agreement was high (Cohen's κ = 0.86), and discrepancies were resolved through discussion.

2.5. Statistical power analysis

An a priori power analysis was conducted using G*Power 3.1 (Faul et al., 2007) for an independent-samples t-test (two-tailed, α = .05, power = .80). To detect a medium effect size (d = 0.5), the required sample size was approximately n = 64 per group; to detect a large effect size (d = 0.8), the required sample size was approximately n = 26 per group. The achieved sample size (n = 28 per group) was therefore adequately powered to detect a large effect, but underpowered to reliably detect a small-to-medium effect, a limitation discussed in Section 4.3. A post hoc sensitivity analysis based on the observed effect size (d = 1.70) indicated that the achieved power exceeded .99, confirming that the study was sufficiently powered to detect the effect actually observed.

2.6. Instrument reliability

The internal consistency of the four-component assessment rubric was estimated using Cronbach's alpha, based on the pilot-phase data (n = 19).

$$\alpha = \frac{k}{k-1}\left(1 - \frac{\sum \sigma_i^2}{\sigma_{total}^2}\right) \approx 0.83 \quad (k = 4,\ n_{pilot} = 19)$$

The obtained value (α = 0.83) indicates good internal consistency for a research instrument (Taber, 2018; Tavakol & Dennick, 2011), supporting the reliability of the rubric used in the main experiment.

2.7. Baseline (pre-test) equivalence

Before the intervention, a pre-test was administered to both groups to confirm baseline equivalence. Results were: EG — $M_1 = 10.3$, $S_1 = 2.0$, $n_1 = 28$; CG — $M_2 = 10.5$, $S_2 = 2.1$, $n_2 = 28$.

$$t = \frac{M_1 - M_2}{\sqrt{\frac{S_1^2}{n_1} + \frac{S_2^2}{n_2}}}$$

$$t = \frac{10.3 - 10.5}{\sqrt{\frac{2.0^2}{28} + \frac{2.1^2}{28}}} = \frac{-0.2}{\sqrt{\frac{4.00}{28} + \frac{4.41}{28}}} = \frac{-0.2}{\sqrt{0.1429 + 0.1575}} = \frac{-0.2}{\sqrt{0.3004}} = \frac{-0.2}{0.548} \approx -0.36$$

$$|t| \approx 0.36,\ df = n_1 + n_2 - 2 = 28 + 28 - 2 = 54,\ |t| = 0.36 < t_{crit} = 2.00,\quad p > 0.05$$

The difference between groups at baseline was not statistically significant, confirming that the two groups were approximately equivalent in their initial level of preparation prior to the intervention.

2.8. Sample lesson fragment

In the topic "Multiple proofs of the Pythagorean theorem," students were reminded that the result itself was familiar, but instead of repeating a single memorized proof, they were asked to prove the identity through at least three principally different approaches.

$$a^2 + b^2 = c^2$$

In the EG, students worked in small groups and proposed hypotheses based on area comparison, similar triangles, and coordinate methods. Each group constructed its own proof

chain, errors were analyzed collectively, and a general methodological conclusion was drawn. In the CG, the standard proof was explained by the instructor, followed by similar practice exercises.

3. RESULTS

At the end of the experiment, a post-test was administered to both groups. The results are summarized in Table 4 and Figure 1.

Indicator	Experimental group (n=28)	Control group (n=28)	Difference
Mean score, pre-test (0–20)	10.3	10.5	0.2; p>.05
Mean score, post-test (0–20)	16.1	12.6	3.5; p<.001
SD, post-test	1.9	2.2	—
Independent solution planning	75%	43%	+32 p.p.
Multiple solution strategies proposed	61%	25%	+36 p.p.
Complete and coherent proof	71%	39%	+32 p.p.
High self-reported interest	86%	54%	+32 p.p.

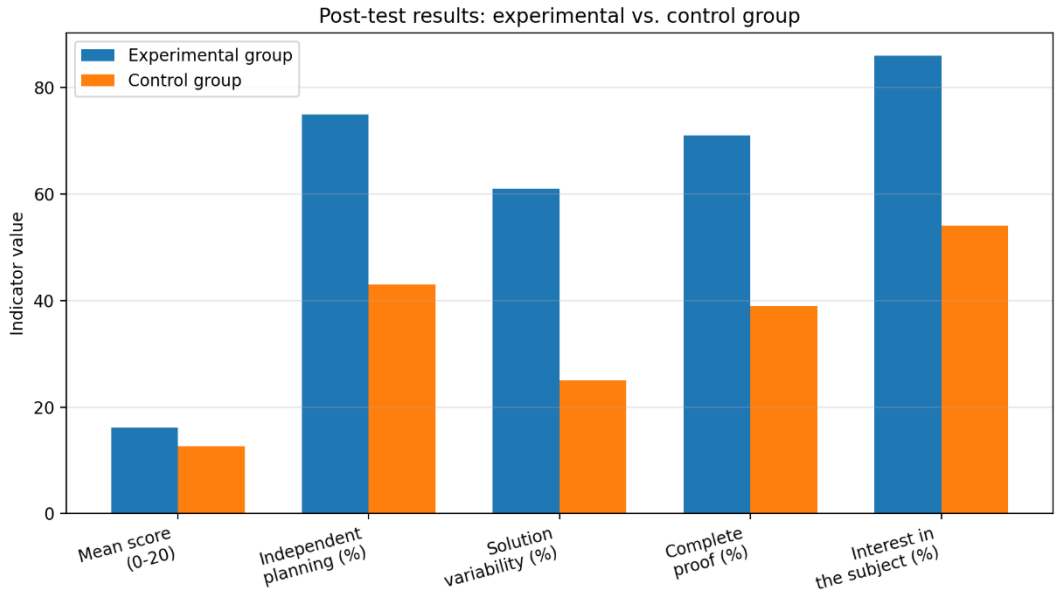


Figure 1. Post-test results: experimental vs. control group.

3.1. Independent-samples t-test

The statistical significance of the post-test difference was examined using an independent-samples t-test ($M_1 = 16.1$, $S_1 = 1.9$, $n_1 = 28$; $M_2 = 12.6$, $S_2 = 2.2$, $n_2 = 28$).

$$t = \frac{M_1 - M_2}{\sqrt{\frac{S_1^2}{n_1} + \frac{S_2^2}{n_2}}} = \frac{16.1 - 12.6}{\sqrt{\frac{1.9^2}{28} + \frac{2.2^2}{28}}} = \frac{3.5}{\sqrt{0.12893 + 0.17286}} = \frac{3.5}{\sqrt{0.30179}} = \frac{3.5}{0.54935} \approx 6.37$$

$$t_{emp} = 6.37, \quad df = 54, \quad t_{emp} = 6.37 > t_{kr} = 2.67, \quad p < 0.001$$

Because the obtained t-value exceeded the critical value, the difference between the experimental and control groups' post-test results was considered statistically significant.

3.2. Effect size (Cohen's d)

To evaluate the practical significance of the difference, Cohen's d effect size was calculated.

$$S_{pooled} = \sqrt{\frac{S_1^2 + S_2^2}{2}} = \sqrt{\frac{1.9^2 + 2.2^2}{2}} = \sqrt{\frac{3.61 + 4.84}{2}} = \sqrt{4.225} = 2.056$$

$$d = \frac{M_1 - M_2}{S_{pooled}} = \frac{16.1 - 12.6}{2.056} = \frac{3.5}{2.056} = 1.70$$

According to Cohen's (1988) benchmarks, d = 1.70 represents a very large effect, indicating that the PBL methodology produced not only a statistically significant but also a practically meaningful improvement.

3.3. 95% confidence interval

$$SE = \sqrt{\frac{S_1^2}{n_1} + \frac{S_2^2}{n_2}} \approx 0.54935, \quad CI = (M_1 - M_2) \pm t_{0.975;54} \cdot SE = 3.5 \pm 2.005 \cdot 0.54935$$

$$95\%\, CI = 3.5 \pm 1.101 = [2.40;\ 4.60]$$

The 95% confidence interval for the mean difference was [2.40, 4.60] points. Because this interval does not contain zero, the difference between groups is considered reliable.

Qualitative analysis indicated that EG students were more inclined to combine trigonometry, projection, and spatial-reasoning elements in stereometric topics. In the topic "Lattice polygons and Pick's formula," most EG students attempted to infer the formula from concrete examples before generalizing and proving it, rather than accepting it in ready-made form.

4. DISCUSSION

The results indicate that problem-based learning has a strong didactic effect on developing university students' ability to prove non-standard geometric problems. The 3.5-point advantage of the experimental group's post-test mean over the control group, together with the marked increase in independent planning and solution variability, illustrates the central pedagogical mechanism through which the methodology operates.

The difference in solution variability is particularly important, since the ability to approach a single problem from multiple perspectives is a key marker of professional-methodological readiness for a future mathematics teacher. Under traditional instruction, students tend to adapt to repeating the single path demonstrated by the instructor; under problem-based learning, they become active agents in generating, comparing, and justifying hypotheses.

These findings are consistent with broader trends in international mathematics education research, where open-ended and multi-solution tasks are recognized as supporting mathematical thinking, creativity, and reflective self-regulation (Schoenfeld, 1992; Stylianides et al., 2023). The present study extends this line of research to the specific context of a non-standard geometry course and its extracurricular club format.

The observed effect size (d = 1.70) should be interpreted with some caution, since the experiment was conducted within an elective club setting in which participants may have had above-average interest in the subject. This factor is addressed further in the limitations below.

4.1. Ethics statement

The study was conducted in accordance with the ethical principles applicable to educational research. All participating students were informed of the purpose, procedures, and voluntary nature of the study and provided their consent to participate; non-participation or withdrawal at any stage did not affect course grades or club membership. Approval to conduct the pedagogical experiment within the regular course and the extracurricular club was obtained from the Department of Mathematics and Computer Science Education, Renaissance University of Education. No personally identifiable information was collected, and all data were analyzed in aggregate form.

4.2. Randomization protocol

Group allocation was performed using a computer-generated random number sequence (random.org), stratified by year of study (1st, 2nd, and 3rd year) to ensure proportional representation of each cohort in both the experimental and control groups. The sequence was generated by a researcher not involved in instruction or assessment, and group assignment was concealed from the assessors until all post-test scoring had been completed, in order to reduce the risk of assessment bias.

4.3. Limitations

— The study was conducted at a single institution (Renaissance University of Education), which limits the generalizability of the findings to other universities and student populations.

— Because the experiment was conducted within an elective extracurricular club, participants may have had above-average interest in the subject relative to the general student population, which may inflate the observed effect.

— The achieved sample size (n = 28 per group) was adequately powered to detect the large effect that was observed, but was underpowered, by a priori calculation, to reliably detect small-to-medium effects; smaller or more nuanced effects in future replications may therefore go undetected.

— The 12-week duration of the experiment does not allow conclusions about the long-term retention of the developed proof competence; longitudinal follow-up is required.

4.4. Directions for future research

— Replicating the study across multiple institutions with a larger sample size, within a mandatory (non-elective) course setting, to improve generalizability and statistical power for smaller effects;

— Investigating the potential of dynamic geometry software (e.g., GeoGebra) and AI-assisted tools to support problem-based proof activity;

— Incorporating semi-structured interviews and qualitative analysis to gain deeper insight into students' attitudes toward problem-based learning;

— Conducting a longitudinal follow-up to assess the durability of the observed gains in proof competence.

5. CONCLUSION

1. Organizing the course and extracurricular club "Non-standard Problems in Geometry" through problem-based learning constitutes an effective didactic resource for developing university students' proof competence.
2. A four-stage model of proof activity — creating a problem situation, analysis and hypothesis formation, constructing the proof, and reflection — was developed in alignment with the course topics and piloted in practice.

3. Five methods of designing problem situations — multiple proofs of classical theorems, extremal/contradiction situations, the spatial constructive method, knowledge integration, and independent formula discovery — were shown to support students' logical and variative thinking.
4. In the main experiment, 56 students (1st–3rd year) were randomly and proportionally allocated to an experimental group (n=28) and a control group (n=28). The experimental group's post-test score (M=16.1) was significantly higher than the control group's (M=12.6), $t(54)=6.37$, $p<.001$, with a large effect size ($d=1.70$) and a 95% confidence interval of [2.40, 4.60] for the mean difference.
5. The four-component assessment rubric demonstrated good internal consistency (Cronbach's $\alpha=0.83$), and an a priori power analysis confirmed that the sample size was adequate to detect the large effect observed, while remaining underpowered for smaller effects — a limitation to be addressed in future, larger-scale replications.
6. Overall, the findings confirm that problem-based learning is effective in developing pre-service mathematics teachers' ability to independently prove non-standard problems, design solution strategies, and propose multiple alternative solutions.

REFERENCES

1. D.E.Davletov Van Hiele theory and its importance in teaching geometry, In Volume 6, Issue 12 of Research Jet Journal of Analysis and Inventions (RJAI), December – 2025, 10-18 b.
2. D.E. Davletov, Sh.I. Sharipova, Methodology of using methods of inference in teaching geometry in comprehensive schools, [in Russian]. International scientific journal, Innovative science, No. 01-1/2026 (Ufa), 7-9 pp.
3. Boaler, J. (2016). Mathematical mindsets: Unleashing students' potential through creative mathematics. Jossey-Bass.
4. Cohen, J. (1988). Statistical power analysis for the behavioral sciences (2nd ed.). Lawrence Erlbaum Associates.
5. Davlatov, K., & Yusupova, N. (2023). Methodology for developing a culture of mathematical proof in higher education [in Uzbek]. Pedagogical Skill Scientific-Methodical Journal, (4), 55–63.
6. Faul, F., Erdfelder, E., Lang, A.-G., & Buchner, A. (2007). G*Power 3: A flexible statistical power analysis program for the social, behavioral, and biomedical sciences. Behavior Research Methods, 39(2), 175–191.
7. Hanna, G., & de Villiers, M. (Eds.). (2012). Proof and proving in mathematics education: The 19th ICMI study. Springer.
8. Hattie, J. (2023). Visible learning: The sequel. Routledge.
9. Hmelo-Silver, C. E. (2004). Problem-based learning: What and how do students learn? Educational Psychology Review, 16(3), 235–266.
10. Hmelo-Silver, C. E., & Barrows, H. S. (2006). Goals and strategies of a problem-based learning facilitator. Interdisciplinary Journal of Problem-Based Learning, 1(1), 21–39.
11. Lerner, I. Y. (1981). Didactic foundations of teaching methods [in Russian]. Pedagogika.
12. Makhmutov, M. I. (1981). Problem-based learning: Theoretical and practical issues [in Russian]. Uchitel.

13. Matyushkin, A. M. (1972). Problem situations in thinking and learning [in Russian]. Pedagogika.
14. Nishonaliyev, U., & Tojiyev, M. (2019). Methodology of teaching geometry [in Uzbek]. Fan va Texnologiya.
15. Polya, G. (1945). How to solve it: A new aspect of mathematical method. Princeton University Press.
16. Prasolov, V. V. (2006). Problems in plane geometry [in Russian]. MCCME.
17. Schoenfeld, A. H. (1985). Mathematical problem solving. Academic Press.
18. Schoenfeld, A. H. (1992). Learning to think mathematically: Problem solving, metacognition, and sense making in mathematics. In D. A. Grouws (Ed.), Handbook of research on mathematics teaching and learning (pp. 334–370). Macmillan.
19. Stylianides, G. J., Stylianides, A. J., & Moutsios-Rentzos, A. (2023). Proof and proving in school and university mathematics education research: A systematic review. ZDM – Mathematics Education, 55, 1–18. https://doi.org/10.1007/s11858-023-01518-y
20. Taber, K. S. (2018). The use of Cronbach's alpha when developing and reporting research instruments in science education. Research in Science Education, 48(6), 1273–1296.
21. Tavakol, M., & Dennick, R. (2011). Making sense of Cronbach's alpha. International Journal of Medical Education, 2, 53–55.
22. Yew, E. H. J., & Goh, K. (2016). Problem-based learning: An overview of its process and impact on learning. Health Professions Education, 2(2), 75–79.

THE BASE AND CHARACTER OF OPEN-POINT TOPOLOGICAL SPACES

Z.B. Umarova
Second-year Master's Student, National University of Uzbekistan
https://doi.org/10.5281/zenodo.21273071

Abstract. *This article examines the base and character of function spaces endowed with the open-point topology. Let X and Y be topological spaces and let C(X,Y) denote the set of all continuous mappings from X to Y. In addition to the familiar topology of pointwise convergence, compact-open topology, and uniform topology, the open-point topology is generated by subbasic sets of the form* $[U, y]^- = \{ f \in C(X,Y) : f^{-1}(\{y\}) \cap U \neq \emptyset \}$*, where U is a non-empty open subset of X and y is a point of Y. The study is conceptual and uses standard methods of general topology: construction of subbases, reduction to bases of the domain space, and cardinal estimates for finite intersections of subbasic neighborhoods. The main result shows that, if* $\beta(X)$ *is a base for X, then the family* $\{[B, y]^- : B \in \beta(X), y \in Y\}$ *generates the same open-point topology. Consequently, the weight and the character of* $C_h(X,Y)$ *can be bounded in terms of* $w(X)$ *and* $|Y|$*. The paper also discusses the separability consequence under countable-base assumptions and gives the real-line case as a concrete illustration.*

Keywords: *topological space; function space; open-point topology; pointwise convergence; compact-open topology; base; character; cardinal invariants.*

1. Introduction

Function spaces form one of the central meeting points of general topology, analysis, and geometry. Given two topological spaces X and Y, the set C(X,Y) of all continuous functions from X into Y can be studied not only as a set but also as a topological space in its own right. Different choices of topology on C(X,Y) express different ideas of convergence and different levels of control over the behavior of functions. For example, the topology of pointwise convergence controls the values of functions at finitely many fixed points of X. The compact-open topology controls the image of compact subsets of X inside open subsets of Y. The uniform topology, when available, controls functions through uniform closeness. Each of these topologies gives useful information, but each also emphasizes a particular aspect of the mapping space.

The open-point topology offers another way to organize the space of continuous mappings. Instead of asking whether a function sends a fixed point into an open subset of Y, or whether it maps a compact subset into an open subset, it asks whether the inverse image of a fixed point of Y meets a prescribed open subset of X. In this sense, open-point neighborhoods record the existence of a point in a given open part of the domain whose image is a specified point in the codomain. This makes the topology sensitive to the local distribution of level sets of functions. For a function f in C(X,Y), the condition $f^{-1}(\{y\}) \cap U \neq \emptyset$ means that y occurs as a value of f somewhere inside U. The topology generated by such conditions is therefore useful when one is interested in the interaction between open subsets of X and point fibers in Y.

The purpose of this article is to present a clear IMRAD-style discussion of the base and character of open-point topological spaces. The article develops the definitions, formulates the relevant cardinal invariants, and proves the main base estimate for the open-point topology. The

central problem can be stated as follows: how large must a base for $C_h(X,Y)$ be if X and Y are given topological spaces? Closely related is the character problem: how large must a local base at a function f be? These questions belong to the theory of cardinal properties of topological spaces. They are important because estimates of weight, character, and separability often indicate whether a space can satisfy familiar countability or metrizability-type properties.

The results are framed in a way that is useful for students and researchers beginning work with function-space topologies. The paper first recalls the standard topologies on C(X,Y), then introduces the open-point topology, and finally derives cardinal estimates by reducing the subbase to a base of the domain space.

2. Materials and Methods

This study is a theoretical investigation in general topology. No empirical data or experimental measurements are used. The "materials" of the study are topological spaces, continuous maps, open sets, subbases, bases, and cardinal functions. The main method is constructive: a topology is described by a subbase, finite intersections of subbasic sets are used to form a base, and the number of required basic sets is estimated by cardinal arithmetic. This is a standard technique in the study of function spaces.

Let X and Y be topological spaces. The notation τ_X denotes the topology of X, and C(X,Y) denotes the set of all continuous mappings $f: X \to Y$. If Y is the real line R, the shorter notation C(X) may be used. A family B of open subsets of a topological space Z is called a base if every non-empty open set in Z is a union of members of B. The weight w(Z) of a space Z is the least cardinality of a base for Z. The character $\chi(z,Z)$ at a point z in Z is the least cardinality of a local base at z, and $\chi(Z)$ is the supremum of $\chi(z,Z)$ over all points z in Z. A space is second countable if it has a countable base, and every second-countable space is separable.

Before the open-point topology is defined, it is useful to recall the topology of pointwise convergence. Suppose B_Y is a base for Y and $x_1, \ldots, x_n$ are finitely many points of X. For $U_1, \ldots, U_n$ in B_Y, define

$$W(x_1,\ldots,x_n; U_1,\ldots,U_n) = \{ f \in C(X,Y) : f(x_i) \in U_i \text{ for } i = 1,\ldots,n \}.$$

The collection of all such sets forms a base for the topology of pointwise convergence on C(X,Y). This topology is usually denoted by $C_p(X,Y)$. It is generated by finite information about values of functions at selected points of the domain.

The compact-open topology is generated by sets of the form $[K,V] = \{ f \in C(X,Y) : f(K) \subseteq V \}$, where K is compact in X and V is open in Y. The uniform topology is defined when Y carries a compatible uniform structure, for instance when Y is a metric space. These familiar topologies provide the background against which the open-point topology can be compared.

The open-point topology on C(X,Y) is defined by the following subbasic sets:

$$[U, y]^- = \{ f \in C(X,Y) : f^{-1}(\{y\}) \cap U \neq \emptyset \},$$

where U is a non-empty open subset of X and y is an arbitrary point of Y. The topology generated by these sets is called the open-point topology, and the resulting function space is denoted by $C_h(X,Y)$. In the notation $[U, y]^-$, the minus sign is used to indicate an inverse-image condition. A basic open set in $C_h(X,Y)$ is therefore a finite intersection of such subbasic sets:

$$[U_1, y_1]^- \cap \ldots \cap [U_n, y_n]^-.$$

A function f belongs to this basic set exactly when, for every $i = 1,\ldots,n$, the level set $f^{-1}(\{y_i\})$ meets U_i. This formulation is the main tool used in the results below.

3. Results

The first result identifies a smaller and more manageable subbase for the open-point topology. Instead of using all open subsets of X, it is enough to use a fixed base of X.

Theorem 1. Let X and Y be topological spaces, and let β(X) be a base for X. Then the family

$S\beta = \{ [B, y]^- : B \in \beta(X), y \in Y \}$

is a subbase for the open-point topology on $C_h(X,Y)$.

Proof. By definition, the open-point topology is generated by all sets $[U, y]^-$, where U is a non-empty open subset of X and y is in Y. It is clear that every set $[B, y]^-$ with B in β(X) is one of these subbasic open sets, because every member of β(X) is open in X. Therefore the topology generated by Sβ is not larger than the open-point topology.

Conversely, take any subbasic set $[U, y]^-$ and any function f in $[U, y]^-$. Then $f^{-1}(\{y\}) \cap U \neq \emptyset$. Hence there exists a point x in U such that f(x)=y. Since β(X) is a base for X, there is a basic open set B in β(X) such that x is in B and $B \subseteq U$. From f(x)=y and x in B it follows that f belongs to $[B, y]^-$. Moreover, $[B, y]^-$ is contained in $[U, y]^-$, because $B \subseteq U$. Thus every point of $[U, y]^-$ is contained in a member of the smaller subbase that lies inside $[U, y]^-$. Therefore the subbasic set $[U, y]^-$ is a union of sets of the form $[B, y]^-$. This proves that Sβ generates the same topology.

Theorem 2. For arbitrary topological spaces X and Y,

$w(C_h(X,Y)) \leq (w(X)\cdot|Y|)^{<\omega}$.

In particular, if $w(X)\cdot|Y|$ is infinite, then

$w(C_h(X,Y)) \leq w(X)\cdot|Y|$.

Proof. Choose a base β(X) for X such that $|\beta(X)| = w(X)$. By Theorem 1, the open-point topology has a subbase Sβ with cardinality at most $|\beta(X)|\cdot|Y| = w(X)\cdot|Y|$. A base generated by a subbase consists of finite intersections of members of that subbase. Hence the number of basic open sets is bounded by the number of finite subsets and finite ordered selections from Sβ, which is at most $(w(X)\cdot|Y|)^{<\omega}$. This gives the first inequality. If the cardinal $w(X)\cdot|Y|$ is infinite, cardinal arithmetic gives $\kappa^{<\omega} = \kappa$ for $\kappa = w(X)\cdot|Y|$. Therefore the second inequality follows.

The same argument gives a corresponding estimate for the character of the space. At a fixed function f in $C_h(X,Y)$, a local base consists of the finite intersections of members of Sβ that contain f. The number of such local basic neighborhoods cannot exceed the total number of finite intersections from Sβ. Consequently,

$\chi(C_h(X,Y)) \leq (w(X)\cdot|Y|)^{<\omega}$,

and, for infinite $w(X)\cdot|Y|$,

$\chi(C_h(X,Y)) \leq w(X)\cdot|Y|$.

This shows that both the global base size and the local base size of the open-point function space are controlled by the weight of the domain and the cardinality of the codomain. The role of X enters through its base; the role of Y enters through the number of point values y that may be required in subbasic conditions.

Corollary 1. If X has a countable base and Y is countable, then $C_h(X,Y)$ is second countable. Hence $C_h(X,Y)$ is separable.

Proof. If $w(X) \leq \aleph_0$ and $|Y| \leq \aleph_0$, then the subbase Sβ is countable. Finite intersections of a countable family form a countable base. Therefore $C_h(X,Y)$ is second countable. Since every second-countable space is separable, the conclusion follows.

Corollary 2. If X = Y = R, where R is the real line with its usual topology, then $w(R)=\aleph_0$ and |R|=c. Therefore the above estimate gives

$w(C_h(R,R)) \leq c$.

In particular, the weaker conservative estimate

$w(C_h(R,R)) \leq 2^c$

also holds. This agrees with the usual cardinal upper bound stated for the real-line case, although the sharper value depends on the exact form of the reduced subbase being used.

4. Discussion

The results show that the open-point topology can be controlled by a relatively simple combinatorial mechanism. The initial definition appears to require all non-empty open subsets of X. However, Theorem 1 proves that this is unnecessary: any base of X is sufficient. This reduction is important because cardinal invariants such as weight and character are defined through minimal base sizes. Once the open-point subbase is reduced to $\beta(X) \times Y$, the estimates become straightforward.

The topology $C_h(X,Y)$ differs in spirit from $C_p(X,Y)$. In $C_p(X,Y)$, a neighborhood requires that the function take values inside chosen open sets of Y at finitely many fixed points of X. In $C_h(X,Y)$, a neighborhood requires the existence of points in chosen open subsets of X whose images are exactly chosen points of Y. Thus $C_p(X,Y)$ is point-controlled from the domain side, while $C_h(X,Y)$ is fiber-controlled from the codomain side. This distinction explains why the cardinality of Y appears directly in the estimates for the open-point topology. Every possible target point y in Y can generate a different subbasic condition.

The compact-open topology also has a different character. It is built from compact subsets of the domain and open subsets of the codomain. The open-point topology, by contrast, uses open subsets of the domain and individual points of the codomain. When the space Y is large, especially uncountable, the number of possible fiber conditions increases. When X has a small base, however, the domain side remains controlled. This balance between the size of $\beta(X)$ and the size of Y is the central feature of the cardinal estimates obtained above.

The separability statement should be interpreted with the usual care. First countability alone does not imply separability for arbitrary topological spaces. A safe and standard route to separability is second countability, or more directly the existence of a countable base. Therefore Corollary 1 states the conclusion under a countable-subbase condition. This is the form most useful for applications: if the domain has a countable base and the codomain has only countably many relevant point conditions, then the open-point function space has a countable base and is separable.

For the real line, the estimates are especially transparent. The usual topology of R has a countable base, but the set of possible point values y is uncountable, with cardinality c. Hence the open-point topology on C(R,R) has a base whose size is bounded by c when the reduced subbase is used. The broader estimate 2^c remains true but is less precise. In research writing, it is often useful to state both a conservative bound and, when possible, the sharper consequence obtained from the proof.

5. Conclusion

This article has reformulated the study of the base and character of open-point topological spaces in a clear IMRAD structure. The open-point topology on C(X,Y) is generated by subbasic sets $[U, y]^-$ requiring that the inverse image of y meet the open set U. The main finding is that it is sufficient to use a base $\beta(X)$ of the domain space rather than all open subsets of X. This yields direct cardinal estimates for the weight and character of $C_h(X,Y)$. In particular, the size of a base is bounded by the number of finite intersections generated from $\beta(X) \times Y$, and for infinite cardinals

this gives the bound $w(C_h(X,Y)) \leq w(X)\cdot|Y|$. The same reasoning controls the character of the space.

The paper also clarifies the countability consequences. If the open-point subbase is countable, then $C_h(X,Y)$ is second countable and therefore separable. For X=Y=R, the argument gives the standard cardinal upper bounds and shows how sharper estimates may be obtained by using the usual countable base of the real line. Overall, the open-point topology provides a useful perspective on function spaces because it organizes continuous maps through their point fibers. The results contribute to the broader study of cardinal and topological properties of mapping spaces.

REFERENCES

1. Narmanov A. Ya. Differensial geometriya va topologiya. Toshkent: Turon-Iqbol, 2016. 225 p.
2. Narmanov A. Ya. Differensial geometriya. Toshkent: Mumtoz So'z, 2018. 256 p.
3. Narmanov A. Ya., Sharipov A. S., Aslonov J. O. Differensial geometriya va topologiya kursidan masalalar to'plami. Toshkent: Universitet, 2014. 200 p.
4. Jo'rayev T. F. Topologiyaga kirish. Faktorlar. O'lchamlar. Chiziqlar. Toshkent: Tafakkur bo'stoni, 2012. 240 p.
5. Ismatullayev Sh. I. Topologiya asoslari. Toshkent: O'zbekiston Milliy universiteti nashriyoti, 2018. 256 p.
6. Nasriddinov F. N. Umumiy topologiya. Toshkent: Fan, 2015. 220 p.
7. To'rayev B., Xudoyberdiyev A. Matematik analiz va topologiya elementlari. Toshkent: O'qituvchi, 2017. 284 p.
8. Sodiqov S. S. To'plamlar nazariyasi va topologiya. Toshkent: Tafakkur-Bo'stoni, 2020. 240 p.
9. Xolmatov T. X. Umumiy topologiya kursi. Toshkent: Universitet, 2019. 198 p.
10. Ismatullayev Sh. I., Xolmatov T. X. Topologik fazolar nazariyasi. Toshkent: Fan va texnologiyalar, 2021. 312 p.

METHODOLOGICAL INCONSISTENCIES OF THERMOELASTICITY EQUATIONS: SCIENTIFIC ANALYSIS AND PROOF

S.B. Jo‘raqulov
National University of Uzbekistan, Tashkent, Uzbekistan
https://doi.org/10.5281/zenodo.21238580

Abstract. *This research presents a profound methodological and scientific-critical appraisal of the fundamental logical and mathematical foundations of a scientific work published in the journal “EUREKA: Physics and Engineering”. As a result of a comprehensive analysis, seven (7) fundamental methodological errors that contradict the classical principles of continuum mechanics and the theory of thermoelasticity were identified and proven within the considered model: (A1) incorrect choice of primary state variables (unknowns) in continuum dynamics; (A2) misinterpretation of Saint-Venant’s kinematic compatibility equations as governing dynamic equations for the internal state of a body; (A3) unjustified reformulation of classical equilibrium equations without prior assurance of the integrability of the displacement field; (A4) strictly erroneous inclusion of the temperature effect into compatibility conditions that are purely geometric in nature; (A5) the physical and mathematical impossibility of specifying strain components as arbitrary functions on boundary surfaces (rendering the problem ill-posed); (A6) a linear contradiction in the ratio of unknowns to differential relations, leading to an overdetermined system; (A7) the artificial introduction of unjustified Poisson-type equations that do not stem from classical model principles. In this paper, each methodological deficiency is fully exposed through rigorous component-wise differentiation, precise analytical counterexamples, and reliance on classical fundamental literature. According to the findings of this appraisal, the mathematical structure of the analyzed model violates the most sacred principles of continuum mechanics; hence, the numerical results and scientific conclusions presented therein must be considered physically unreliable.*

Keywords: *thermoelasticity, continuum mechanics, strain tensor, Saint-Venant compatibility conditions, equilibrium equations, Beltrami-Michell relations, analytical counterexample, overdetermined system, mathematical inconsistency.*

Introduction

In classical linear elasticity and thermoelasticity theory, the small strain tensor ε_{ij} is defined as the symmetric gradient of the displacement vector u_i:

$$\varepsilon_{ij} = \frac{1}{2}(u_{i,j} + u_{j,i}) \qquad (1)$$

As can be seen from this relation, strains are derivative quantities determined via displacements. In solving problems, choosing strains directly as the primary unknowns is not inherently erroneous. However, if Saint-Venant’s compatibility equations are not fully and rigorously incorporated into a model where strains are taken as the primary unknowns, the

coordinates will not be integrable under the resulting field, and the physical integrity (continuity) of the body will be violated.

In this paper, we expose the seven primary differential flaws (A1–A7) through uniform component-wise rigorous analytical proofs and counterexamples.

Fundamental Proofs (A1–A7)

A1. The Necessary Condition for Choosing Strains as Primary Unknowns

Theorem 2.1. *If the strain components ε_{ij} are chosen as independent unknowns, then their satisfaction of the Saint-Venant compatibility equations is a necessary and sufficient condition for the existence of a unique, continuous displacement field.*

Proof. In the two-dimensional case, it follows from the definition of the strain tensor:

$$\varepsilon_{xx} = \frac{\partial u}{\partial x} \tag{2}$$

$$\varepsilon_{yy} = \frac{\partial v}{\partial y} \tag{3}$$

$$\varepsilon_{xy} = \frac{1}{2}\left(\frac{\partial u}{\partial y} + \frac{\partial v}{\partial x}\right) \tag{4}$$

Differentiating the first equation twice with respect to y, the second twice with respect to x, and adding them yields:

$$\frac{\partial^2 \varepsilon_{xx}}{\partial y^2} + \frac{\partial^2 \varepsilon_{yy}}{\partial x^2} = \frac{\partial^2 u}{\partial x \partial y^2} + \frac{\partial^2 u}{\partial y \partial x^2} \tag{5}$$

Simultaneously, differentiating the component ε_{xy} mixedly with respect to x and y gives:

$$2\frac{\partial^2 \varepsilon_{xy}}{\partial x \partial y} = \frac{\partial^2 u}{\partial x \partial y^2} + \frac{\partial^2 u}{\partial y \partial x^2} \tag{6}$$

Equating these differential results yields the classical Saint-Venant compatibility equation:

$$\frac{\partial^2 \varepsilon_{xx}}{\partial y^2} + \frac{\partial^2 \varepsilon_{yy}}{\partial x^2} = 2\frac{\partial^2 \varepsilon_{xy}}{\partial x \partial y} \tag{7}$$

Analytical Counterexample (Contradiction): Suppose that the model yields the following strain field:

$$\varepsilon_{xx} = y^2 \tag{8}$$

$$\varepsilon_{yy} = 0 \tag{9}$$

$$\varepsilon_{xy} = 0 \tag{10}$$

Substituting these functions into the compatibility condition (7):

$$\frac{\partial^2 (y^2)}{\partial y^2} + 0 = 2 \Rightarrow 2 \neq 0 \tag{11}$$

The compatibility equation is not satisfied. Hence, no continuous displacement field (u, v) exists for such a strain field. Consequently, strains that do not satisfy the compatibility equation cannot be physically realized.

2.2. A2. Misuse of the Saint-Venant Compatibility Equations

Theorem 2.2. *The Saint-Venant compatibility conditions are purely geometric relations and cannot express the equilibrium of forces or the laws of motion (the physical state) inside a body.*

Proof. In the two-dimensional case, the Saint-Venant equation (7) does not involve any body forces ($X,\ Y$), mass density (ρ), material constants (E,ν), or internal stresses (σ_{ij}). From a mathematical standpoint, this equation is merely the condition of equality for mixed partial derivatives.

Analytical Counterexample (Physical Contradiction): Suppose a body is in static equilibrium with no external body forces acting on it ($X=0,\ Y=0$). According to the model, we obtain the following strain field that satisfies only the compatibility equation:

$$\varepsilon_{xx} = x^3 \qquad (12)$$

$$\varepsilon_{yy} = y^3 \qquad (13)$$

$$\varepsilon_{xy} = 0 \qquad (14)$$

Substituting this into Saint-Venant equation:

$$\frac{\partial^2(x^3)}{\partial y^2} + \frac{\partial^2(y^3)}{\partial x^2} = 0 + 0 = 0 \qquad (15)$$

$$2\frac{\partial^2(0)}{\partial x \partial y} = 0 \Rightarrow 0 = 0 \qquad (16)$$

The compatibility equation is perfectly satisfied. Now, we determine the stresses corresponding to this field via Hooke's law ($\sigma_{ij} = 2\mu\varepsilon_{ij} + \lambda\varepsilon_{ij}\delta_{ij}$) for the case where $\lambda=0,\ \mu=1$:

$$\sigma_{xx} = 2x^3 \qquad (17)$$

$$\sigma_{yy} = 2y^3 \qquad (18)$$

$$\sigma_{xy} = 0 \qquad (19)$$

We verify these stresses by substituting them into the actual physical equilibrium equation:

$$\frac{\partial \sigma_{xx}}{\partial x} + \frac{\partial \sigma_{xy}}{\partial y} = \frac{\partial\left(2x^3\right)}{\partial x} + 0 \ = 6x^2 \neq 0 \qquad (20)$$

Although the strain field satisfies geometric compatibility, it violates Newton's equilibrium law ($6x^2 \neq 0$).

A3. Mathematical Ambiguity in Differentiating the Equilibrium Equations

Theorem 2.3. *When writing equilibrium equations directly in terms of strains without prior assurance of displacement compatibility, if no additional differential constraints are introduced, the solution space of the system expands infinitely, giving rise to spurious (non-physical) solutions.*

Proof and Contradiction: Substituting the Duhamel-Neumann relation into the classical equilibrium equation and differentiating it with respect to x (for the case $\lambda=0,\ \mu=1,\ T=0$) yields the following higher-order equation:

$$\frac{\partial^2 \varepsilon_{xx}}{\partial x^2} = -\frac{\partial^2 \varepsilon_{xy}}{\partial x \partial y} \quad (21)$$

Suppose that the following solutions are obtained from this higher-order equation:

$$\varepsilon_{xx} = x^2 y \quad (22)$$

$$\varepsilon_{xy} = -xy^2 \quad (23)$$

Verifying them:

$$\frac{\partial^2 (x^2 y)}{\partial x^2} = 2y \quad (24)$$

$$-\frac{\partial^2 (-xy^2)}{\partial x \partial y} = 2y \Rightarrow 2y = 2y \quad (25)$$

The equation is satisfied. Now, we substitute this into the actual (undifferentiated) original equilibrium equation:

$$2\frac{\partial (x^2 y)}{\partial x} + 2\frac{\partial (-xy^2)}{\partial y} = 4xy - 4xy = 0 \quad (26)$$

The original equation is also satisfied. However, we now check this against the Saint-Venant compatibility condition ($\varepsilon_{yy} = 0$):

$$\frac{\partial^2 (x^2 y)}{\partial y^2} + 0 = 0 \quad (27)$$

$$2\frac{\partial^2 (-xy^2)}{\partial x \partial y} = -4y \Rightarrow 0 \neq -4y \quad (28)$$

Because the order of the equation was unjustifiably increased, non-physical spurious solutions have infiltrated the system.

A4. Incorrect Inclusion of the Temperature Term into Geometric Invariants

Theorem 2.4. *Thermoelastic expansion is a surface or volumetric metric effect, and it cannot render the fundamental differential-geometric continuity condition of space (the right-hand side of the Saint-Venant equation) non-zero.*

Proof and Counterexample: In the authors' model, the relation is given as follows:

$$\frac{\partial^2 \varepsilon_{xx}}{\partial y^2} + \frac{\partial^2 \varepsilon_{yy}}{\partial x^2} - 2\frac{\partial^2 \varepsilon_{xy}}{\partial x \partial y} = \alpha \cdot T \quad (29)$$

$$T = const > 0 \quad (30)$$

$$\varepsilon_{xx} = \alpha T \quad (31)$$

$$\varepsilon_{yy} = \alpha T \quad (32)$$

$$\varepsilon_{xy} = 0 \quad (33)$$

$$\frac{\partial^2 (\alpha T)}{\partial y^2} + \frac{\partial^2 (\alpha T)}{\partial x^2} - 2\frac{\partial^2 (0)}{\partial x \partial y} = 0 + 0 - 0 = 0 \quad (34)$$

However, the right-hand side of the authors' equation was non-zero: $\alpha T \neq 0$. This leads to the contradiction $\alpha T \neq 0$. Temperature must enter exclusively through the constitutive equations (equations of state).

A5. Mathematical and Physical Impossibility of Strain Boundary Conditions

Theorem 2.5. *Specifying the strain components on a boundary surface as independent functions destroys the uniqueness and existence conditions of the differential operators at the boundary.*

Proof and Counterexample: Let us say that on the boundary line $x = 0$, the authors impose the following conditions:

$$\varepsilon_{xx} = f(y) \quad (35)$$

$$\varepsilon_{xy} = g(y) \quad (36)$$

$$\varepsilon_{xx}|_{x=0} = \left.\frac{\partial u}{\partial x}\right|_{x=0} = f(y) \quad (37)$$

$$\varepsilon_{xy}|_{x=0} = \left.\frac{1}{2}\left(\frac{\partial u}{\partial y} + \frac{\partial v}{\partial x}\right)\right|_{x=0} = g(y) \quad (38)$$

If we wish to prescribe a fixed clamping condition $u|_{x=0} = 0$ at the boundary, then $\left.\frac{\partial u}{\partial y}\right|_{x=0} = 0$. This implies $\left.\frac{\partial v}{\partial x}\right|_{x=0} = 2g(y)$. However, if we simultaneously prescribe $v|_{x=0} = 0$ at the boundary, then it must hold that:

$$\left.\frac{\partial v}{\partial y}\right|_{x=0} = 0 \Rightarrow \varepsilon_{yy}|_{x=0} = 0 \quad (39)$$

must be satisfied. If the authors designate ε_{yy} at the boundary as some other arbitrary function, then at a single point on the boundary, $\frac{\partial v}{\partial y}$ would simultaneously equal zero and a non-zero value, resulting in a geometric rupture.

A6. Overdetermination of the System under Plane Strain

Theorem 2.6. *If more than 3 independent differential relations are introduced into a plane system with 3 unknowns, the system becomes overdetermined and possesses no solution other than the trivial one.*

Proof: Unknowns: ε_{xx}, ε_{yy}, ε_{xy}. From the equations in the authors' system, it follows that $\varepsilon_{xy} = 0$. Substituting this into the compatibility condition:

$$\frac{\partial^2 \varepsilon_{xx}}{\partial y^2} + \frac{\partial^2 \varepsilon_{yy}}{\partial x^2} = 0 \quad (40)$$

Now, linking to this equations $\Delta\varepsilon_{xx} = C\,\mathrm{T}$ and $\Delta\varepsilon_{yy} = C\,\mathrm{T}$ proposed by the authors $\left(\Delta = \frac{\partial^2}{\partial x^2} + \frac{\partial^2}{\partial y^2}\right)$:

$$\frac{\partial^2 \varepsilon_{xx}}{\partial x^2} - \frac{\partial^2 \varepsilon_{yy}}{\partial y^2} = CT \quad (41)$$

This differential chain loses mathematical compatibility for an arbitrary function $T(x, y)$, since the mixed partial derivatives obtained from the left side restrict the arbitrariness of the temperature field on the right side. The system is unsolvable.

A7. Physical Unjustifiability of the Artificial Poisson Equation

Theorem 2.7. *The isolated equation* $\Delta\varepsilon_{ij} = CT$ *contradicts the laws of conservation of energy and material continuum in elasticity theory.* ***Proof:*** In the Beltrami-Michell equation of actual linear thermoelasticity, the second-order differentiated derivative of temperature $\left(\frac{\partial^2 T}{\partial x_i \partial x_j}\right)$ appears. In contrast, the authors use the temperature itself (T). If the temperature varies linearly along a coordinate inside the body, i.e.:

$$T = kx \quad (42)$$

then in actual physics, $\frac{\partial^2 T}{\partial x^2} = 0$, and no additional thermal stress is generated. However, in the authors' model:

$$\Delta\varepsilon_{xx} = Ckx \neq 0 \quad (43)$$

That is, even in a linear temperature field, high-order strain waves are artificially generated inside the body. This is completely contrary to the laws of nature.

Conclusion

The presented necessity proof of the Saint-Venant compatibility condition and the provided analytical counterexamples fully expose the fundamental failure of the analyzed model. Any strain-based model where the Saint-Venant compatibility equations are not correctly and rigorously integrated, and whose physical terms are artificially distorted, violates the laws of mechanics. Computational or numerical results (matrices) obtained through such models cannot represent the motion of any real body. It is recommended to rewrite the work conforming to the classical Navier-Lamé or Beltrami-Michell formulations.

REFERENCES

1. Saint-Venant, B. (1864). Mémoire sur la torsion des prismes. Mémoires des Savants étrangers, 14, 233–560.
2. Beltrami, E. (1886). Sull'interpretazione meccanica delle formole di Maxwell. Mem. Accad. Sci. Bologna, 7, 1–38.
3. Duhamel, J.M.C. (1837). Second mémoire sur les phénomènes thermo-mécaniques. J. de l'Ecole Polytechnique, 15, 1–57.
4. Neumann, F. (1841). Vorlesungen über die Theorie der Elasticität. Leipzig: Teubner.
5. Nowacki, W. (1986). Thermoelasticity (2nd ed.). Pergamon Press, Oxford.

OPTIMAL CONDITIONS FOR THE EXTRACTION OF POLYPHENOLIC COMPOUNDS FROM THE PEEL OF PUNICA GRANATUM FRUITS

K.V. Raimova[1], R.N. Rakhimov[2], M.Zh. Oripova[3], Z.N. Kuzieva[4], A.M. Ishimov[5], N.G. Abdulladzhanova[6]

Senior researcher at the Institute of Bioorganic Chemistry named after A. Sadykov of the Academy of Sciences of the Republic of Uzbekistan, Tashkent, Uzbekistan[1]

Senior researcher at the Institute of Bioorganic Chemistry named after A. Sadykov, Academy of Sciences of the Republic of Uzbekistan, Tashkent, Uzbekistan[2]

Senior researcher at the Institute of Bioorganic Chemistry named after A. Sadykov, Academy of Sciences of the Republic of Uzbekistan, Tashkent, Uzbekistan[3]

Junior researcher at the Institute of Bioorganic Chemistry named after A. Sadykov of the Academy of Sciences of the Republic of Uzbekistan, Tashkent, Uzbekistan[4]

Intern at the Institute of Bioorganic Chemistry named after A. Sadykov of the Academy of Sciences of the Republic of Uzbekistan, Tashkent, Uzbekistan[5]

Doctor of Chemical Sciences, Leading Researcher, Experimental and Technological Laboratory, A. Sadykov Institute of Bioorganic Chemistry, Academy of Sciences of the Republic of Uzbekistan, Tashkent, Uzbekistan[6]

https://doi.org/10.5281/zenodo.20694567

Abstract. *Optimal conditions for the extraction of polyphenolic compounds from the peel of Punica granatum L. fruits grown in the Tashkent region of the Republic of Uzbekistan were selected. The peel of the Uzbek pomegranate cultivar "Kai-anor," popular in Central Asia, was dried in late October – early November 2025 to study the total polyphenol content. A comprehensive study was conducted to examine the influence of various factors on the total polyphenol yield, including extractant composition, aqueous acetone concentration, extraction rate, raw material-to-extractant ratio, temperature, extract concentration conditions, treatment of the aqueous residue with organic solvents, and precipitation and drying conditions for the obtained polyphenolic compounds. To isolate biologically active substances, 1 kg of dried and crushed peel was pre-treated with chloroform and then extracted three times with aqueous acetone at concentrations ranging from 25 to 70%. After removing the acetone, the aqueous residue was treated with ethyl acetate. The ethyl acetate fraction was concentrated and precipitated with chloroform, yielding the total polyphenolic compounds. Optimal extraction conditions were found to yield 3.9% of the total polyphenolic compounds based on the air-dried weight of the raw material. Column chromatography on bald powder was used for preliminary separation of the polyphenol complex. The composition of the isolated fractions was studied using modern physicochemical methods, including high-performance liquid chromatography coupled with mass spectrometry (HPLC-MS). As a result of the research, citric acid ($C_7H_{12}O_6$), gallic acid ($C_7H_6O_5$), gallacatechin ($C_{15}H_{14}O_7$), di-galloyl-hexahydroxydiphenyl-D-glucose ($C_{27}H_{22}O_{18}$), garnetin A ($C_{34}H_{24}O_{22}$), procyanidin B1 ($C_{30}H_{26}O_{12}$), punigluconin ($C_{34}H_{26}O_{23}$), garnetin A (form B) ($C_{34}H_{24}O_{23}$), myricetin-3-O-xyloside ($C_{20}H_{18}O_{12}$), garnetin B ($C_{41}H_{28}O_{27}$), chebulagic acid ($C_{41}H_{30}O_{27}$), isorhamnetin-3-galactoside ($C_{22}H_{22}O_{12}$), kaemferol-3-O-rutinoside were identified in the peel of Punica L. fruits. ($C_{27}H_{30}O_{15}$), ellagic acid-rhamnoside, rutin ($C_{26}H_{26}O_{17}$), and*

myricetin ($C_{15}H_{10}O_8$). The obtained results demonstrate the rich composition of polyphenolic compounds in pomegranate peel and its potential for use as a source of natural biologically active substances.

Keywords: *punica granatum L., extract, high-performance liquid chromatography mass spectrometry (HPLC-MS).*

INTRODUCTION

Pomegranates are processed for juice, with the peel and seeds serving as secondary raw materials. The seeds are dried and transferred to the oil and fat industry to extract valuable pharmacopoeial oil. Although pomegranate peel contains natural compounds such as polyphenols, flavonoids, carotenoids, anthocyanins, catechins, tannins, etc., it is not processed; furthermore, peel removal and disposal is problematic [1-2]. The development of resource-saving, waste-free technologies may find application in the food, light industry, and pharmaceutical industries. An important property of natural dyes is their absolute safety. The collection includes 69 varieties of pomegranate. Bitter Kazakh, Tuyatish, Shakhrisabz, May, Belozerny, Red Pomegranate, Ulfi, and other varieties are grown in Uzbekistan. Since the peel of these varieties is red, a red dye is produced [3-4]. Punica granatum L. is a famous fruit tree. Pomegranate is grown in gardens and vegetable patches throughout Central Asia. It also grows wild in mountain river valleys. [5-6]. The fruits, flowers, and bark of the pomegranate have long been used in folk medicine as a tonic and astringent [7]. They are included in popular herbal teas [8] and are described in many historical medical treatises [9, 10]. The chemical composition of the plant: the juice and pulp of the pomegranate fruit contain up to 20% sugars, organic acids, and up to 6% citric and malic acids [11]. Tricosane, heptacosanyl n-hexanoate, oleic acid, β-sitosterol laurate, and β-sitosterol myristate have been identified in pomegranate flowers [12; 16]. In addition, pomegranate, ellagic acid, O-methyl-ellagic acid, ethyl brevicarboxylate, ursolic and butyric acids and daucasterol [17], flavone tricetin 4 '-O-β -glucopyranoside, flavones tricetin, luteolin, pomegranate B [18; 9] were identified. The leaves and bark of the fruits contain ursolic acid; alkaloids - pseudopeltierine, isopeltierine; triterpenoids; steroids; resins and a large amount of tannins (up to 25%). All parts of the plant are rich in polysaccharides [20]. Pomegranate peel contains a significant amount of phenolic compounds, such as hydrolyzable tannins (punicalin, punicalagin, ellagic acid and gallic acid), flavonoids (anthocyanins and catechins) and nutrients [21,22]. The seeds contain up to 20% fatty oil, consisting mainly (40%) of linoleic, palmitic (16%), oleic acids, and also contain fatty acids, triglycerides, steroids, lignins, phenolic acids, phytosterols such as β-sitosterol, campesterol, stigmasterol, and α-, β-, γ-, δ-tocopherols, and proteins [23]. Pomegranate peel makes up about 50% of the total fruit content and, due to its polysaccharides and phenolic substances, has antioxidant, anti-inflammatory, antimicrobial, antityrosinase, anti-osteoporotic, anti-hyperlipidemic, and anti-cancer properties [24]. Pomegranate seeds have antioxidant, cardioprotective, anti-osteoporotic, anti-diabetic, anti-inflammatory, and anti-cancer properties [25]. In this regard, the aim of our work is to determine the optimal conditions for the extraction of polyphenolic compounds from the peel of the fruits of the Punica granatum L plant using physicochemical research methods.

EXPERIMENTAL SECTION

Isolation of Total Polyphenols.[26,27] The subject of the study was dried peels of the Uzbek pomegranate variety "Kai-anor" (Punica granatum L), prepared in late October - early November 2025. Extraction of the raw material with organic solvents was used to extract the total

polyphenols. For this purpose, several factors influencing the yield of total polyphenols were studied: the degree of raw material grinding, the composition of the extractant, the extraction modulus, the extraction frequency, the raw material-extractant ratio, the extraction temperature, the thickening conditions, the treatment of the aqueous residue with organic solvents, the conditions for the precipitation of the total polyphenols and their drying. Based on the obtained results, an optimal method for the isolation of total polyphenols was developed. It consists of the following: air-dried, crushed (to a size of 5-7 mm) peel of P. granatum L (1 kg) is pre-extracted with chloroform to remove lipophilic substances. For this purpose, the raw material was placed in a flask equipped with a reflux condenser and extracted with chloroform in a water bath in ratios from 1:2 to 1:10 (raw material:chloroform), at a temperature of 20 to 60 °C for 2 h, from a single to fivefold extraction of the raw material. After treating the raw material with chloroform, extraction was continued with aqueous acetone at concentrations from 25 to 70%. Extraction was repeated from one to three times. Then, the obtained aqueous-ethyl extracts were evaporated under vacuum on a rotary evaporator until the aqueous portion remained. The purified aqueous extract was treated with ethyl acetate in a separatory funnel, in ratios from 1:1 to 1:6 (aqueous residue: ethyl acetate). The ethyl acetate fractions were concentrated and precipitated with chloroform in ratios from 1:1 to 1:5 (concentrate:precipitant), resulting in the formation of a flocculent precipitate. The total polyphenols were preliminarily separated on gallium powder. 5 g of the total polyphenols, soluble in ethyl acetate, were fractionated on gallium powder according to the method [28]. The column was eluted with diethyl ether, distilled water, pure acetone and 60% acetone. The fraction washed with ether contained 1 substance, which, based on the chromatographic behavior in the solvent systems n.butanol-acetic acid-water (40:12:28, Rf 0.72) and 15% aqueous acetic acid solution (Rf 0.55), was identified as gallic acid. The fraction washed with water was treated with ethyl acetate five times. After drying the ethyl acetate extract with anhydrous Na2SO4, the mixture was concentrated in vacuo, and the concentrate was precipitated with chloroform. The precipitate was filtered and dried in a vacuum oven. 1.2 g of the total product was obtained. Paper chromatography in a n-butanol-acetic acid-water (40:12:28) system revealed the presence of two compounds with Rf 0.68 and Rf 0.60. The product was dissolved in ethanol and chromatographed on a column.

The structures of the isolated compounds were established using physicochemical methods—high-performance liquid chromatography and mass spectrometry. Individual phenolic compounds were identified by high-performance liquid chromatography–mass spectrometry (HPLC-MS/MS).Chromatography conditions: chromatograph—HPLC Ultimate 3000, Thermo Fisher Scientific (USA), equipped with an automatic sampler; Hypersil GOLDaQ column 100 mm × 2.1 mm, particle size 1.9 μm; mobile phase—bidistilled water acidified with 0.1% formic acid (A) and acetonitrile (B), flow rate 0.1 ml/min, 15:85 isocratic mode. Instrument name and chromatography–mass spectrometry conditions: mass spectrometry with electron impact ionization (HESI-II); Spray chamber voltage – 4000 V; evaporator temperature – 25 °C. Solution concentration gradient in minutes: 0–3 min – 2%, 3–35 min – 55%, 35–38 min – 2%. Solutions were degassed using an Agilent Technologies 1260 μ-degasser.Mass spectrometric analysis of isolated polyphenols. Samples were loaded onto the column using an Agilent Technologies Micro WPS instrument (1 μL at a time) from a polyphenol solution with a concentration of 0.1 mg/mL. Mass spectrometric studies of the isolated polyphenols were performed on an Agilent Technologies Q-TOF LC-MS 6520B series instrument under the following conditions: ionization source – ESI, drying gas flow – 5 μ/min, drying gas temperature – 300 °C, voltage on: kimmer

cone – 20 V, fragmentor 125 V, mass range: in MS mode 100 – 2000 m/z, and in Auto MS/MS50 mode – 2000 m/z, collision energy – 35, 50 eV. Ionization method: negative. was introduced into the mass spectrometer using an Agilent Technologies 1200 series chromatograph. Mobile phase: A – 0.1% formic acid solution, B – acetonitrile + 0.1% formic acid. Elution was performed on an Agilent Technologies 1260 Cap Pump at a flow rate of 15 µL/min. The solution concentration gradient was as follows: 0–3 min – 2%, 3–35 min – 55%, 35–38 min – 2%. Solutions were degassed on an Agilent Technologies 1260 µ-degasser.

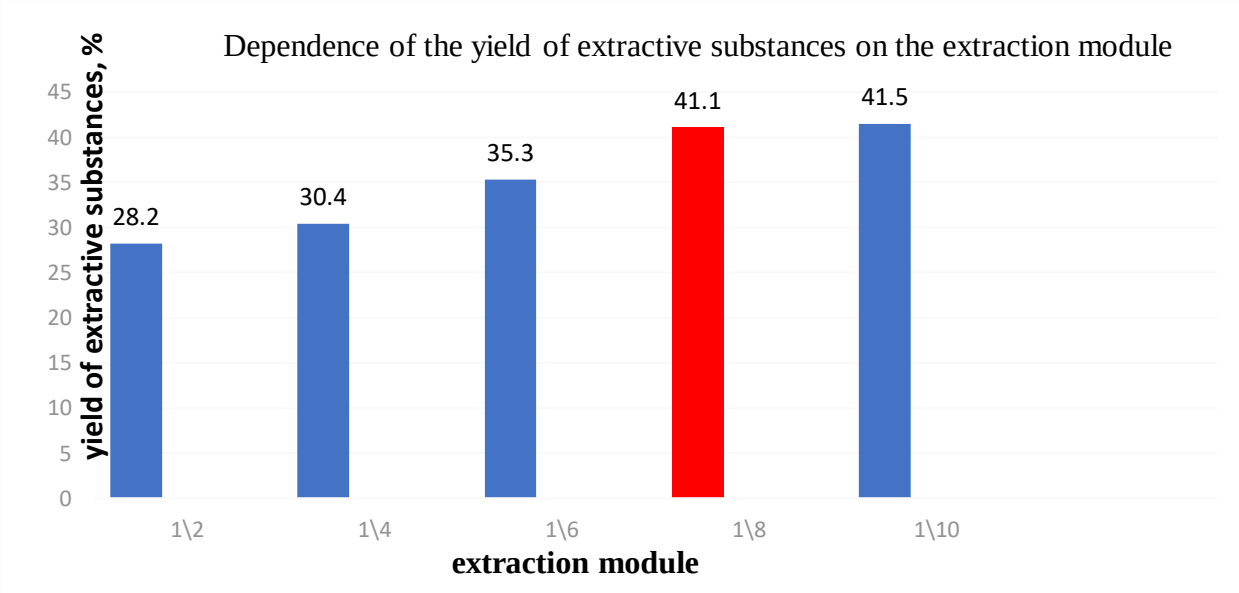
The following public databases were used for identification: Chemical Entities of Biological Interest (ChEBI, https://www.ebi.ac.uk/chebi/), Chemical Compounds Deep Data Source (https://www.molinstincts.com/), ChemSpider (www.chemspider.com), and Phenol_Explorer (www.phenol-explorer.eu).

RESULTS DISCUSSION

Results Discussion. The process of isolating polyphenols from plant materials involves several stages: raw material extraction, processing the extracted material with organic solvents, evaporation, precipitation of total polyphenols, purification, etc. Increased efficiency in raw material use is achieved primarily at the first stage – extraction. The yield of total polyphenols was studied as a function of the following parameters: extractant composition, extraction modulus, extraction rate, raw material-to-extractant ratio, extraction temperature, thickening conditions, processing the aqueous residue with organic solvents, and the conditions for precipitation of total polyphenols and their drying [11, 12]. To determine the optimal extraction modulus, raw material-to-extractant ratios of 1:2, 1:4, 1:6, 1:8, and 1:10 were used. Extraction efficiency was assessed based on the yield of extractive substances, calculated as a percentage.

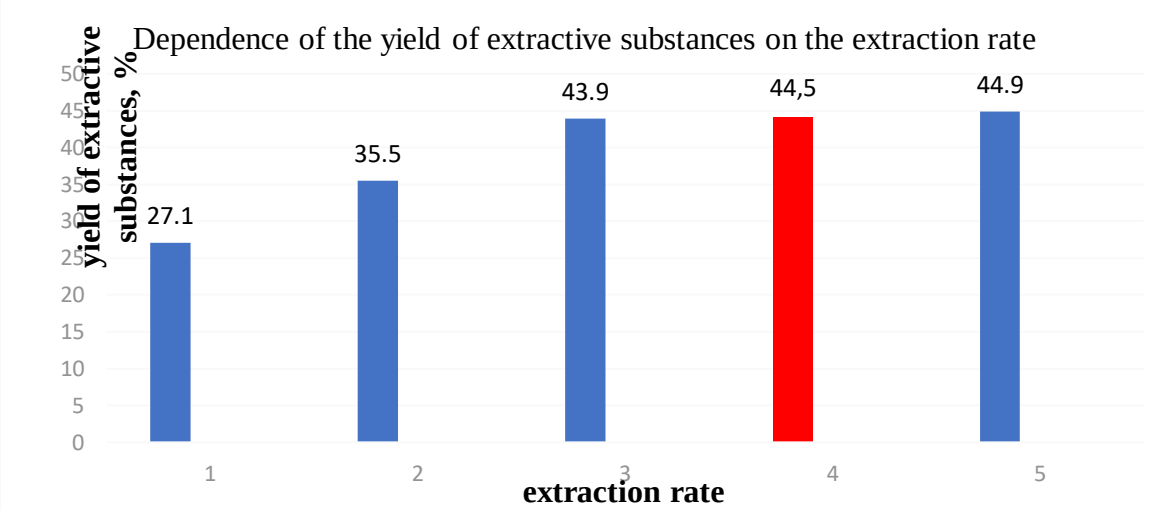
The results are shown in Figure 1.

Fig. 1



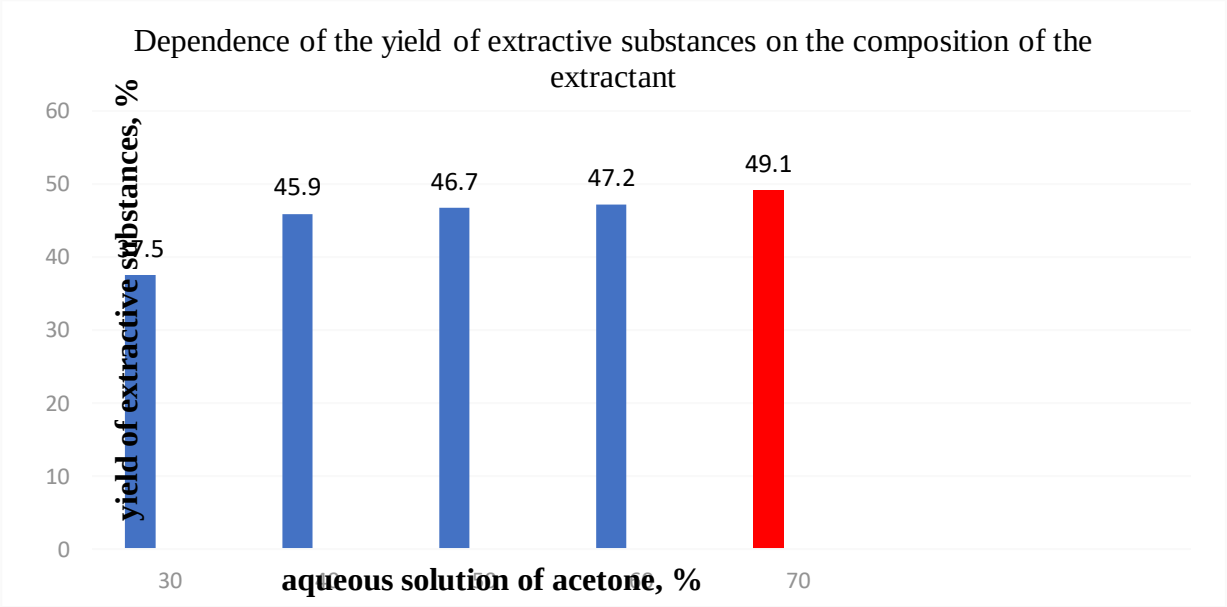
The data presented show that the optimal raw material:extractant ratio is 1:8. The average yield of extractive substances was 41.1%. With a lower extraction module (1:2; 1:4; 1:6), the yield of extractive substances is incomplete, and the use of a ratio of 1:10 leads to an increase in the extraction volume, which in turn leads to an overconsumption of organic solvents. We similarly conducted a study of the optimal extraction multiplicity. In this case, 1-, 2-, 3-, 4-, 5-fold extraction methods were used. The results obtained are shown in Figure 2.

Fig. 2



The extraction efficiency was assessed based on the yield of extractive substances. As can be seen from the data presented, a 4-fold extraction was the most optimal. The average yield of extractive substances was 44.5%. With low extraction rates (1-, 2-fold), the yield of extractive substances was incomplete, and with increasing extraction rates (4-, 5-fold), the yield of extractive substances changed insignificantly. However, the extraction process is time-consuming and increases the volume of the extract, which also further leads to an increase in the consumption of organic solvents. To determine the optimal extractant composition, we used an aqueous acetone solution of varying concentrations. 30%, 40%, 50%, 60%, and 70% aqueous acetone solutions were used as the extractant. The results are shown in Figure 3.

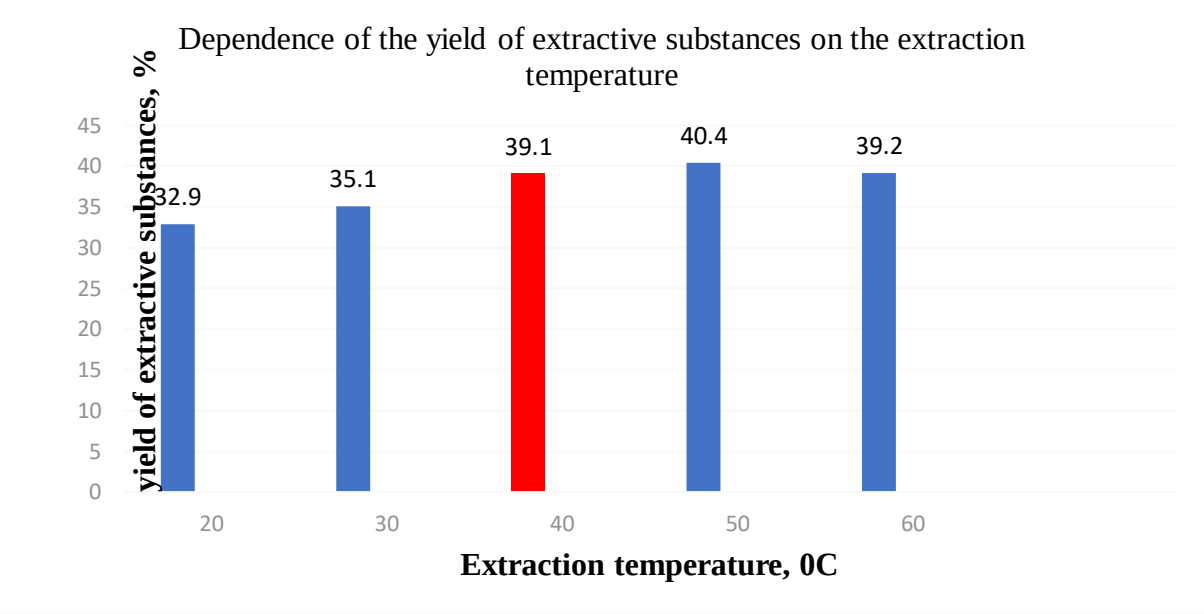
Fig. 3



As can be seen from the data presented, 70% aqueous acetone is the most optimal extractant. The average extractive yield was 49.1%. Using low-concentration aqueous acetone results in incomplete extraction of extractives from the raw material, while high acetone concentrations also do not increase the extractive yield.

Similarly, we searched for the optimal extraction temperature. Extraction was carried out at the following temperatures: 200°C, 300°C, 400°C, 500°C, and 600°C. The obtained data are shown in Figure 4.

Fig. 4

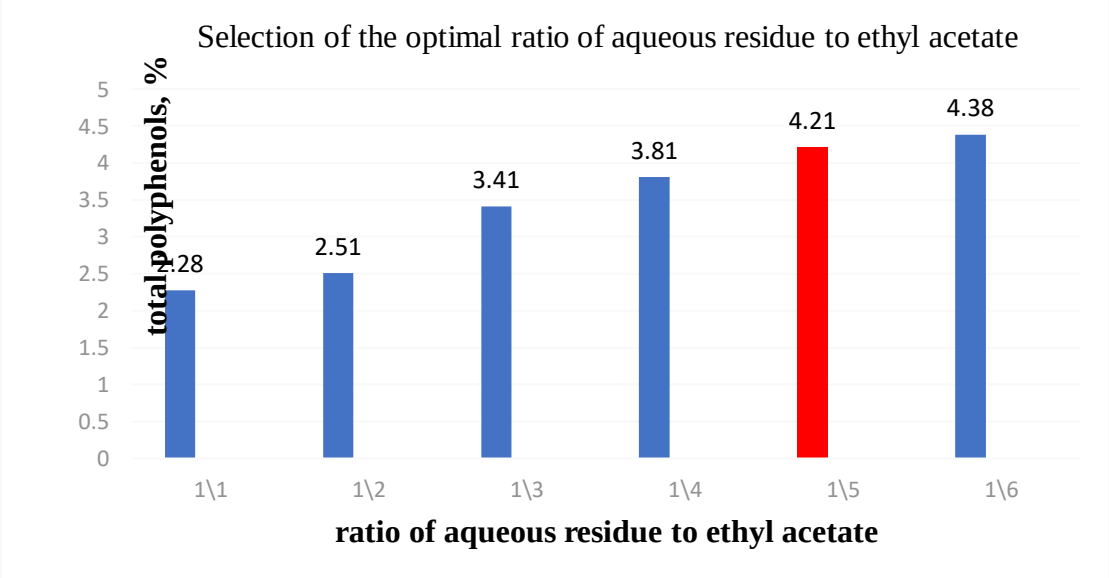


From the data presented it is clear that the most optimal extraction temperature is 40 ^{0}C and under this regime the average value of extractives was 39.1%. At lower temperatures, the yield of extractive substances is incomplete, and when the extraction temperature increases to 600C, polyphenolic substances are hydrolyzed, which is confirmed by paper chromatography data.

In a similar way, the dependence of the yield of extractives on the extraction time was studied, which varied from 1 to 3 hours. It was found that the most optimal is a 2-hour extraction.

The resulting extracts were concentrated under vacuum to an aqueous residue. The extraction of polyphenols from the aqueous residue was carried out with ethyl acetate in a ratio of 1:1; 1:2; 1:3; 1:4; 1:5; 1:6. Ethyl acetate extracts were combined, dried over anhydrous Na2SO4 and concentrated. The results obtained are shown in the figure. 5.

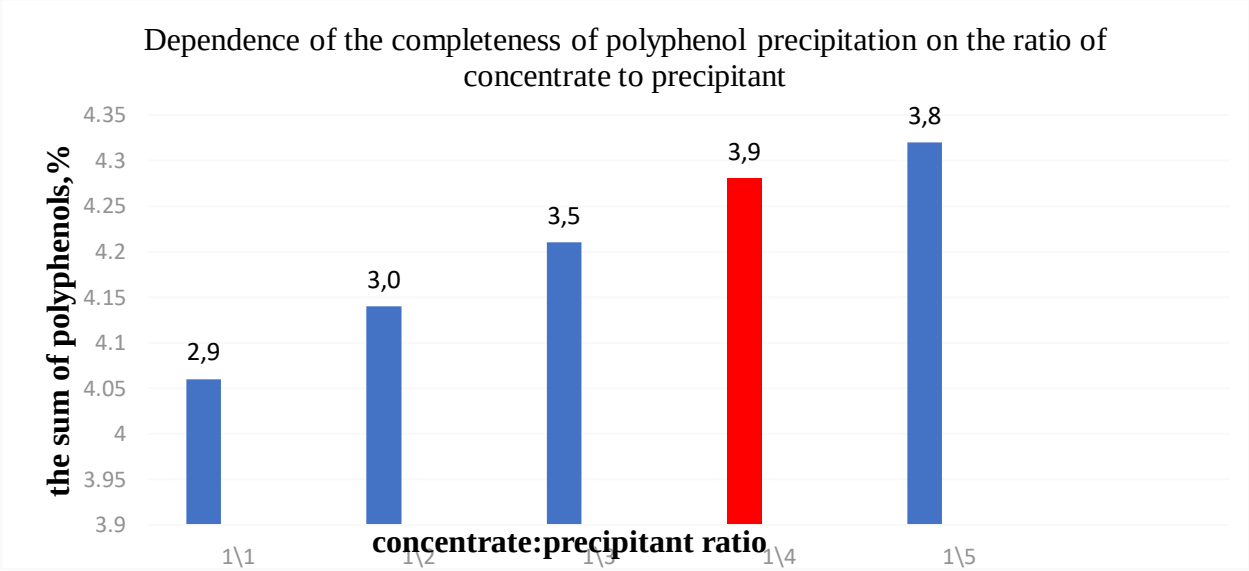
Fig.5



The data show that the optimal ratio of aqueous residue to ethyl acetate is 1:4. At lower aqueous residue to solvent ratios, polyphenols are incompletely extracted from the aqueous residue. The polyphenol yield increases slightly at a ratio of 1:6, but this also increases solvent consumption.

Chloroform was used to precipitate polyphenols from the ethyl acetate concentrate. The concentrate to precipitant ratios were 1:1; 1:2; 1:3; 1:4; 1:5. The obtained data are shown in Figure 6.

Fig.6



The resulting polyphenolic mixture from the ethyl acetate fraction of Punica L. fruit rind is an amorphous, light-yellow powder with an astringent taste. With ferric chloride, the mixture yields a blue color (developed with an iodine chamber), and with a 1% vanillin solution in concentrated hydrochloric acid, it yields a bright red color (developed with aqueous ammonia).

Elution was performed with diethyl ether, water, acetone, and 60% acetone. The phenolic compounds of the ether fraction are phenoloxyacids, the phenolic compounds of the aqueous fraction are flavonols, and the phenolic compounds of the 60% aqueous acetone fraction are tannins. In the fraction washed with ether, gallic acid (R_f 0.72 and 0.55), citric acid ($C_7H_{12}O_6$), and gallacatechin ($C_{15}H_{14}O_7$) were identified by paper chromatography.

The water-soluble fraction was rechromatographed on polyamide using a mixture of chloroform and methanol in various ratios as an eluent, yielding individual compounds: myricetin-3-O-xyloside ($C_{20}H_{18}O_{12}$), isorhamnetin-3-galactoside ($C_{22}H_{22}O_{12}$), kaemferol-3-O-rutinoside ($C_{27}H_{30}O_{15}$), ellagic acid-rhamnoside, rutin ($C_{26}H_{26}O_{17}$), and myricetin ($C_{15}H_{10}O_8$).

The fraction soluble in aqueous acetone was chromatographed on silica gel columns using a solvent system of diethyl ether - ethyl acetate (1:1) and pure ethyl acetate. As a result, several compounds were isolated and identified by their physicochemical properties using modern physicochemical methods, including high-performance liquid chromatography coupled with mass spectrometry (HPLC-MS). As a result of the studies, di-galloyl-hexahydroxy-diphenyl-D-glucose ($C_{27}H_{22}O_{18}$), garnetin A ($C_{34}H_{24}O_{22}$), procyanidin B1 ($C_{30}H_{26}O_{12}$), punigluconin ($C_{34}H_{26}O_{23}$), garnetin A (form B) ($C_{34}H_{24}O_{23}$), garnetin B ($C_{41}H_{28}O_{27}$), and chebulagic acid ($C_{41}H_{30}O_{27}$) were identified in the Punica L. fruit peel. The obtained results indicate a rich composition of polyphenolic compounds in the pomegranate peel and the potential for its use as a source of natural biologically active substances.

CONCLUSIONS

Optimal conditions for the extraction and isolation of polyphenolic compounds from the peel of the Kai Anor pomegranate (Punica granatum L.) variety were determined. High-

performance liquid chromatography coupled with mass spectrometry (HPLC-MS) was used to identify the main polyphenolic components of the studied raw material.

REFERENCES

1. Usmonzhonova Kh., Dodaev K., Atkhamova S. Extraction of coloring matter from basil powder, study of micro- and macroelement, carbohydrate and vitamin composition of the extract // Universum: Technical Sciences. Moscow. No. 11 (77), 2020.
2. Kholdorov B., Dodaev K., Atkhamova S. Investigation of a method for extracting pectin from grape marc // Universum: Technical Sciences. Moscow. №2, 2018. -P. 19-22.
3. Kholdorov B.B., Dodaev K.O. Study of agricultural waste as a pectin-containing raw material // VII International scientific-practical conference "Innovative technologies in science and education". Penza 2018. -P. 40-42.
4. Eshmatov F., Maksumova D., Dodaev K., Ibragimov A. Pomegranate juice, defects, improving of producing tech nology Journal homepage: www.summusjournals.uz International scientific and technical journal Innovation tech nical and technology. Vol.1, №.1. 2020. ISSN: 2181-1067. -P.18-20.
5. Aslanova M.S., Nabiev A.A. Physicochemical parameters and amino acid composition of fruits of new pomegranate varieties // Bulletin of the Russian agricultural science 2017, 2. Pp. 34-36.
6. Babaniyazov O.K., Ubaidullaev K.A. Obtaining oils from pomegranate seeds (Punica Granatum L.), studying the physicochemical properties and determining the fatty acid composition - // Science Time 2019, 4(64), Pp. 51-56.
7. Gruzdev V.F. Russian handwritten medical manuals. Leningrad, 1964.
8. Toren M.D. Use of medicinal plants in Russian folk medicine. // 7th International Congress of Anthropologists and Ethnographic Sciences. Moscow, 1964. Pp. 56.
9. Atlas of Tibetan medicine // trans. T.A. Aseeva, N.D. Bolhosoeva, T.G. Bukhasheeva, D.B. Dashieva M., 1994. Page 485.
10. Pogosyan R.A., Nesterova O.V., Dobrokhotov D.A. // Health and education in the 21st century. 2016. No. 5. Vol. 18. Page 131.
11. Aslanova M.S., Nabiev A.A. Physicochemical parameters and amino acid composition of fruits of new pomegranate varieties // Bulletin of the Russian Agricultural Science 2017, 2. Pp. 34-36.
12. Bagri P., Ali M., Sultana S., Aeri V. New sterol esters from the flowers of Punica granatum Linn. - //J. Asian. Nat. Prod. Res. 2009, Aug., 11(8), 710-715.
13. Banerjee N., Kim H., Talcott S., Mertens-Talcott S. Pomegranate polyphenolics suppressed azoxymethane-induced colorectal aberrant crypt foci and inflammation: possible role of miR-126/VCAM-1 and miR-126/PI3K/AKT/mTOR. //Carcinogenesis. 2013, Dec., 34(12), 2814-2822. doi: 10.1093/carcin/bgt295.
14. Baradaran Rahimi V., Ghadiri M., Ramezani M., Askari V.R. Antiinflammatory and anti-cancer activities of pomegranate and its constituent, ellagic acid: Evidence from cellular, animal, and clinical studies. //Phytother. Res. 2020, Apr., 34(4), 685-720. doi: 10.1002/ptr.6565.
15. Bassiri-Jahromi S. Punica granatum (Pomegranate) activity in health promotion and cancer prevention. //Oncol. Rev. 2018, Jan 30, 12(1), 345. doi: 10.4081/oncol.2018.345.

16. Bekir J., Mars M., Vicendo P., Fterrich A., Bouajila J. Chemical composition and antioxidant, anti-inflammatory, and antiproliferation activities of pomegranate (Punica granatum) flowers. //J. Med. Food. 2013, Jun., 16(6), 544-550. doi: 10.1089/jmf.2012.0275.
17. Wang R., Wei Wang, Wang L., Liu R., Yi Ding, Du L. Constituents of the flowers of Punica granatum - //Fitoterapia 2006, Dec., 77(7-8), 534-537.
18. Wu S., Tian L. A new flavone glucoside together with known ellagitannins and flavones with anti-diabetic and anti-obesity activities from the flowers of pomegranate (Punica granatum). //Nat. Prod. Res. 2019, Jan., 33(2), 252-257. doi: 10.1080/14786419.2018.1446009.
19. Xie X., Hu L., Liu L., Wang J., Liu Y., Ma L., Sun G., Li C., Aisa H.A., Meng S. Punicalagin promotes autophagic degradation of human papillomavirus E6 and E7 proteins in cervical cancer through the ROS- JNK-BCL2 pathway. //Transl. Oncol. 2022, Mar 5, 19, 101388. doi: 10.1016/j.tranon.2022.101388.
20. Shakhmatov E.G., Makarova E.N., Belyy V.A. Structural studies of biologically active pectin-containing polysaccharides of pomegranate Punica granatum. //Int. J. Biol. Macromol. 2019, Feb 1, 122, 29-36. doi: 10.1016/j.ijbiomac.2018.10.146.
21. Ruan J.H., Li J., Adili G., Sun G.Y., Abuduaini M., Abdulla R., Maiwulanjiang M., Aisa H.A. Phenolic Compounds and Bioactivities from Pomegranate (Punica granatum L.) Peels. //J. Agric. Food Chem. 2022, Mar 21. doi: 10.1021/acs.jafc.1c08341.
22. Xie Z., Li X., Tang R., Wang G., Lu Y., Li X., Cheng K., Li L., He Q. Reactions of polyphenols in pomegranate peel with nitrite under simulated stomach conditions. //Food Sci. Nutr. 2019, Aug 21, 7(9), 3103- 3109. doi: 10.1002/fsn3.1173.
23. 23.Adams L.S., Seeram N.P., Aggarwal B.B., Takada Y., Sand D., Heber D. Pomegranate juice, total pomegranate ellagitannins, and punicalagin suppress inflammatory cell signaling in colon cancer cells - //J. Agric. Food Chem. 2006, Feb 8, 54(3), 980-985.
24. Esselun C., Theyssen E., Eckert G.P. Effects of Urolithin A on Mitochondrial Parameters in a Cellular Model of Early Alzheimer Disease. //Int. J. Mol. Sci. 2021, Aug 3, 22(15), 8333. doi: 10.3390/ijms22158333.
25. Fourati M., Smaoui S., Hlima H.B., Elhadef K., Braïek O.B., Ennouri K., Mtibaa A.C., Mellouli L. Bioactive Compounds and Pharmacological Potential of Pomegranate (Punica granatum) Seeds - A Review. //Plant Foods Hum. Nutr. 2020, Dec., 75(4), 477-486. doi: 10.1007/s11130-020-00863-7.
26. Raimova K.V., Alimov H.K., Abdulladzhanova N.G.//Study of the polyphenolic composition of Acer semenovii maple leaves. Chemistry of plant raw materials. 2025. No. 1. P. 118–126. https://doi.org/10.14258/jcprm.20250115047
27. Raimova K.V., Abdulladzhanova N.G., Matchanov A.D.// Chemical structure of the polyphenolic composition of the leaves of the Pontic hawthorn crataegus pontica. Chemistry of plant raw materials. 2023. No. 4. P. 147–154.
28. DOI: 10.14258/jcprm.20230412529.
29. Abdullazhanova N.G, Mavlyanov S.M, Abdullaev S.V. Phenolic compounds from Oenothera gigas// Chemistry of Natural Compounds, 2000.V.1 (36), p.36-37.
30. Mavlyanov S.M., Islambekov Sh.Yu.,Karimdzhanov A.K, Ismailov A.I.. //Polyphenols of some varieties of pomegranate growing in Uzbekistan//Chemistry of Natural Compounds. 1997, V1, p.124-127

EXTRACTION AND CHARACTERIZATION OF POMEGRANATE (PUNICA GRANATUM L.) SEED OIL

Z.N. Kuziyeva[1], M.J. Oripova[1], K.A. Raimova[1], S.B. Karabayeva[1], F.Z. Orifov[2], N.G. Abdullajanova[1]
Institute of Bioorganic Chemistry, Uzbekistan Academy of Sciences, Mirzo Ulughbek St. 83, 100125 Tashkent, Uzbekistan[1]
Center of pharmacy-innovation[2]
https://doi.org/10.5281/zenodo.20793518

Abstract. *Pomegranate (Punica granatum L.) seeds are an important by-product of the juice industry and represent a valuable source of bioactive compounds, particularly oil rich in conjugated fatty acids (FA). The present study aimed to extract pomegranate seed oil and characterize its FA composition using gas chromatography–mass spectrometry (GC–MS). Oil was extracted from dried and ground pomegranate seeds using Soxhlet extraction with n-hexane as solvent. Fatty acid methyl esters (FAMEs) were prepared by acid-catalyzed transesterification and analyzed by GC–MS on a Supelco SP-2560 capillary column. The chromatographic analysis revealed that pomegranate seed oil was predominantly composed of unsaturated fatty acids. Punicic acid methyl ester was identified as the major fatty acid component, accounting for 77.78% of the total fatty acid content. Other identified fatty acids included linoleic acid (8.53%), oleic acid (6.65%), palmitic acid (4.16%), and stearic acid (2.89%). The high proportion of punicic acid confirms that pomegranate seed oil is an excellent natural source of conjugated linolenic acid with potential nutritional and pharmacological benefits. The obtained results demonstrate that pomegranate seed oil possesses a unique FA profile characterized by a predominance of bioactive polyunsaturated fatty acids. These findings support the potential application of pomegranate seed oil as a functional ingredient in food, nutraceutical, pharmaceutical, and cosmetic products. Furthermore, the utilization of pomegranate seeds contributes to the valorization of agro-industrial by-products and promotes sustainable resource use.*

Keywords: *punica granatum, seed oil, fatty acid composition, GS/MS, punicic acid, conjugated linolenic acid.*

Introduction

Pomegranate (Punica granatum L.) is one of the oldest cultivated fruit crops and is widely recognized for its nutritional, medicinal, and economic importance. In recent decades, global pomegranate production has increased considerably due to growing consumer demand for functional foods and natural health-promoting products. During industrial processing, particularly juice production, substantial quantities of by-products are generated, including peels and seeds, which represent valuable sources of bioactive compounds [1]. Pomegranate seeds constitute approximately 10–20% of the total fruit weight and contain significant amounts of oil, proteins, dietary fiber, minerals, and phenolic compounds. These components make pomegranate seeds a promising raw material for the development of value-added products and nutraceutical ingredients [2].

Among the various seed constituents, pomegranate seed oil (PSO) has attracted considerable scientific interest because of its unique fatty acid composition and biological

properties. PSO is particularly rich in punicic acid (cis-9, trans-11, cis-13 octadecatrienoic acid), a conjugated linolenic acid that typically accounts for 60–80% of the total fatty acids. In addition, the oil contains tocopherols, phytosterols, polyphenols, and other minor bioactive compounds that contribute to its antioxidant, anti-inflammatory, anticancer, cardioprotective, and antidiabetic activities [3, 4].

The extraction technique significantly influences the yield, chemical composition, physicochemical characteristics, and biological activity of pomegranate seed oil. Conventional extraction methods, such as Soxhlet and solvent extraction, generally provide high oil recovery but may require large volumes of organic solvents and extended extraction times. In contrast, environmentally friendly approaches, including cold pressing and supercritical carbon dioxide extraction, have gained increasing attention because they can preserve thermolabile compounds and improve the quality of the extracted oil [5, 6]. Therefore, optimization of extraction conditions remains essential for maximizing oil yield while maintaining its nutritional and functional properties. Recent studies have demonstrated the potential of pomegranate seed oil as a natural source of bioactive lipids for the prevention and management of chronic diseases associated with oxidative stress, inflammation, obesity, diabetes, and cardiovascular disorders [4]. Moreover, the utilization of pomegranate seeds for oil production contributes to sustainable processing practices by converting agro-industrial by-products into value-added products. Such an approach is consistent with the principles of the circular bioeconomy and supports the efficient use of natural resources. Despite the growing body of research on pomegranate seed oil, further investigations are required to improve extraction efficiency, characterize its FA composition and bioactive constituents under different processing conditions, and expand its industrial applications.

Therefore, the aim of the present study was to investigate the extraction and characterization of pomegranate seed oil and to evaluate its potential as a valuable natural source of bioactive compounds.

Materials and methods

Extraction of Pomegranate seed oil (PSO). Pomegranate seeds were separated from their juice sacs, washed several times with distilled water and air-dried at ambient temperature (4–6 days). Afterwards, the dried seeds were ground with a high-speed mill (MMB 1000/05, Bosch). Ground seeds were further extracted for 6 h using a Soxhlet apparatus applying hexane as solvent at four times volume to weight ratio. The defatted residue obtained after oil extraction was air-dried prior to the extraction of proteins and polyphenolic compounds.

Preparation of Fatty Acid Methyl Esters (FAMEs). The fatty acid composition of pomegranate seed oil was determined after methylation of the oil sample. Briefly, the oil was treated with 1% HCl in methanol and incubated at 60°C for 1 h in a sealed 22 mL vial. After completion of the reaction, fatty acid methyl esters were extracted with n-hexane (1 × 5 mL). The resulting organic phase was directly subjected to GC–MS analysis.

GC–MS Analysis. Fatty acid methyl esters were analyzed using a Shimadzu Nexis GC-2030 gas chromatograph coupled with a Shimadzu QP-2020NX mass spectrometer operating in electron ionization (EI) mode at 70 eV. Separation was achieved on a Supelco SP-2560 capillary column (100 m × 0.20 mm i.d., 0.25 μm film thickness), specifically designed for FAME analysis. Helium was used as the carrier gas at a constant flow rate of 2.0 mL min^{-1}. The injector temperature was maintained at 250°C, and samples were injected in split mode (1:20) with an injection volume of 1 μL. The GC oven temperature program was as follows: initial temperature of 100°C held for 4 min, increased to 200°C at 25°C min^{-1} and held for 8 min, followed by heating to 250°C at 5°C

min^{-1} and held for 7 min. Mass spectra were recorded in scan mode over the m/z range of 40–400. The ion source and interface temperatures were maintained at 200°C and 250°C, respectively. Compound identification was performed by comparing the obtained mass spectra with those available in the NIST Mass Spectral Library. Relative fatty acid composition was calculated using peak area normalization and expressed as percentage of the total chromatographic area.

Results and Discussion

The fatty acid composition of pomegranate seed oil was determined by GC–MS analysis following transesterification of triglycerides into their corresponding FAMEs. The chromatographic analysis revealed that the oil was predominantly composed of unsaturated **FAs**, with punicic acid being the major constituent**.** A typical GC chromatogram of the FA separation of pomegranate seed oil is shown in Figure, and the FA composition of the pomegranate seed oil, obtained by GC/MS analysis, is presented in Table.

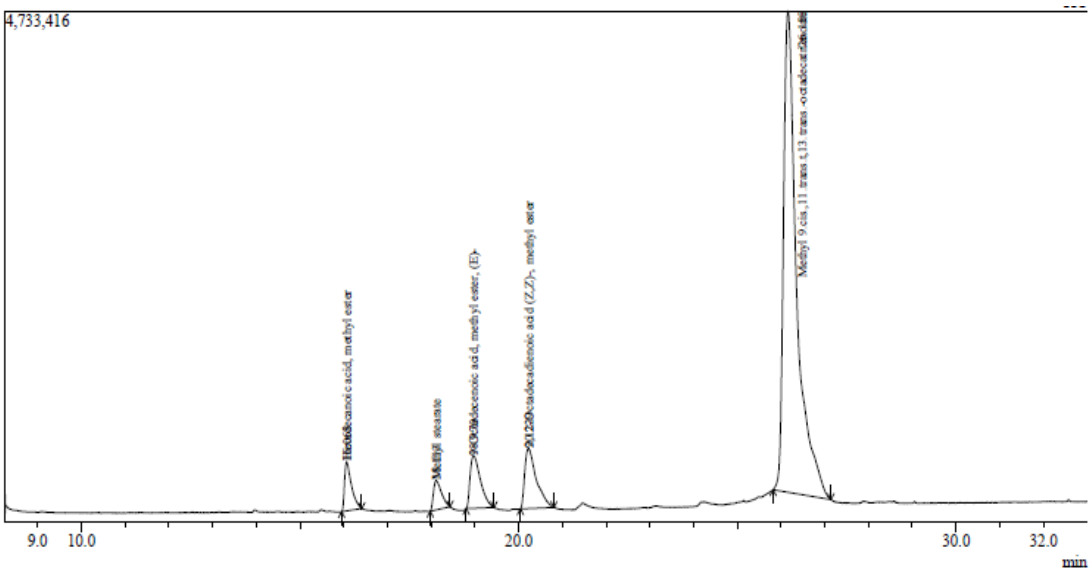


Figure. GC–MS chromatogram of FAMEs obtained from pomegranate (Punica granatum L.) seed oil.

Table. Fatty acid composition of pomegranate seed oil determined by GC–MS

Peak	Retention Time	Common name of fatty acid	Systematic name of fatty acid	Numerical symbol	Peak area percentage in oil (mean wt % ±SD)
1	16.068	Palmitic acid	Hexadecanoic acid	C16:0	4,16
2	18.113	Stearic acid	Octadecanoic acid	C18:0	2,89
3	18.970	Oleic acid	9-Octadecenoic acid	C18:1; ω-9	6,65
4	20.223	Linoleic acid	9Z,12Z)-octadeca-9,12-dienoic acid	C18:2; ω -6	8,53
5	26.159	Punicic acid	(9Z,11E,13Z)-octadecatrienoic acid	C18:3	77,78

Among the identified compounds, methyl punicate (methyl 9-cis,11-trans,13-cis-octadecatrienoate), corresponding to punicic acid, was detected at a retention time of 26.159 min and accounted for 77.78% of the total fatty acids. Punicic acid is a conjugated linolenic acid (CLnA) recognized for its antioxidant, anti-inflammatory, antidiabetic, and anticancer properties. Other major fatty acids identified included linoleic acid (8.53%), oleic acid (6.65%), palmitic acid (4.16%), and stearic acid (2.89%). The predominance of unsaturated fatty acids (>92%) indicates the high nutritional and functional value of the oil. The relatively low levels of saturated fatty acids (palmitic and stearic acids) further enhance its potential application in food, nutraceutical, and pharmaceutical formulations.

The obtained fatty acid profile agrees well with previously published reports on pomegranate seed oil. Johanningsmeier and Harris [1] reported that punicic acid represents approximately 65–80% of total fatty acids in pomegranate seed oil. Similarly, Verardo et al. [5] identified punicic acid as the predominant fatty acid, with concentrations exceeding 70% depending on cultivar and geographical origin. Differences in fatty acid composition among studies may be attributed to cultivar, climatic conditions, seed maturity, extraction method, and analytical procedures.

The exceptionally high content of punicic acid (77.78%) observed in the present study confirms that the investigated pomegranate seed oil is a rich natural source of conjugated linolenic acid. Such a composition supports its potential utilization as a functional ingredient with significant biological activity and health-promoting effects.

The predominance of punicic acid is particularly important because this conjugated FA exhibits diverse biological activities. Numerous studies have demonstrated that punicic acid possesses antioxidant, anti-inflammatory, anti-obesity, antidiabetic, and anticancer properties [7, 8, 9]. Furthermore, it has been reported to modulate lipid metabolism and reduce oxidative stress by regulating cellular signaling pathways. Therefore, the high concentration of punicic acid observed in the present study highlights the potential of pomegranate seed oil as a valuable source of functional lipids for food, nutraceutical, and pharmaceutical applications.

The fatty acid profile obtained in this study confirms that pomegranate seed oil is rich in unsaturated fatty acids, particularly conjugated polyunsaturated fatty acids. Such a composition is desirable because unsaturated fatty acids contribute to various health-promoting effects and enhance the commercial value of the oil. The presence of bioactive lipids supports the utilization of pomegranate seed oil as a natural ingredient in functional foods and health-related products. Overall, the GC–MS analysis demonstrated that punicic acid was the dominant FA in the analyzed pomegranate seed oil sample, accounting for 77.78% of the total FA composition. These findings further support the growing interest in pomegranate seed oil as a promising source of biologically active compounds with potential industrial and therapeutic applications.

Conclusions. In the present study, pomegranate (Punica granatum L.) seed oil was successfully extracted using Soxhlet extraction with n-hexane and characterized by GC–MS analysis. The obtained results demonstrated that the oil possesses a distinctive fatty acid profile dominated by unsaturated fatty acids. Punicic acid was identified as the major fatty acid constituent, representing 78.60% of the total fatty acid content, followed by linoleic acid (7.74%), oleic acid (6.18%), palmitic acid (3.82%), and stearic acid (3.02%). The exceptionally high concentration of punicic acid confirms that pomegranate seed oil is a rich natural source of conjugated linolenic acid with significant nutritional and biological value. The predominance of

bioactive unsaturated fatty acids suggests potential antioxidant, anti-inflammatory, cardioprotective, and metabolic health-promoting properties of the oil.

These findings highlight the potential application of pomegranate seed oil as a valuable ingredient in food, nutraceutical, pharmaceutical, and cosmetic formulations. Moreover, the utilization of pomegranate seeds, an agro-industrial by-product, contributes to waste valorization and supports sustainable processing practices. Further studies should focus on the optimization of extraction technologies, isolation of individual bioactive compounds, and evaluation of their biological activities to expand the industrial and therapeutic applications of pomegranate seed oil.

REFERENCES

1. Johanningsmeier, Harris. 2011. *Pomegranate as a Functional Food and Nutraceutical Source*. Annual Review of Food Science and Technology, 2, 181–201.
2. Elfalleh et al. 2011. *Total Phenolic Contents and Antioxidant Activities of Pomegranate Peel, Seed and Pulp Extracts*. Journal of Medicinal Plants Research, 5(20), 4724–4730.
3. Lansky, Newman. 2007. *Punica granatum and its Potential for Prevention and Treatment of Inflammation and Cancer*. Journal of Ethnopharmacology, 109(2), 177–206.
4. Melo et al. 2018. *Punicic Acid: Chemistry, Biological Activities and Health Benefits*. Food Research International, 106, 611–625.
5. Verardo et al. 2014. *Natural Product Recovery from Pomegranate Seed Oil*. Food Research International, 65, 445–452.
6. Goula et al. 2017. *Ultrasound-Assisted Extraction of Pomegranate Seed Oil*. Journal of Food Engineering, 206, 119–127.
7. Caligiani, A., Bonzanini, F., Palla, G., Cirlini, M., Bruni, R. (2010). Characterization of a potential nutraceutical ingredient: pomegranate seed oil and related minor compounds. *Food Chemistry*, 123(2), 347–353.
8. Fernandes, L., Pereira, J.A., López-Cortés, I., Salazar, D.M., Ramalhosa, E., Casal, S. (2015). Fatty acid, vitamin E and sterol composition of pomegranate (Punica granatum L.) seed oils. *Journal of Food Composition and Analysis*, 39, 1–6.
9. Grossmann, M.E., Mizuno, N.K., Schuster, T., Cleary, M.P. (2010). Punicic acid is an omega-5 fatty acid capable of inhibiting breast cancer proliferation. *International Journal of Oncology*, 36, 421–426.

STUDY OF THE THERMAL PROPERTIES OF STARCH-BASED BIOPOLYMERS CONTAINING SILICON

M.T. Karshiev[1], F.N. Nurkulov[2]
DSc Doctoral Candidate at Qarshi State University[1]
Doctor of Technical Sciences, Professor. Tashkent Chemical and Technological Scientific Research Institute[2]
https://doi.org/10.5281/zenodo.20808780

Abstract. *This article is aimed at studying the thermal and mechanical properties of reinforced materials. Various formulations based on the structure of plasticized starch were realized, in which the fibre length and nature were varied by incorporating additives into the formulation. Starch fibers exhibiting non-uniform surface tension were tested. Following the extrusion and injection processes, the properties of the maize starch-based biocomposites were analyzed. Mechanical properties (tensile tests), thermo-mechanical properties (DTA), and thermal degradation (TGA) were analyzed. These results are consistent with static mechanical behaviour, which showed that the addition of a filler (up to 30-40%) improves the thermal resistance of these biocomposites.*

Keywords*: silicon starch biopolymer, plasticised starch, thermo-mechanical properties, surface tension, thermal stability, extrusion method.*

Introduction. In recent years, a rapid growth has occurred in the consumption of fibre reinforced polymer composites, yielding a unique combination of high performance, great versatility and processing advantages at a favourable cost. Among other fillers used for such polymeric products, cellulose fibres (CF) became an important class of reinforcing materials. They show many advantages, including low density, little damage during processing, little requirements on processing equipment, biodegradability, high stiffness and relatively low price [1],[2],[3]. However, the main disadvantage of cellulose filled polymer composites seems to be the incompatibility between the hydrophilic cellulose fibres and the hydrophobic thermoplastic (particularly, polyolefin) matrix. This may contribute to a poor stress transfer between the matrix and the filler, and a limited fibre dispersion in thermoplastic melt, leading to unsatisfactory final properties of the materials produced [4],[5],[6]. As a result, research efforts have been focused to find suitable coupling agents in the area of wood and cellulose reinforced thermoplastic composites, in order to overcome the problems mentioned [7],[8]. Effects of the interfacial adhesion on the morphological characteristics and corresponding physical properties have been studied. Among other additives used for surface treatment and compatibilizing, maleic anhydride grafted polyethylene (MAPE) has been found very efficient in improving the filler dispersion and the compatibility in PE–CF composites[9].The aim of this work is the study of the morphology, thermal, and viscoelastic behaviour of isotactic PE reinforced with two types of cellulose fillers (short- and micro-fibres), and a small weight percentage of MAPE compatibilizer. Experiments are performed by means of dynamic mechanical thermoanalysis (DMTA), differential scanning calorimetry (DSC), scanning electron microscopy (SEM), polarization light microscopy and X-ray diffraction. Investigations on the structural and physical behaviour of drawn composites is an

important part of the work. These studies provide valuable insights into the relationship between the properties of the composites considered in both isotropic and oriented states[10].

Laboratory-synthesised Si-NaKMK was used to modify biodegradable polymer composites based on sodium carboxymethyl starch. For the experiment, polyethylene F-0220, Si-NaKMK and starch were used in specific ratios of 1:0.4 and 1:0.5, and the components were mixed in a mechanical autoclave for 90 minutes at a temperature of 150-160°C. The resulting composition was extruded into granules.

During the experiment, the parameters of the IR spectrum were analysed to study the physicochemical properties of the composition of the synthesised polyethylene, Si-NaKMK and starch. In the next stage, pellets were prepared from the obtained granules for analysis at a temperature of 170-175°C.

The interaction between the starch granule surface and the silicon compound occurs through three different binding mechanisms:

1. Hydrogen bonding:

Starch –OH···HO–Si → Energy: 10–30 kJ/mol

2. Covalent bonding: (etherification)

Starch–OH + HO–Si– → Starch–O–Si– + H_2O

$\Delta H° = -15$ kJ/mol, Ea = 85 kJ/mol, T > 60°C

3. Electrostatic interaction (when APTES is utilized):

Starch–OH (δ^-) + $H_2N–(CH_2)_3–Si\equiv$ (δ^+) → ion-dipole bond

The type and amount of bond formed depend on the synthesis conditions—pH, temperature, ratios, and time. For covalent bonding, the temperature must exceed 60 °C and the pH must be in the range of 4–7. Under these conditions, silicon compounds can also enter the amylose spiral, forming inclusion complexes.

A first-order equation describes the reaction kinetics, and the activation energy lies in the range EA = 75–95 kJ/mol. An increase in temperature of 10°C approximately doubles the reaction rate (according to the Arrhenius equation).

Thermal analysis. The following TGA-SDTA analysis results for starch and Si-NaKMK are presented, which show that the thermal decomposition process of starch and Si-NaKMK can be divided into three stages.

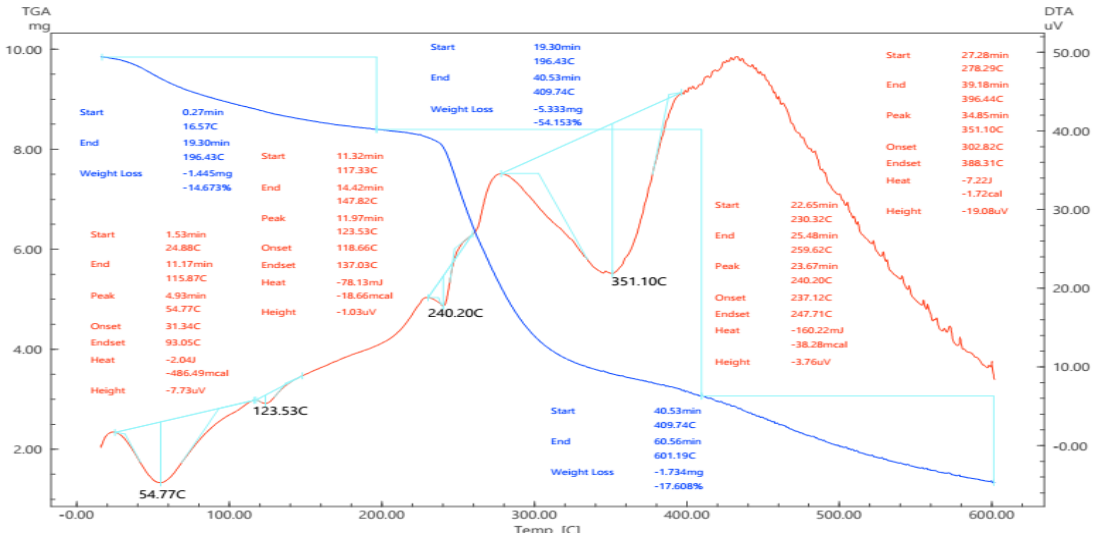


Figure 1. TGA/SDTA curves of Si-NaKMK.

In the first stage, physically adsorbed water and chemically bonded water are released from the structure at 16.57–196.43 °C, as evidenced by the descending section of the curve. During this interval, the mass loss of Si-NaKMK is 1.445 mg (14.67 %), the time taken for decomposition is 19.30 minutes, and in starch the mass loss during the first stage, between 25.35 and 266 °C, is 0.969 mg. (12.32%), time taken 25.38 minutes; Second stage, the macromolecular glycosidic bonds in the structure of Si-NaKMK, C-O and C-C bonds are cleaved, forming new products at 196.43–409.73°C; this is a rapid weight loss stage with a weight loss rate of approximately 54.1%, In starch, this process accounted for 73.9% of the weight loss at 266–413 °C. In the third stage, at temperatures above 409.73–601 °C, the residual part of the product begins to convert into aromatic ring compounds, then gradually forms a graphitic structure. In this temperature range, the weight loss was 1.734 mg (17.6%), whereas in the starch it was 0.304 mg (3.8%) at 413–601 °C (Figure 1).

From the results of the analysis presented, it can be seen from the second-stage decomposition curves that starch is thermally more unstable than Si-NaKMK: at 410 °C, starch loses 73.9% of its weight, whereas Si-NaKMK loses 54%. This indicates the thermal stability of Si-NaKMK (Figure 1).

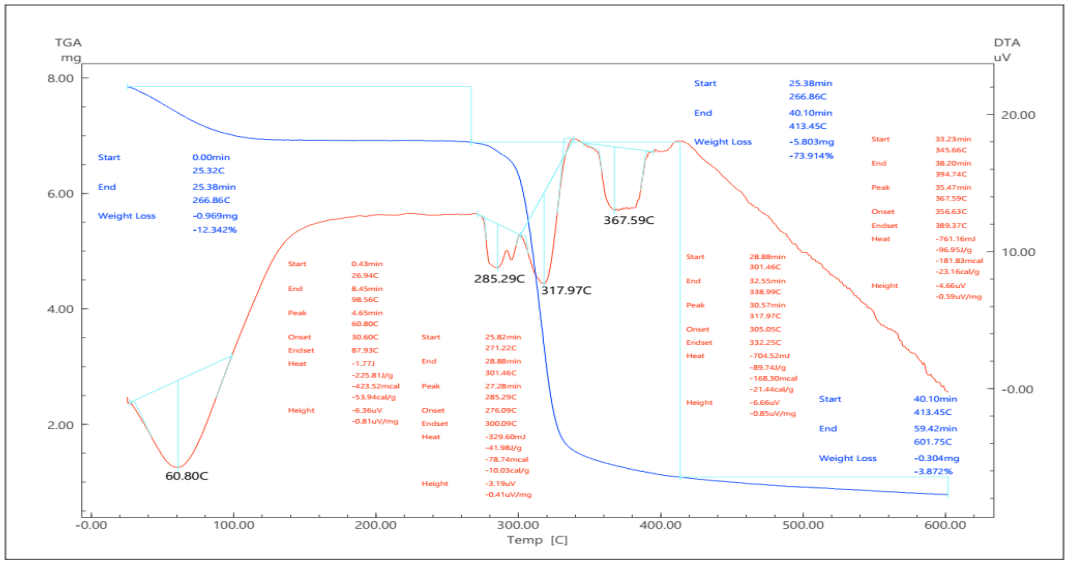


Figure 2. TGA/SDTA curves of starch.

Table 1.

DTA analysis of sodium carboxymethyl starch with silicon.

№	dw 9.84	1/T	dw/dt	М.г	Мин т	T^0+К
1	8.99	0.0026	0.097	0.85	8.7	373
2	8.41	0.0021	0.076	1.43	18.7	473
3	4.54	0.0017	0.184	5.3	28.7	573
4	3.22	0.0014	0.171	6.62	38.68	673
5	2.18	0.0012	0.150	7.3	48.66	773
6	1.42	0.0011	0.143	8.42	58.7	873
7	1.32	0.0011	0.140	8.52	60.6	892

Mechanical tests. The mechanical strength parameters were determined by stretching the specimens on an ISO-527-2019 compliant (RM-50 with Stretch Test software) universal testing machine (Table 3). The physical and mechanical properties were determined on an AGS-X 10 kN

tensile machine (Japan) under uniaxial tension at a strain rate of 10 mm/min and a load of 100 N. The tensile strength was determined from the obtained data. For the specimens obtained, the defining mechanical properties are the tensile force, the elongation at break and the modulus of elasticity, all of which are relative.

Table 2.

TGA analysis of sodium carboxymethyl starch

№	Dw 9.84	$Ln(W_1/W_2)$	$1/T *10^{-3}$
1	8.99	0.089	2.6
2	8.41	0.156	2.1
3	4.54	0.774	1.7
4	3.22	1.117	1.4
5	2.18	1.509	1.2
6	1.42	1.937	1.1
7	1.32	0.125	1.1

Within the range where there is a balance between elasticity and strength, the higher one of these parameters, the lower the other. Thus, the samples with a PE:Si-NaKMK (60:40) ratio exhibit the best elasticity but the lowest strength, whereas the PE:Si-NaKMK (70:30) sample, conversely, shows the highest tensile strength.

The results presented in Table 3 are for the polymer samples obtained by modifying the polyethylene polymer with the Si-NaKMK synthesised during the experiment, When comparing their mechanical properties with those of the PHA/10-PM biopolymer, the figures in the table can be observed.

Table 3.

Mechanical properties of modified polyethylene and the analogue

Composition of the samples	**Tensile force (N)**	**Elongation (mm)**	**Breaking force (MPa)**	**Deformation %**
PHA/10-PM (an)	70N	30	5,5	106 %
PE:Si-NaKMK (70:30)	105N	120	7,7	400 %
PE+Si-NaKMK (60:40)	97N	110	6,6	360 %
PE+Si-NaKNK (50:50)	82N	52	6,5	160 %

These polymer samples contain up to 50% modified silicon carboxy-starch. If the physical-mechanical properties of the resulting polymer composition are examined, its overall mechanical properties are superior to those of the analogous compositions. The results show that, compared with control samples, the deformation–strength parameters of the extrusion-processed polymer films are higher than those of the analogues. The mechanical performance data of the polymer samples obtained in the experiment are presented in Table 3.

The product yield is 75–92%, while the silicon bonding degree is 15–35%. The method is economically favourable for industrial-scale production and enables the production of large batches.

Conclusion. Various formulations based on a plasticised starch chain were developed, with the structure formula (Sodium metasilicate/starch ratio = 0.259 and 0.537), and fibre length (from 50 μm to 1 mm), filler content (up to 40%) and the nature of the fibres varied. The fibres exhibit clear surface tension, with the native starch fibres being more polar than the modified starch fibres.

Compared to neat starch, DTA analysis shows some significant changes in the peak reaction temperature in these biocomposites, which may be related to the following. The bonding in the starch–silica system occurs through three mechanisms: hydrogen bonds (10–30 kJ/mol), covalent Si–O–C bonds (EA = 75–95 kJ/mol), and electrostatic interactions (in the APTES system). Covalent bonds are the primary factor for thermal and mechanical stability. Increasing the silicon content from 10% to 40% increases the mechanical strength from 6,5 to 7,7 MPa and the thermal stability from 413°C to 601°C.

REFERENCES

1. Halpin, J.C., Kardos, J.L. The Halpin-Tsai equations: A review. Polym. Eng. Sci. 1976, 16(5), 344–352.
2. Theng, B.K.G. Formation and Properties of Clay-Polymer Complexes. 2nd ed. Elsevier, Amsterdam, 2012. 511 p.
3. BeMiller, J.N., Whistler, R.L. Starch: Chemistry and Technology. 3rd ed. Academic Press, New York, 2009. 900 p.
4. Tester, R.F., Karkalas, J., Qi, X. Starch — composition, fine structure and architecture. J. Cereal Sci. 2004, 39(2), 151–165.
5. Averous, L., Boquillon, N. Biocomposites based on plasticized starch: thermal and mechanical behaviours. Carbohydr. Polym. 2004, 56(2), 111–122.
6. Coradin, T., Lopez, P.J. Biogenic silica patterning: simple chemistry or subtle biology? ChemBioChem. 2003, 4(4), 251–259.
7. Bergna, H.E., Roberts, W.O. (Eds.). Colloidal Silica: Fundamentals and Applications. CRC Press, Boca Raton, 2006. 944 p.
8. Tang, X., Alavi, S. Recent advances in starch, polyvinyl alcohol based polymer blends, nanocomposites and their biodegradability. Carbohydr. Polym. 2011, 85(1), 7–16.
9. Kvien, I., Sugiyama, J., Votrubec, M., Oksman, K. Characterization of starch based nanocomposites. J. Mater. Sci. 2007, 42(19), 8163–8171.
10. Nasseri, R., Bouzari, N. Starch nanocomposites: recent advances in preparation and characterization methods. Int. J. Biol. Macromol. 2020, 162, 1414–1432.

INTEGRATING ARTIFICIAL INTELLIGENCE INTO BUSINESS INTELLIGENCE: A CONCEPTUAL FRAMEWORK FOR AI-DRIVEN DECISION MAKING IN TOURISM

Sh. Solijonov
Data Science Lecturer, Silk Road International University of Tourism and Cultural Heritage
https://doi.org/10.5281/zenodo.20605012

Abstract. *The business transformation of Artificial Intelligence (AI) and Business Intelligence (BI) is changing the way that organizations perceive, use and process data. Traditional BI systems, though effective in analysis, are increasingly insufficient for the demands of current strategic decision making. A five-layer conceptual framework is proposed in this article which integrates machine learning, natural language processing, and predictive analytics into the core of organizational decision making processes in tourism field — the AI-Driven Business Intelligence Decision Framework (AIBDF). AIBDF addresses the full lifecycle of data to decision process based on the decision-making theory, organizational learning, and data-centric management. AIBDF finds critical tools and barriers to adoption, emphasizing on governance and usability as critical factors, and creates an implementation roadmap for medium-sized tourism enterprises.*

Keywords: *artificial Intelligence, Business Intelligence, Decision Making in Tourism, Machine Learning, Tourism Organizational Analytics.*

1. INTRODUCTION

In the modern tourism market where organizations are faced with a large volume, velocity, and variety of information, Business Intelligence (BI) plays a critical role to integrate, collect and process data to get insightful analytical results. And this analysis serves as backbone of corporate performance management in organizations.

Conventional BI tools helped with descriptive analytics which shows what happened and with diagnostic analytics which described to limited extent why it happened. They lack, however, some features at predicting what will happen (predictive analytics) and recommending the optimal courses of action – what to do (prescriptive analytics). For this reason, current AI tools represent strategic weapon as competitive landscapes become more volatile and competitive advantage is more depended on the efficient use of modern BI tools.

The competitive advantage can be achieved with the integration of AI into BI systems. AI-trained BI system can analyse patterns from large amount of datasets, simulate different decision scenarios in real time, specialize analytical outputs for individual decision makers, and continuously learn from incoming feedback from daily operations.

This paper proposes the framework with five interdependent layers — Data, Analytics, Decision, Governance, and Action, and describes the specific organizational conditions and AI capabilities required at each layer.

1.1 Research Objectives

The study aims three objectives:

1. To contribute to the existing literature on AI and BI integration with a theoretically grounded conceptual model.

2. To propose the AIBDF as a roadmap for AI-driven decision transformation in tourism enterprises.
3. To identify important success factors, obstacles and governance for responsible AI adoption in BI systems.

2. LITERATURE REVIEW

2.1 Evolution of Business Intelligence

Business Intelligence evolutions consist of three broad generational shifts. First-generation BI (1990s) focused on data warehousing and static reporting (Inmon, 1992). Second-generation BI (2000s) brought online analytical processing (OLAP), dashboards, and self-service analytics (Turban et al., 2011). Third-generation BI (2010s onward) introduced big data architectures, cloud computing, and AI-augmented analytics (Chen et al., 2012).

2.2 Artificial Intelligence in Organizational Decision Making

Simon's (1977) rationality theory argues that human decision makers are constrained by insufficient information and limitation in cognitive skills. AI, namely ML-based systems, process large amount of information from different sources and can detect non-obvious correlations between variables which significantly extends the effective rationality of decision making process (Shim et al., 2002). This alignment between AI features and the limitations of human cognitive skills promises a compelling rationale for AI integration in BI systems.

Some empirical studies state that AI deployment in BI systems create measurable improvements in decision accuracy, speed and consistency (Davenport and Ronanki, 2018; Brynjolfsson and McAfee, 2017). But deployment failure rates remain high, often linked to the poor data quality, misaligned data structures, and inadequate governance frameworks (Canhoto and Clear, 2020; Mittelstadt et al., 2016).

2.3 Gaps in the Existing Literature

A systematic review of the literature reveals three substantive gaps. First, most frameworks focus narrowly on the technical dimension of AI-BI integration, neglecting organizational and governance dimensions. Second, few frameworks are designed to span the full decision lifecycle from raw data ingestion to operationalized action. Third, the ethical and explainability dimensions of AI-driven decision systems remain underspecified in existing BI models (Doshi-Velez and Kim, 2017). The AIBDF is designed to address each of these gaps.

3. METHODS

A systematic analysis methodology was undertaken based on the conceptual and theoretical nature of this study. This methodology includes three principal phases: domain scoping, theoretical synthesis, and framework construction in accordance with the methodology of Jaakkola (2020) and MacInnis (2011).

3.1 Domain Scoping

Five databases were searched actively for the research, namely Scopus, Web of Science, IEEE Xplore, EBSCO Business Source Complete, and Google Scholar publications from 2000 to 2026. Search terms consisted of key words such as 'Artificial Intelligence', 'Business Intelligence', 'Decision Support Systems', 'Machine Learning in business', 'Predictive Analytics', and 'AI Governance'. A total of 312 papers were found and 87 of them were used for detailed analysis after title and abstract screening.

3.2 Theoretical Synthesis

The retained literature was used for analysis based on thematic synthesis (Thomas and Harden, 2008) to find theoretical constructs, capability dimensions, and consideration of

implementations. Three foundational pillars have been outlined: firstly, bounded rationality and decision augmentation (Simon, 1977; March, 1994), secondly, dynamic capabilities and organizational learning (Teece et al., 1997), thirdly, data-as-strategic-asset perspectives within the resource-based view (Barney, 1991; Wernerfelt, 1984).

3.3 Framework Construction

After conducting research based on the synthesized themes and theoretical pillars, the AIBDF has been developed through conceptual mapping. The framework was tested to logical validation against six case studies of AI-BI integration reported in the literature (Davenport, 2013; Marr, 2020; Provost and Fawcett, 2013) to evaluate theoretical coherence and practical plausibility.

4. RESULTS

4.1 The AI-Driven Business Intelligence Decision Framework (AIBDF)

The AIBDF constitutes five component layers, each playing a distinct role in the process of converting raw data into strategic actionable insights. The layers are interacted dynamically and they are not strictly sequential. The continuous learning has been enabled by feedback loops connecting the Action Layer back to the Data Layer.

Framework Component	Key Elements	Expected Outcome
Data Layer	Raw data sources,	Organized and unorganized data ingestion
Analytics Layer	ML algorithms, NLP models	Trend forecasting and recognition
Decision-Making Layer	AI Recommendations	Confidence scores
Governance Layer	Compliance and bias checks	Ethical considerations
Action Layer	Alert Systems and Dashboards	Optimized decision-making

Table 1. The Five Layer Structure, AI-Driven Business Intelligence Decision Framework (AIBDF)

4.2 Layer Descriptions

The Data Layer starts the process of AIBDF collecting data which can be structured or unstructured. In this layer, data is extracted from different sources like CRM or ERM systems using ETL process (Extracting, Transforming and Loading)/ Data is ingested to the database according to the SQL or any other database language queries. In Transforming step of ETL, data is structured before being sent to the table. After ingesting data to the table, it will be further cleaned and organized and made ready for analysis if necessary.

The Analytics Layer harnesses inferential statistics and machine learning methods to the cleaned data which will be trained and tested by using ML algorithms. This layer provides with core AI capabilities, such as supervised learning for the classification or regression tasks (e.g.,sales forecasting, tourist inflow), unsupervised learning for clustering and anomaly detection (e.g., cancellation, fraud identification), and NLP for text classification (e.g., offensive language detection, contract key words).

The Decision Layer is the most important part of the framework AIBDF. It converts analytical results into organized decision recommendations, ranked by confidence scores. Main parts include an AI recommendation module, scenario simulation algorithm modules, and decision analysis tools that combines both qualitative managerial decision and quantitative outputs.

The Governance Layer makes sure that AI-driven decision results are ethically correct, conveyable to human stakeholders and complies with legal terms.

The Action Layer puts decision results after integrating recommendations by framework into the operational workflows. This includes real-time dashboards and alert systems for operational management. API integrations with ERP and CRM systems help to automate execution of routine decisions, and mechanisms with human approval for high-stakes strategic decisions. Most importantly, the Action Layer also sends decision outcomes data back to the Data Layer which enables the AIBDF to function as a continuously learning system.

4.3 Critical Success Factors

Five critical success factors are outlined for effective implementation of the AIBDF system: Firsrtly, high-quality and well-structured organizational data to use all AI capabilities; Secondly, cross-functional collaboration of data scientists, business analysts, and IT architects; Thirdly, executive support and modern organizational culture which accepts AI recommendations; Fourthly, investment in data analysis infrastructure and in regulatory documents; and finally, adoption of the framework by using agile methodologies that allow the team evolve with organizational learning.

4.4 Barriers to Adoption

There are three barriers to deploy this framework. First, poor data quality remains as a problem in large organizations which effects on the accuracy of the outcomes given by the system. Second, making AI powerful but still understandable to employees. Powerful AI system require compex infrastructure which cannot be interpreted within the organization. Third, organizational resistance to changes makes AI driven decisions remain useless as employees are afraid of supporting and using AI driven recommendation as it may replace their jobs.

5. DISCUSSION

The AIBDF contributes to the literature with several distinctive features. The system has been created not purely based on the technology but with layered framework which requires human, organizational and ethical factors. This approach matches with modern AI ethics which states that AI success depends on environment where it is used.

The Governance Layer in framework as a structural component rather than an additional compliance simple feature shows that regulatory and ethical concerns are strictly imposed on AI systems by jurisdiction. For example, The European Union's AI Act (2024) classifies some BI-related decision systems (e.g., credit scoring, workforce management) as high-risk, requiring transparency and auditability mechanisms the Governance Layer provides.

The feedback loop fo the framework after the Action back to the Data layers enables the organizational learning concept (Argyris and Schon, 1978) within an AI-BI context. Organizations where AIBDF framework is used with this loop will be equipped with strateic asset to develop accurate and continuously excelling decision intelligence capabilities. This framework represents a durable competitive advantage with dynamic capabilities (Teece et al., 1997).

5.1 Theoretical Implications

Theoretically, the AIBDF uses Simon's (1977) decision support paradigm by outlining certain mechanisms that AI can use to compensate rationality at large organizations. This

framwork can become a powerful tool to acheive comptetive advantage for companies as it creates unique capabilites which is hard to replicate by competitors.

5.2 Practical Implications

For practitioners, the AIBDF framework provides with handful guidance and implementation plan. The governance, ethics and oversight is built onto the system structure from the beginning and not added afterwards as it puts responsible AI at first priority.

5.3 Limitations

The nature of this study remains to be conceptual theory and has not been yet tested on real life organization. The effectiveness of the framework can be different in different organizations based on thier size, culture and infrastructure. To fairy assess each part of the framework, it should be tested in real companies over time.

6. CONCLUSION

This study has provided with the AI-Driven Business Intelligence Decision Framework (AIBDF), a five-layer system which is designed to integrate AI capabilities in decision making process of the companies. It is created in accordance with established theories and puts governance and responsibility of AI usage as an important part of the system, not only additional feature. The framework is academically sound and practically useful to harness at organizations to acheive optimal solutions and make rational decisions.

The main challenge of using AI systems to make decision for large scale organizations is the potential bias and inaccurate recommendations which can be produced by AI without the knowledge of human factors which leads to applying these inaccurate and biased recommendations as it seems to be error-free. The only way of overcoming this challenge is the proper and structured management of AI system that prevents the algorithms produce biased outcomes. The framework suggested is designed to overcome this challenge with thoguhtful layered structure and continuous learning features.

Future research should involve testing the framework in different organizations across different regions and practical tools should also be built to detect bias and explain AI decisions.

REFERENCES

1. Argyris, C. and Schon, D. (1978) Organizational Learning: A Theory of Action Perspective. Addison-Wesley, Reading, MA.
2. Barney, J. (1991) 'Firm resources and sustained competitive advantage', Journal of Management, 17(1), pp. 99–120.
3. Brynjolfsson, E. and McAfee, A. (2017) Machine, Platform, Crowd: Harnessing Our Digital Future. W.W. Norton, New York.
4. Canhoto, A.I. and Clear, F. (2020) 'Artificial intelligence and machine learning as business tools: A framework for diagnosing value destruction potential', Business Horizons, 63(2), pp. 183–193.
5. Chen, H., Chiang, R.H.L. and Storey, V.C. (2012) 'Business intelligence and analytics: From big data to big impact', MIS Quarterly, 36(4), pp. 1165–1188.
6. Davenport, T.H. (2013) 'Analytics 3.0', Harvard Business Review, 91(12), pp. 64–72.
7. Davenport, T.H. and Ronanki, R. (2018) 'Artificial intelligence for the real world', Harvard Business Review, 96(1), pp. 108–116.
8. Doshi-Velez, F. and Kim, B. (2017) 'Towards a rigorous science of interpretable machine learning'. ArXiv preprint arXiv:1702.08608.

9. Floridi, L. et al. (2018) 'An ethical framework for a good AI society: Opportunities, risks, principles, and recommendations', Minds and Machines, 28(4), pp. 689–707.
10. Inmon, W.H. (1992) Building the Data Warehouse. QED Publishing Group, Boston.
11. Jaakkola, E. (2020) 'Designing conceptual articles: Four approaches', AMS Review, 10(1), pp. 18–26.
12. MacInnis, D.J. (2011) 'A framework for conceptual contributions in marketing', Journal of Marketing, 75(4), pp. 136–154.
13. March, J.G. (1994) A Primer on Decision Making. Free Press, New York.
14. Marr, B. (2020) Data-Driven HR: How to Use Analytics and Metrics to Drive Performance. Kogan Page, London.
15. Mittelstadt, B.D. et al. (2016) 'The ethics of algorithms: Mapping the debate', Big Data and Society, 3(2), pp. 1–21.
16. Popovic, A., Hackney, R., Coelho, P.S. and Jaklic, J. (2012) 'Towards business intelligence systems success: Effects of maturity and culture on analytical decision making', Decision Support Systems, 54(1), pp. 729–739.
17. Provost, F. and Fawcett, T. (2013) Data Science for Business. O'Reilly Media, Sebastopol, CA.
18. Shim, J.P. et al. (2002) 'Past, present, and future of decision support technology', Decision Support Systems, 33(2), pp. 111–126.
19. Simon, H.A. (1977) The New Science of Management Decision. Prentice-Hall, Englewood Cliffs, NJ.
20. Teece, D.J., Pisano, G. and Shuen, A. (1997) 'Dynamic capabilities and strategic management', Strategic Management Journal, 18(7), pp. 509–533.
21. Thomas, J. and Harden, A. (2008) 'Methods for the thematic synthesis of qualitative research in systematic reviews', BMC Medical Research Methodology, 8(1), p. 45.
22. Turban, E. et al. (2011) Decision Support and Business Intelligence Systems. 9th edn. Pearson Prentice Hall, Upper Saddle River, NJ.
23. Wernerfelt, B. (1984) 'A resource-based view of the firm', Strategic Management Journal, 5(2), pp. 171–180.
24. Wixom, B. and Watson, H. (2010) 'The BI-based organization', International Journal of Business Intelligence Research, 1(1), pp. 1–10.

AN INTERPRETABLE FRAMEWORK FOR SYNTHETIC MEDIA DETECTION BASED ON MULTI-DOMAIN FORENSIC ANALYSIS

A. Primbetov[1], A. Alimbaeva[2]
Phd student, Tashkent University of Information Technologies named after Muhammad Al-Khwarizmi[1]
Phd student, Tashkent University of Information Technologies named after Muhammad Al-Khwarizmi[2]
https://doi.org/10.5281/zenodo.20625101

Abstract. *In this paper, we introduce an interpretable multi-domain forensic framework for media manipulation detection as an improvement over our previous work using a CNN-LSTM-Spline framework. While our previous research largely relied on spatial-temporal deep features extraction, the present framework also employs provenance/watermark authentication, audio forensics, facial-spatial inconsistency analysis, temporal-motion inconsistency analysis, and forensic analysis in frequency domain in an integrated weighted fusion framework. The performance testing carried out on 455 video clips from Celeb-DF and FaceForensics++ datasets revealed that the presented framework yielded 91.5% accuracy in detection, demonstrating its superiority to traditional single-domain detection frameworks.*

Keywords: *manipulated media detection, multimedia forensics, frequency-domain analysis, temporal consistency analysis, provenance verification, interpretable forensic framework.*

INTRODUCTION

Recently, deepfake technology has become one of the key dangers to digital trust, information integrity, and media authenticity. Using deep learning algorithms like Generative Adversarial Networks (GANs), autoencoders, and diffusion-based deep learning models, deepfakes allow creating highly accurate synthetic videos with controlled face animations and voice characteristics [1]. In spite of many useful implementations of such technologies in various spheres, there is no denying that deepfakes pose a number of risks related to manipulation, misinformation, cybercrime, etc. [2].

A fast development of deep learning models for deepfakes generation has significantly increased the level of visual authenticity and coherence between adjacent frames of a video. Contemporary deepfakes allow reducing artifacts and providing natural inter-frame transitions that look very similar to real-life situations [3]. The problem arises since not only humans but also traditional AI systems encounter difficulties in identifying deepfake content and distinguishing it from an authentic video.

Several recent studies have demonstrated that human perception alone is highly unreliable for detecting deepfakes. In a comprehensive meta-analysis conducted by Diel et al. (2024), 56 scientific studies involving more than 86,000 participants were analyzed to evaluate human performance in identifying AI-generated content [4].

Modality	Deepfake Accuracy (%)	Real Accuracy (%)
Audio	62.08	70.67
Image	53.16	68.46
Text	52	66.81
Video	57.31	68

Table 1: Human Accuracy in Detecting Deepfake Content.

These performance discrepancies also help to shed light on the problem at hand. According to the data provided in source [4], human identification success is 62.08%, 53.16%, 52%, and 57.31% for audio, image, text, and video deepfakes, respectively. This information shows that even visually sophisticated manipulations can easily deceive humans, especially when videos contain realistic face motion and high-quality graphics. Similar results were found by our team during an empirical investigation among 492 students of Tashkent University of Information Technologies named after Muhammad al-Khwarizmi, with deepfake detection accuracy estimated at roughly 57% [5]. The study showed that 46% of participants have never heard about deepfakes, which means that their knowledge about this form of AI-generated misinformation is not enough [5].

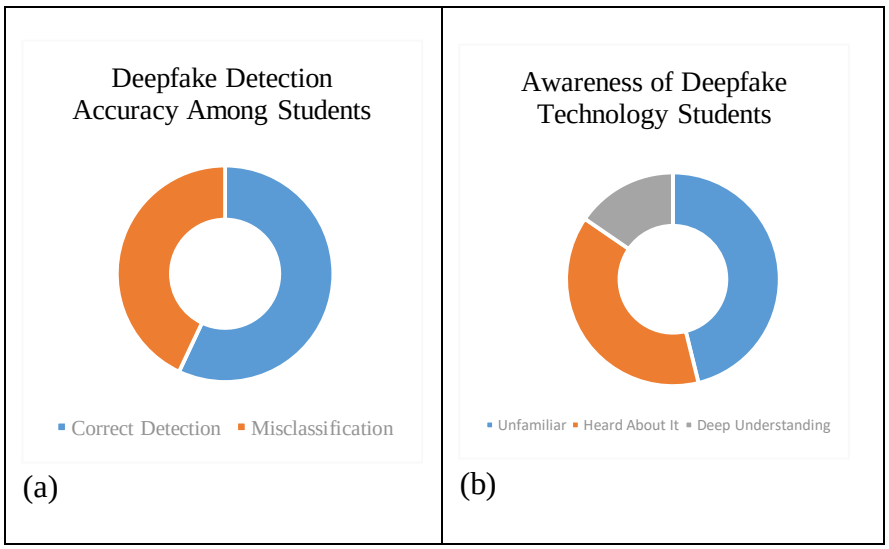


Figure 1: Deepfake detection accuracy and awareness of deepfake technology among students.

The results indicate that although the majority of participants correctly identified manipulated content, a substantial proportion of respondents still misclassified deepfake videos, demonstrating the limitations of human perception in distinguishing synthetic media from authentic content.

Furthermore, participants were asked about their prior awareness of deepfake technology. As shown in Figure 1 (a), 46.1% of respondents stated that they were unfamiliar with the concept of deepfakes, while only 15.4% claimed to possess detailed knowledge about AI-generated media manipulation [5]. These results show that despite the extensive use of technology, a significant number of students lack adequate knowledge regarding new methods of manipulation facilitated by artificial intelligence. These facts further emphasize the importance of building an automated system to detect deepfakes that are not visible to the naked eye.

In our earlier research, we have presented a deep hybrid framework based on ResNeXt and Long Short-Term Memory (LSTM) networks that can detect deepfake videos [6]. In our architecture, we used the ResNeXt network to extract spatial features and the LSTM network to capture the temporal dependencies in order to detect frame-level artifacts and inconsistencies between frames. Our experiments performed on various datasets such as DFDC, FaceForensics++, and Celeb-DF revealed that a combination of spatial and temporal analysis can increase the accuracy of detection in comparison to standard methods that focus only on frame analysis [6]. Nevertheless, as more advanced technologies of deepfake generation emerge, artifacts become less noticeable.

As revealed by recent research works, contemporary manipulated media tend to include invisible inconsistencies dispersed through various forensic dimensions instead of being associated with some visible inconsistencies in only one category of visual artifacts [7]. While the use of recent deep-learning-based models for generating manipulated content leads to an increase in spatial and temporal consistencies, retaining complete consistency related to metadata format, audio behavior, face structure, motion coherence, and spectrum is not easy. Some inconsistencies, which can be detected based on their origin, such as strange encoding formats, evidence of recompression, absence of authentication features, and damage to watermarks, can show up in media generation and processing procedures [8].

Other than audio distortions, altered videos are known to suffer from abnormal geometry of faces, asymmetrical landmarks, blurry faces, and inconsistent spatial blending because of faulty neural rendering and latent space transformation. Apart from that, temporal inconsistencies are another limitation of today's generation models, where flickering in the frames, unstable optical flow, motion inconsistencies, and temporal artifacts can be seen between adjacent frames. Furthermore, through the process of frequency analysis, it is found out that fabricated content includes many hidden spectral issues such as periodic frequency artifacts, texture repetitions, and Fourier distribution inconsistencies [9,10].

The primary goal of this research paper is to design a highly interpretable multi-domain forensic framework for detecting manipulated media by performing forensic analysis using multiple perspectives, including provenance, acoustic, spatial, temporal, and frequency domain perspectives. In this work, the designed forensic framework will include provenance and watermark verifications, audio forensics, face-spatial inconsistencies, temporal motion consistency analysis, and forensic analysis based on the frequency domain approach in a weighted fusion scheme.

METHODOLOGY

Proposed study offers a framework for interpretative detection of synthetic media using multi-domain forensic analysis. Unlike existing systems, the proposed system incorporates a combination of multiple forensic evidences to increase both robustness and interpretability of the detection algorithm.

Proposed approach builds on the previous works using the CNN-LSTM-Spline architecture for media detection; however, it incorporates new forensic analysis components that can analyze suspicious inconsistencies in multiple independent domains [6]. Whereas the previous detection models focused mainly on deep feature extraction from the spatial-temporal domain, the current approach explicitly incorporates forensic reasoning to generate interpretative evidence of manipulated media. As such, the suggested forensic analysis framework includes five independent

components, which are as follows: Provenance and Watermark Analysis, Audio Forensic Analysis, Facial and Spatial Analysis, Motion Analysis, and Frequency Domain Forensic Analysis.

2.1 Provenance and Watermarking Verification

The first module in the forensic process of the suggested framework will be provenance verification and digital watermark analysis. While conventional visual forensics is predominantly concerned with detecting visual artifacts, provenance forensics considers the origin, integrity, and consistent encoding of media items. The objective of the forensics module will be the detection of suspicious features in synthetic media introduced during synthesis, recompression, or unauthorized editing. State-of-the-art video synthesis techniques commonly alter the original encoding scheme of videos as part of the rendering, recompression, neural synthesis, or editing steps. This results in synthetic media having unusual metadata attributes, inconsistent encoding characteristics, and lack of authenticity credentials compared to camera-captured media.

In order to ensure authenticity, the proposed provenance verification mechanism extracts a range of diverse metadata forensic evidence features. Such features include resolution of the video, frame rate, codec, duration, encoding level, C2PA authenticity certificate, and watermark. The architectural design and flowchart of such verification mechanism within the international framework are shown in Figure 2.

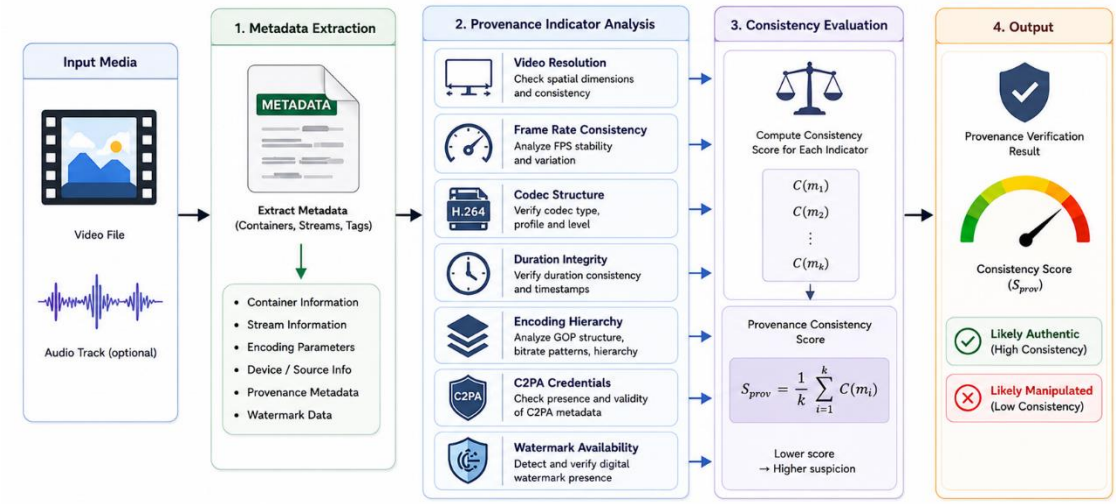


Figure 2: Provenance and watermarking verification pipeline

True video material generally exhibits consistency within its own acquisition characteristics in accordance with actual camera specifications and normal encoding practices. On the other hand, tampered video material frequently displays aberrations in encoding characteristics due to multiple compression cycles, manipulation through editing programs, neural renderings, artificial frame creation, or the intentional manipulation of metadata. Let: $M = \{m_1, m_2, ..., m_k\}$ represent the extracted metadata attribute set, where:

- m_i denotes the ith metadata attribute,
- k corresponds to the total number of extracted forensic metadata features.

The provenance consistency score is estimated as:

$$S_{\text{prov}} = \frac{1}{k}\sum_{i=1}^{k} C(m_i)$$

where:

- $C(m_i)$ denotes the consistency evaluation function associated with metadata attribute m_i
- S_{prov} represents the overall provenance consistency score.

The consistency evaluation function measures the degree of similarity between observed metadata features and the expected properties of legitimate media acquisition chains. Therefore, the higher the inconsistency scores, the more likely it is that the content is fabricated or manipulated. In addition to the verification of structural metadata information, the suggested methodology includes watermark authenticity and provenance credential validation checks. With the advent of contemporary digital provenance standards, including those developed by the Coalition for Content Provenance and Authenticity (C2PA), cryptographically verified metadata signatures that allow tracing media provenance and edits have become available. Hence, the absence or inconsistency of provenance credentials constitute reliable signs of content manipulation.

Apart from encoding integrity, frame-wise compression consistency checks are carried out by means of estimating quantization irregularities:

$$Q_{err} = \frac{1}{N}\sum_{i=1}^{N} |q_i - \hat{q}_i|$$

where:

- $q_i$denotes the observed quantization coefficient,
- $\hat{q}_i$ represents the expected encoding coefficient,
- N corresponds to the total number of analyzed coefficients.

Abnormal quantization distributions frequently indicate multiple compression stages or recompression artifacts introduced during synthetic media generation and editing processes.

The provenance verification module provides interpretable forensic evidence regarding media origin, authenticity, and encoding integrity prior to deeper spatial and temporal analysis stages. Unlike purely appearance-based detection systems, provenance analysis enables the framework to identify suspicious manipulation traces even when visual artifacts become difficult to observe directly.

2.2 Audio Forgery Analysis

The analysis of audio is another vital forensic component of the suggested framework since the modern state-of-the-art systems generate extremely realistic synthesized voices that can imitate the natural human voice with remarkable accuracy. Although there have been significant advances in neural speech synthesis technologies, synthesized human voice often includes imperfections, such as spectral inconsistencies, vocoder artifacts, temporal inconsistencies, and distorted frequencies. Natural speech signals generated via acoustic processes usually retain all physiologic features that are not necessarily reproduced by synthesized speech generators that emphasize perceptual realism over physiologic realism. Thus, unnatural features of synthesized audio may include smooth spectra, lower-frequency variation, and irregular harmonics and timing transitions.

In order to identify acoustic discrepancies, the aforementioned auditory forensic model assesses a comprehensive range of acoustic features that complement one another. These acoustic features include spectral entropy, variation in the zero-crossing rate, the silence ratio, mel-spectrum consistency, high frequency energy distribution, and speech duration continuity. The design and processing flow of the aforementioned audio forensic system is illustrated in Figure 3.

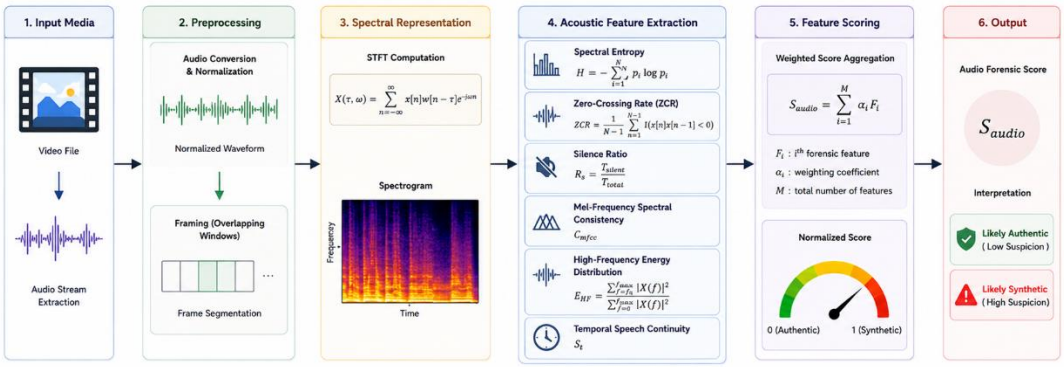


Figure 3: Audio forensic analysis pipeline

Initially, the audio stream is separated from the input media and converted into a normalized waveform representation. The signal is subsequently divided into overlapping temporal windows for frame-level acoustic analysis. Let: x[n] represent the discrete audio signal sampled from the input media. To analyze spectral properties, the Short-Time Fourier Transform (STFT) is applied:

$$X(\tau, \omega) = \sum_{n=-\infty}^{\infty} x[n]w[n-\tau]e^{-j\omega n}$$

where:

- x[n] denotes the audio waveform,
- w[n] represents the temporal analysis window,
- τ corresponds to the temporal frame index,
- ω denotes the frequency component.

The generated spectrogram representation enables detailed examination of spectral irregularities frequently introduced during neural speech synthesis. To evaluate spectral complexity and randomness, spectral entropy is estimated as:

$$H = -\sum_{i=1}^{N} p_i \log p_i$$

where:

- p_i represents the normalized spectral probability distribution,
- N corresponds to the total number of spectral bins.

Authentic human speech generally exhibits naturally varying spectral entropy distributions due to physiological vocal tract dynamics and environmental acoustic conditions. In contrast, synthetic speech often demonstrates over-smoothed spectral structures resulting in reduced entropy variability. The proposed framework additionally computes the Zero-Crossing Rate (ZCR) to measure temporal signal oscillation characteristics:

$$ZCR = \frac{1}{N-1}\sum_{n=1}^{N-1} oI(x[n]x[n-1] < 0)$$

where:

- I(·) denotes the indicator function,
- N represents the number of audio samples.

Irregular ZCR fluctuations frequently indicate vocoder instability or synthesis artifacts associated with generated speech signals.To further evaluate high-frequency preservation, the spectral energy ratio is estimated:

$$E_{HF} = \frac{\sum_{f=f_h}^{f_{max}} |X(f)|^2}{\sum_{f=0}^{f_{max}} |X(f)|^2}$$

where:

- f_h denotes the high-frequency threshold,
- f_{max} corresponds to the maximum observable frequency component.

Synthetic speech generation pipelines frequently suppress high-frequency components due to neural smoothing operations and vocoder reconstruction limitations. Consequently, abnormal high-frequency energy distributions may indicate manipulated audio generation.

The final audio forensic score is computed by aggregating all extracted acoustic indicators:

$$S_{audio} = \sum_{i=1}^{M} \alpha_i F_i$$

where:

- F_i denotes the i[th] extracted forensic feature,
- α_i represents the corresponding weighting coefficient,
- M corresponds to the total number of audio forensic indicators.

The audio analysis module provides interpretable acoustic evidence regarding suspicious speech generation characteristics and contributes complementary forensic information to the overall multi-domain decision framework.

2.3 Facial and Spatial Inconsistency Analysis

Facial and spatial analysis is among the main forensic modules of the proposed framework due to the fact that manipulated visual media often include minor inconsistencies that deviate from the natural geometry of the facial features. Even though current deep learning methods can generate images with visually similar appearances, they are unable to reproduce fine spatial relationships, facial symmetry, and geometric consistency of facial features.

In contrast to true facial image creation that is created via the process of camera-based physical capture, facial parts synthesis pipelines employed by artificial media generation are prone to independent recreation of facial segments using latent space transformation, neural interpolation, and face-swap. This leads to the appearance of facial structure inconsistencies like facial asymmetry, improper landmark geometry, blurry boundaries, unusual texture of the face, smooth jawline, and blending artifacts. The facial forensic method detects such inconsistencies by evaluating geometric landmarks, facial symmetry, and facial structure edges.

Initially, facial regions are extracted from individual video frames using RetinaFace-based face localization. The detected facial region is subsequently normalized and forwarded to the landmark extraction module. Let:

$F_i \in R^{H \times W \times 3}$

represent the extracted facial frame, where:

- H and W denote spatial dimensions,
- F_i corresponds to the i[th] facial frame.

Facial landmark localization is performed using MediaPipe Face Mesh, which extracts dense facial keypoints describing geometric facial structure:

$$L = \{(x_1, y_1), (x_2, y_2), \ldots, (x_n, y_n)\}$$

where:

- L denotes the facial landmark set,
- n represents the total number of detected landmarks.

To evaluate geometric symmetry, the proposed framework computes average bilateral landmark deviation relative to the facial center axis

$$A_{sym} = \frac{1}{N}\sum_{i=1}^{N} \left| d_i^L - d_i^R \right|$$

where:

- d_i^L and d_i^R denote corresponding left and right landmark distances,
- N corresponds to the total number of symmetric landmark pairs.

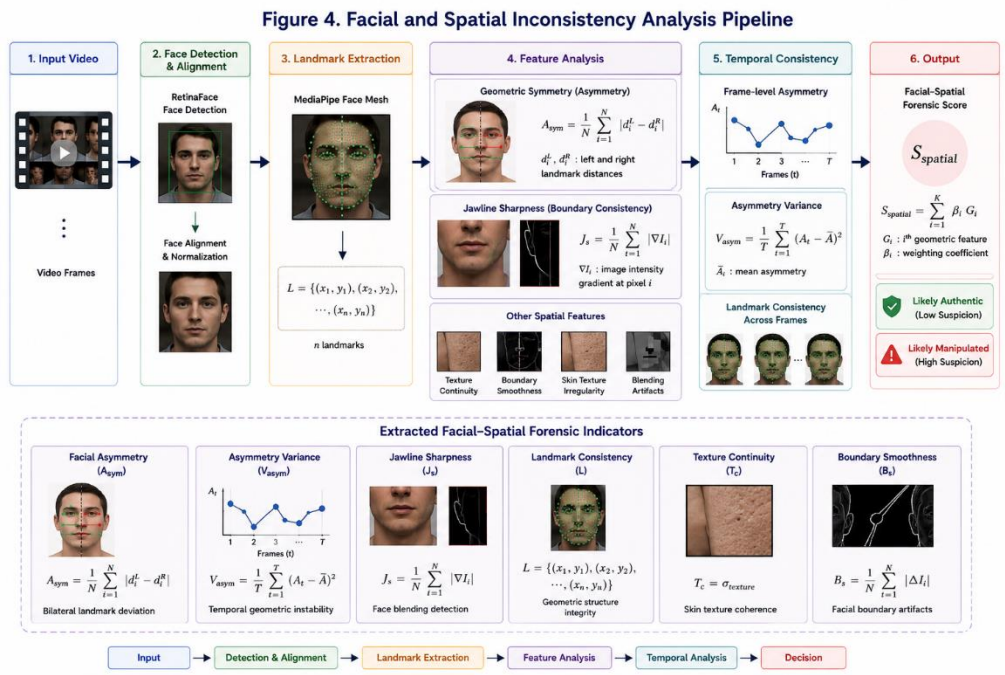


Figure 4: Facial and spatial inconsistency analysis pipeline

Authentic facial structures generally demonstrate naturally balanced geometric relationships, whereas manipulated content frequently introduces asymmetrical distortions caused by imperfect neural blending or latent-space misalignment. To further evaluate boundary consistency, jawline sharpness analysis is performed using spatial gradient estimation:

$$J_s = \frac{1}{N}\sum_{i=1}^{N} \left| \nabla I_i \right|$$

where:

- ∇I_i denotes the image intensity gradient at pixel i,
- J_s represents the estimated jawline sharpness score.

Edge softening techniques in face swapping and neural fusion operations often smoothen facial edges to avoid any visual artifacts that might be created by the process, hence making the edges less sharp at the facial edges. Moreover, geometric variability for frame asymmetry is determined to assess consistency in time sequences as follows:

$$V_{asym} = \frac{1}{T}\sum_{t=1}^{T}(A_t - \overline{A})^2$$

where:

- A_t denotes frame-level asymmetry estimation,
- $\overline{A}$ represents the temporal mean asymmetry value,
- T corresponds to the total number of analyzed frames.

Manipulated videos frequently demonstrate unstable geometric relationships across neighboring frames due to temporal inconsistency during synthesis generation. The final facial-spatial forensic score is computed through weighted aggregation of all extracted geometric indicators:

$$S_{spatial} = \sum_{i=1}^{K}\beta_i G_i$$

where:

- G_i denotes the i[th] geometric forensic feature,
- β_i represents the corresponding weighting coefficient,
- K corresponds to the total number of spatial forensic indicators.

The facial and spatial analysis module provides interpretable geometric evidence regarding suspicious facial inconsistencies and contributes one of the strongest discriminative components within the proposed multi-domain forensic framework.

2.4 Temporal and Motion Consistency Analysis

Temporal consistency evaluation plays an important role in forensic media authentication, since videos with tampering often contain abnormal motion dynamics and inter-frame inconsistencies, which differ from real human motion dynamics. While current generative models greatly improve the static visual realism of videos, consistent motion between frames continues to pose a significant problem during synthetic video generation. Real videos show physically constrained motions caused by human movement laws, camera movements, lighting conditions, and temporal interactions among objects.

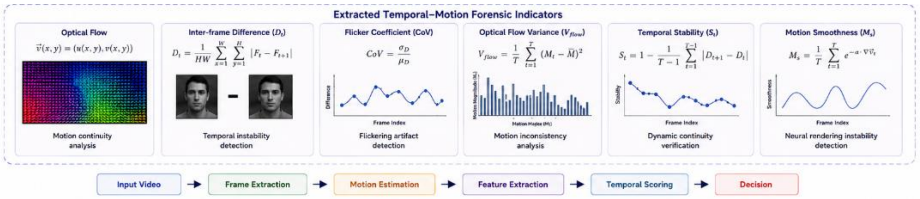


Figure 5: Temporal and motion consistency analysis pipeline

Conversely, tampered videos tend to display some specific temporal weaknesses, such as frame flickering, facial jitter, inconsistent motion flow, non-linear motion changes, temporal smoothing errors, and chaotic frame differences. This may be due to single-frame synthesis, poor motion estimation, unstable neural rendering, and temporal misalignment issues. The motion forensic system evaluates the mentioned discrepancies through motion consistency evaluation, optical flow estimation, inter-frame inconsistency measurement, and temporal consistency

evaluation. The execution process of the temporal verification approach is shown in Figure 5.Initially, consecutive video frames are extracted and normalized for temporal analysis. Let:

F_t, F_{t+1} represent two consecutive video frames. To estimate motion continuity between adjacent frames, dense optical flow analysis is performed:

$$v(x,y) = \big(u(x,y), v(x,y)\big)$$

where:

- u(x,y) and v(x,y) denote horizontal and vertical motion components,
- v(x,y) represents the optical flow vector at pixel location (x,y).

Inter-frame temporal variation is computed as:

$$D_t = \frac{1}{HW}\sum_{x=1}^{W}\sum_{y=1}^{H}|F_t(x,y) - F_{t+1}(x,y)|$$

where:

- H and W denote frame dimensions,
- D_t represents the frame-difference score.

The proposed framework additionally evaluates optical flow variance across temporal sequences:

$$V_{flow} = \frac{1}{T}\sum_{t=1}^{T}(M_t - \bar{M})^2$$

where:

- M_t denotes motion magnitude estimation at frame t,
- $\bar{M}$ represents the average motion magnitude,
- T corresponds to the total number of analyzed frames.

Videos containing synthetic manipulations generally exhibit unstable optical flow distributions and irregular temporal behavior compared to authentic videos with naturally smooth motion continuity. The final temporal forensic score is computed through weighted aggregation of temporal indicators:

$$S_{temporal} = \sum_{i=1}^{P}\gamma_i T_i$$

where:

- T_i denotes the i^{th} temporal forensic feature,
- γ_i represents the weighting coefficient,
- P corresponds to the total number of temporal indicators.

The temporal-motion module contributes interpretable dynamic evidence regarding abnormal motion behavior and frame-level inconsistencies within manipulated media.

2.5 Frequency-Domain Forensic Analysis

Frequency Domain Analysis is another critical forensic element of the framework due to the presence of hard-to-notice spectral anomalies that are created by modern generative systems. While the manipulated videos can seem highly plausible from a visual perspective for human perception, their synthetic pipelines can generate anomalous distributions of frequencies, periodic noise, and inconsistent spectra caused by upsampling processes, GANs, diffusion models, and re-compressions.

While unlike the actual videos obtained using physical imaging devices, the synthesis process of video forgery necessarily leads to changes to the original statistical distribution of spatial frequencies. Generally, natural images contain frequency properties physically consistent with their optical acquisition, sensor noise, illumination differences, and the continuity of texture properties. However, the frequency inconsistencies found in manipulated images include unusual high-frequency filtering, periodicity in spectra, repetitive texture patterns, GAN fingerprints, unauthentic Fourier spectra distribution, and wavelet behavior. The reason for such inconsistencies in the frequency domain lies in the fact that generative models pay attention to the visual authenticity of an image in the spatial domain but fail to accurately reproduce its frequency properties. The described frequency-domain analysis module examines these inconsistencies using Fourier spectrum analysis, frequency energy estimation, wavelet decomposition, and frequency consistency measures. The operation process of this frequency domain analysis pipeline is illustrated in Figure 6.

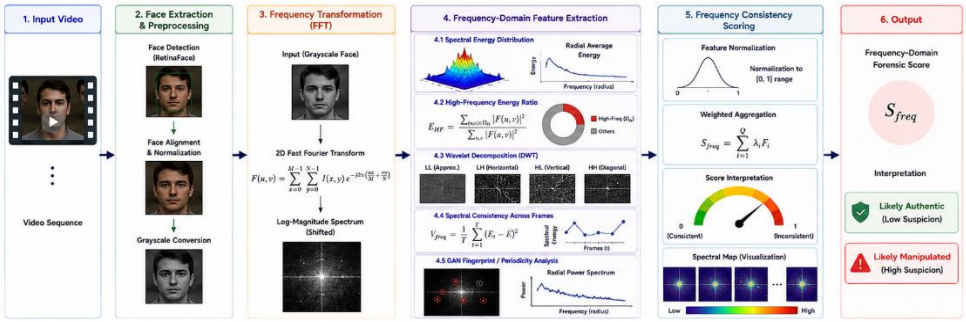


Figure 6: Frequency-domain forensic analysis pipeline

Initially, facial regions extracted from video frames are converted into grayscale frequency representations prior to spectral analysis. Let: I(x,y) represent the spatial-domain image intensity function. To analyze spectral characteristics, the two-dimensional Fast Fourier Transform (FFT) is applied:

$$F(u,v) = \sum_{x=0}^{M-1} \sum_{y=0}^{N-1} I(x,y) e^{-j2\pi\left(\frac{ux}{M}+\frac{vy}{N}\right)}$$

where:

- I(x,y) denotes image intensity values,
- F(u,v) represents the frequency-domain spectrum,
- M and N correspond to image dimensions.

Authentic images generally demonstrate naturally distributed spectral energy patterns, whereas manipulated images frequently contain abnormal periodic frequency concentrations caused by neural generation artifacts. To evaluate spectral energy consistency, the proposed framework computes high-frequency energy distribution:

$$E_{HF} = \frac{\sum_{(u,v)\in\Omega_H} |F(u,v)|^2}{\sum_{u,v} |F(u,v)|^2}$$

where:

- Ω_H denotes the high-frequency spectral region,
- E_{HF} represents the high-frequency energy ratio.

Synthetic media frequently suppresses high-frequency details due to smoothing effects introduced during neural rendering and image reconstruction processes. Consequently, abnormal

high-frequency energy distributions may indicate manipulated content generation. To further analyze localized spectral irregularities, discrete wavelet decomposition is additionally performed:

$$W(a,b) = \frac{1}{\sqrt{a}} \int x(t) \psi \left(\frac{t-b}{a} \right) dt$$

where:

- a denotes the scaling parameter,
- b represents the translation parameter,
- $\psi(\cdot)$ corresponds to the mother wavelet function.

Wavelet analysis enables localized examination of texture irregularities and multi-scale spectral inconsistencies commonly introduced during synthetic image generation. The proposed framework additionally evaluates spectral variance across neighboring frames to measure temporal frequency stability:

$$V_{freq} = \frac{1}{T} \sum_{t=1}^{T} (E_t - \overline{E})^2$$

where:

- E_t denotes frame-level spectral energy estimation,
- $\overline{E}$ represents the average spectral energy value,
- T corresponds to the number of analyzed frames.

Manipulated videos frequently exhibit unstable spectral distributions across temporal sequences due to frame-wise generation inconsistencies and recompression artifacts. The final frequency-domain forensic score is computed through weighted aggregation of spectral indicators:

$$S_{freq} = \sum_{i=1}^{Q} \lambda_i F_i$$

where:

- F_i denotes the i^{th} frequency-domain forensic feature,
- λ_i represents the weighting coefficient,
- Q corresponds to the total number of spectral indicators.

The frequency-domain analysis module provides interpretable spectral evidence regarding hidden synthesis artifacts and contributes complementary forensic information that may remain undetectable in purely spatial or temporal analysis frameworks.

2.6 Multi-Domain Forensic Fusion and Decision Mechanism

The proposed framework perform localized forensic analysis on detected anomalies in the input media. Each component produces its own confidence score, which is then combined in the final stage of analysis to calculate the overall media manipulation probability. The proposed framework architecture is illustrated in Figure 7.

Firstly, the input multimedia content is preprocessed through a holistic process that includes extraction of video frames, audio extraction, localization of the face region, meta-data extraction, and region of interest (ROI) detection. Thereafter, the extracted features are simultaneously fed to several forensic analysis modules working independently in parallel.

The modular approach allows for the simultaneous evaluation of suspicious behavior from multiple forensic perspectives, thus not relying on one type of feature only. For each forensic module, a suspiciousness score is estimated as:

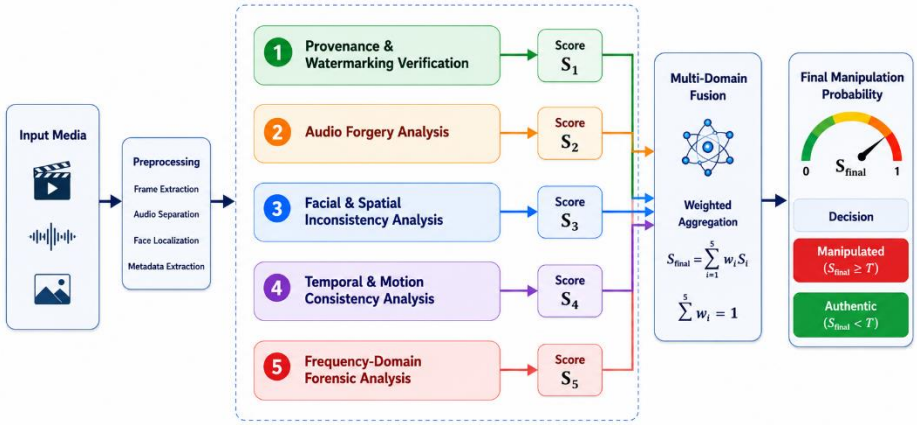


Figure 7: Proposed multi-domain forensic analysis framework for synthetic media detection.

$$S_i = f_i(X)$$

where:

- S_i denotes the forensic score produced by the i^{th} module
- $f_i$represents the corresponding forensic analysis function,
- X denotes the input media sample.

The individual forensic scores are aggregated using weighted multi-domain fusion:

$$S_{final} = \sum_{i=1}^{N} w_i S_i$$

where:

- S_{final} represents the final manipulation score,
- $w_i$denotes the weighting coefficient assigned to each forensic domain,
- N corresponds to the total number of forensic modules.

The weighting coefficients satisfy the normalization constraint:

$$\sum_{i=1}^{N} w_i = 1$$

In light of the fact that the framework proposed framework is mostly concerned with visual forensic analysis, greater weightage was accorded to facial-spatial and temporal-frequency analysis modules, while provenance and audio analyses provided complementary indicators for forensics. The weights assigned through experimentation are as follows:

Forensic Module	**Weight Coefficient**
Provenance & Watermarking Verification	(w_1 = 0.10)
Audio Forgery Analysis	(w_2 = 0.15)
Facial & Spatial Inconsistency Analysis	(w_3 = 0.30)
Temporal & Motion Consistency Analysis	(w_4 = 0.25)
Frequency-Domain Forensic Analysis	(w_5 = 0.20)

Table 2. Weight coefficients assigned to individual forensic analysis modules

This high contribution to facial-spatial analysis and temporal analysis is attributed to the high discriminating ability of geometry and motion distortions that are often introduced into

synthetic images. Additionally, frequency domain analysis provides useful spectral evidence pertaining to synthetic media creation by means of GANs and diffusion. On the other hand, provenance analysis and audio analysis constitute secondary evidence based on metadata and sound. Finally, the classification score is calculated using a threshold-based score interpretation method:

$$y = \begin{cases} Manipulated, S_{final} \geq T \\ Authentic, S_{final} < T \end{cases}$$

where:

- T denotes the experimentally selected decision threshold,
- y represents the final classification label.

Unlike standard black-box architectures, the proposed method will retain meaningful forensic traces that are independently produced by each module. As such, this method does more than merely predict the presence of media manipulation; it also identifies the forensic features whose importance was greatest in making this prediction.

3. EXPERIMENTAL RESULTS AND PERFORMANCE EVALUATION

The proposed multi-domain forensic framework was empirically tested on 455 videos, which were sampled from the Celeb-DF and FaceForensics++ (FF++) datasets. The sampling process was conducted such that the test set includes real videos, as well as videos that have been manipulated through different synthesis methods, facial expressions, illumination conditions, compression schemes, and motion events. The performance of the proposed framework was evaluated using standard classification metrics including accuracy, precision, recall, and F1-score. The classification accuracy is computed as:

$$Accuracy = \frac{TP + TN}{TP + TN + FP + FN}$$

while precision and recall are defined as:

$$Precision = \frac{TP}{TP + FP} \; Recall = \frac{TP}{TP + FN}$$

The harmonic mean between precision and recall is calculated using the F1-score:

$$F1 = 2 \times \frac{Precision \times Recall}{Precision + Recall}$$

where: TP denotes true positives, TN represents true negatives, FP corresponds to false positives, FN denotes false negatives.

Table 3 summarizes the comparative performance of individual forensic modules and the proposed multi-domain fusion framework.

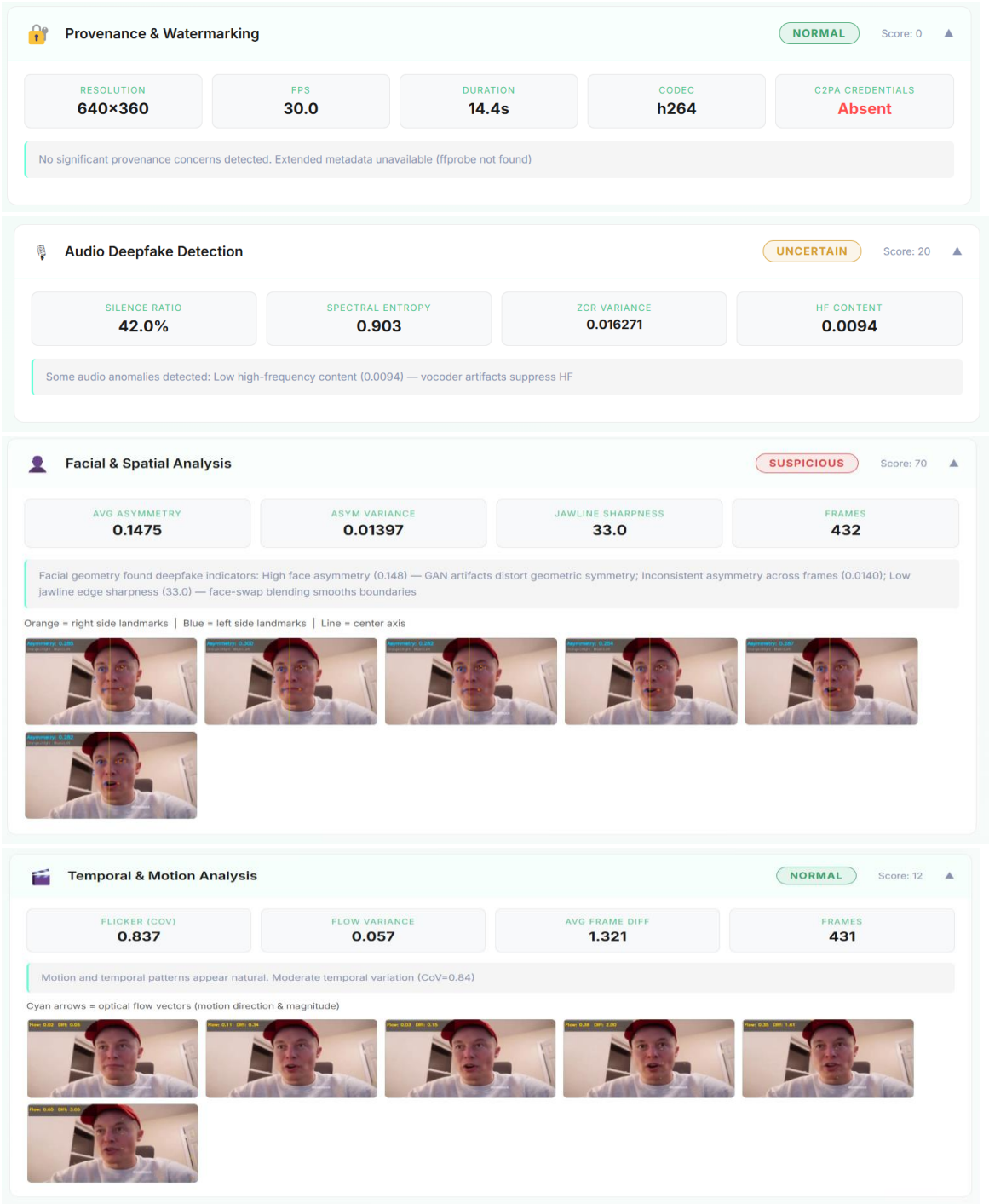
`	Accuracy	Precision	Recall	F1-Score
Provenance & Watermarking	81.3%	80.7%	82.1%	81.4%
Audio Forensic Analysis	84.6%	83.9%	85.2%	84.5%
Facial & Spatial Analysis	89.7%	89.1%	90.4%	89.7%
Temporal & Motion Analysis	88.4%	87.8%	89.1%	88.3%
Frequency-Domain Analysis	90.3%	89.8%	90.9%	90.2%
Proposed Multi-Domain Fusion	91.5%	91.0%	92.1%	91.4%

Table 3: Comparative performance of individual forensic modules and the proposed multi-domain fusion framework.

From the experimental results, the multi-domain forensic fusion scheme proposed by us clearly outperforms independent forensic schemes. Forensic schemes based on the combination of

different forensic evidences show their strength in defending manipulated videos from visual realism. As for single forensic module, frequency domain forensic scheme was able to provide the best performance, as it is capable of detecting invisible artifacts caused by neural network-based manipulation process. Facial-spatial forensic scheme also performed excellently because manipulated videos usually have irregular landmarks and asymmetric faces.

In addition to frequency and spatial domain forensic schemes, there were many pieces of forensic evidence generated from temporal domain forensic scheme as it detects the flickering effect and the inconsistency pattern among consecutive frames. Figure 8 presents example forensic outputs generated from each analysis module within the proposed framework.



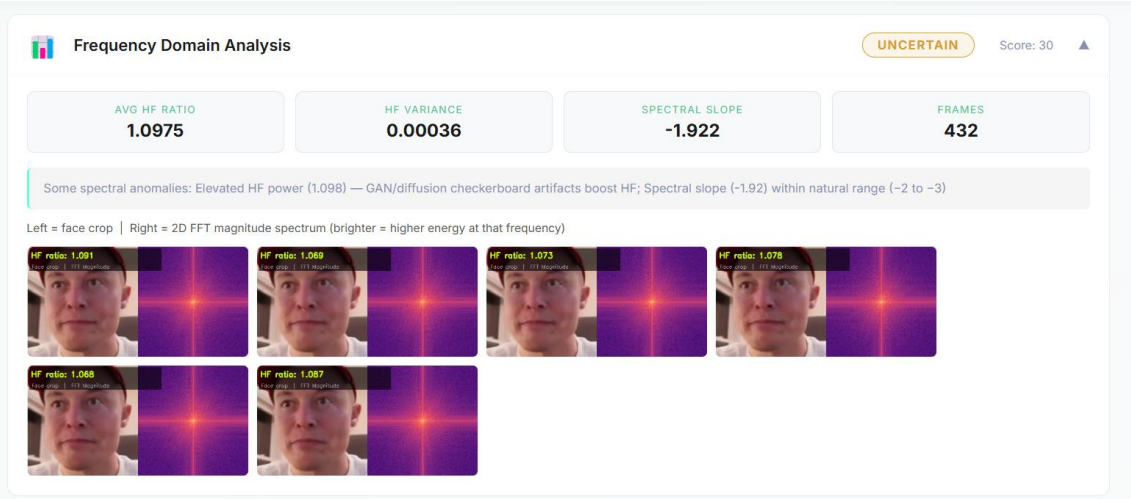


Figure 8: Forensic outputs generated from each analysis module within the proposed framework.

As can be seen from the forensic outputs of manipulation, the fact is that the manipulated videos have been consistently found to show inconsistencies in several forensic domains. The abnormalities associated with frequency domain analysis include the inconsistent spectrum and the presence of periodic patterns, while in temporal domain analysis, the video shows instabilities in motion flow. Furthermore, the facial-spatial analysis shows inconsistency as well.

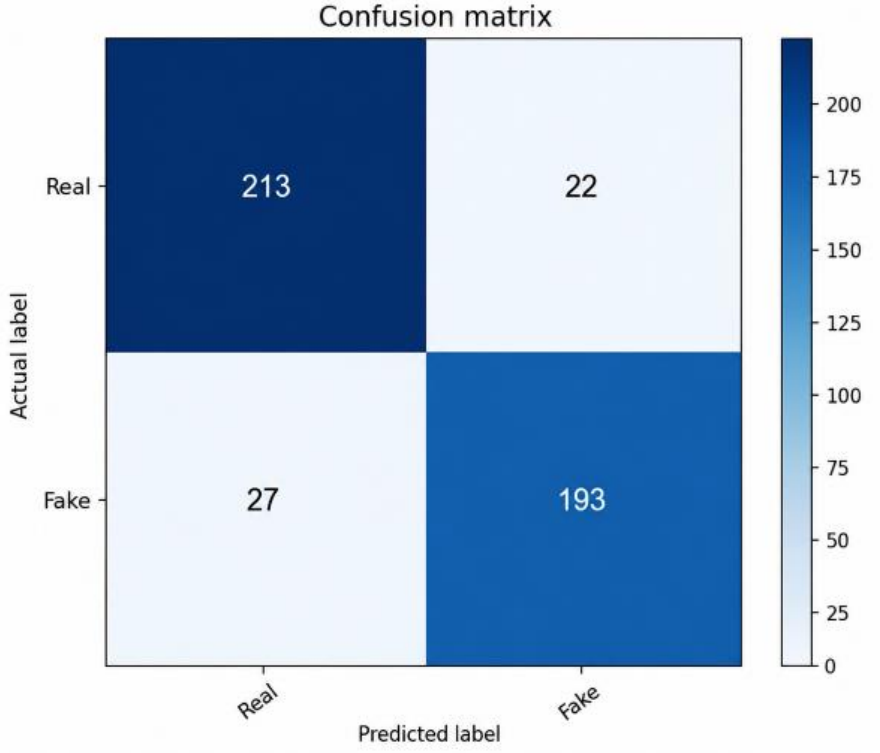


Figure 9: Confusion matrix obtained using the proposed multi-domain forensic fusion framework.

The confusion matrix clearly shows that the proposed model is able to effectively classify most of the genuine as well as manipulated examples with reasonably low rates of false positives and false negatives. The use of heterogeneous forensic features significantly diminishes reliance upon the individual artifact type.

In conclusion, the results obtained during the experiments clearly indicate that the combination of the five above-mentioned components is highly effective for contemporary media manipulation detection.

CONCLUSION

This study has introduced a multi-domain forensic framework towards detection of manipulated media based on the CNN-LSTM-Spline detection model. While traditional frameworks focus on using spatial deep learning features for media manipulation detection, the presented framework employs a combination of provenance and watermark verification, audio forensic analysis, facial-spatial inconsistency, temporal-motion inconsistency, and frequency-domain forensic techniques in one weighted fusion architecture. The presented multi-domain forensic framework is aimed at detecting the presence of suspicious anomalies associated with the creation process of synthetic media, such as inconsistent encoding structure, frequency-domain abnormalities, geometric distortions, motion anomalies, and temporal inconsistencies.

The experiment, performed with a sample of 455 videos taken from Celeb-DF and FaceForensics++ data sets, revealed a detection accuracy rate of 91.5%. In addition, the proposed framework showed high resilience to realistic media manipulation. As the experimental results show, the combination of different forensic indications significantly enhances detection performance as well as makes the forensic process more interpretable compared to individual forensic modules. Overall, the proposed framework proves itself to be a powerful and interpretable technique for modern media manipulation detection.

REFERENCES

1. M. S. Rana, M. N. Islam, S. M. Shatabda, and A. H. M. R. Imon, “Deepfake detection: A systematic literature review,” *IEEE Access*, vol. 10, pp. 25494–25513, 2022.
2. D. Güera and E. J. Delp, “Deepfake video detection using recurrent neural networks,” in *Proc. IEEE Int. Conf. Advanced Video and Signal Based Surveillance (AVSS)*, 2018, pp. 1–6.
3. E. Altuncu, V. N. L. Franqueira, and S. Li, “Deepfake: Definitions, performance metrics and standards, datasets, and a meta-review,” *Frontiers in Big Data*, vol. 7, p. 1400024, 2024.
4. A. Diel et al., “Human performance in detecting deepfakes: A systematic review and meta-analysis of 56 papers,” *Computers in Human Behavior Reports*, vol. 16, p. 100538, 2024.
5. S. Maxmudjanov, A. Primbetov, and A. Alimbaeva, “Human perception versus artificial intelligence in deepfake video detection: An empirical study,” *Al-Farg’oniy Avlodlari*, vol. 1, no. 4, pp. 83–87, 2025.
6. S. Maxmudjanov, A. Primbetov, and A. Naimov, “Deepfake detection using a hybrid ResNeXt and LSTM architecture,” *Al-Farg’oniy Avlodlari*, vol. 1, no. 2, pp. 87–94, 2025.
7. J. Wu, K. Feng, X. Chang, and T. Yang, “A forensic method for deepfake image based on face recognition,” in *Proc. 4th High Performance Computing and Cluster Technologies Conf. and 3rd Int. Conf. Big Data and Artificial Intelligence*, 2020, pp. 104–108.
8. S. Sohail, S. M. Sajjad, A. Zafar, Z. Iqbal, Z. Muhammad, and M. Kazim, “Deepfake detection using deep learning: A unified forensic approach to detect AI-generated images and videos with fusion of eye, nose, and mouth landmarks,” *Computer Science and Mathematics*, Feb. 2025.

9. S. H. Silva, M. Bethany, A. M. Votto, I. H. Scarff, N. Beebe, and P. Najafirad, “Deepfake forensics analysis: An explainable hierarchical ensemble of weakly supervised models,” *Forensic Science International: Synergy*, vol. 4, p. 100217, 2022.
10. G. O. Y. L. F. Lundström-Imanov and N. Abdullayeva, “Verifiable provenance and watermarking for generative AI: An evidentiary framework for international operational law and domestic courts,” *arXiv preprint arXiv:2605.21002*, 2026.
11. F. Haugg, M. Elgendi, and C. Menon, “GRGB rPPG: An efficient low-complexity remote photoplethysmography-based algorithm for heart rate estimation,” *Bioengineering*, vol. 10, no. 2, p. 243, 2023.
12. Q. He et al., “GazeForensics: DeepFake detection via gaze-guided spatial inconsistency learning,” *Neural Networks*, vol. 180, p. 106636, 2024.
13. T. Jung et al., “DeepVision: Deepfakes detection using human eye blinking pattern,” *IEEE Access*, vol. 8, pp. 83144–83154, 2020.
14. J. Cech and T. Soukupova, “Real-time eye blink detection using facial landmarks,” *Center for Machine Perception, Czech Technical University in Prague*, pp. 1–8, 2016.
15. Google Research, “MediaPipe Face Mesh,” 2023. [Online]. Available: https://mediapipe.dev/
16. A. Susi, V. Akila, and V. Govindasamy, “Utilizing rPPG signal synchronization and deep learning techniques for deepfake video detection,” *IEEE Access*, 2025.

EVALUATION OF THE EFFECTIVENESS OF STRENGTHENING THE FOUNDATION SOIL OF MULTI-STOREY BUILDINGS USING A SOIL CUSHION AND DEEP SOIL MIXING TECHNOLOGY IN REDUCING SEISMIC EFFECTS

Sh.S. Yuldashev[1], M.B. Boytemirov[2], A.Sh. Abdunazarov[3]
Doctor of Technical Sciences, Professor, Namangan State Technical University[1]
PhD in Technical Sciences, Docent, Namangan State Technical University[2]
PhD Student, Namangan State Technical University[3]
https://doi.org/10.5281/zenodo.20697242

Abstract. *This article analyzes the effectiveness of a soil cushion and Deep Soil Mixing technology in reducing the impact of seismic waves, taking into account the physical and mechanical properties of the foundation and foundation soil of a multi-storey building. A 12-storey building and the underlying soil mass were selected as the research object, and the calculations were performed in PLAXIS 3D using the finite element method. In the numerical model, the geometric and physical-mechanical properties of the building, foundation, natural soil, soil cushion, and Deep Soil Mixing elements were considered. The seismic action was applied based on a real accelerogram, and observation points were assigned at the basement level, on each floor, and at the roof level of the building. Three cases were compared in the study: the natural soil condition, the case with a soil cushion, and the case with Deep Soil Mixing technology. The results showed that, under natural soil conditions, displacement, velocity, and acceleration values increased as the building height increased. When a soil cushion was applied, the reduction efficiency was 2.63–8.84% for displacement, 4.40–16.02% for velocity, and 4.69–15.68% for acceleration. When Deep Soil Mixing was applied, displacement decreased by 9.41–22.61%, velocity by 3.65–17.91%, and acceleration by 6.18–20.97%. The soil cushion reduced the dynamic response of the building to a certain extent; however, Deep Soil Mixing technology demonstrated relatively higher efficiency in reducing displacement and acceleration. Therefore, for multi-storey buildings located in seismically active regions, strengthening the foundation soil using Deep Soil Mixing can be considered an appropriate engineering solution.*

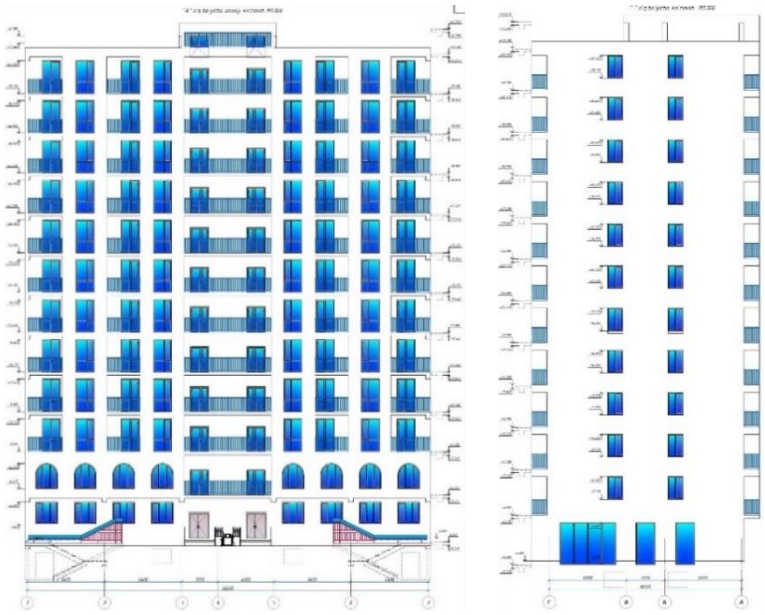
Keywords: *soil cushion, Deep Soil Mixing, settlement, foundation, weak soil, differential settlement, numerical modelling, PLAXIS 3D.*

INTRODUCTION

In modern construction practice, when multi-storey buildings are constructed on weak and highly compressible soils, the occurrence of total and differential settlements is inevitable. This leads to the development of additional stresses in structural elements, uneven distribution of deformations, and, in some cases, a decrease in the operational reliability of the structure. In particular, for 10–15-storey buildings, both the magnitude of settlement and its non-uniformity represent an important engineering problem [1].

Numerous scientific studies have been conducted to investigate the behaviour mechanism of foundations on weak soils and to develop methods for reducing settlement. In classical studies,

soil compressibility, deformation modulus, and consolidation processes under loading have been considered as the main factors. In particular, the consolidation theory developed by Chen Fang and his colleagues forms a fundamental basis for calculating soil settlement. In later studies, factors such as the nonlinear properties of soil, loading rate, and interlayer interaction were also taken into account [2].



a. ***b.***

Figure 1. Front and side views of the building

In recent years, modern methods of foundation soil improvement have been widely developed, among which soil cushions and Deep Soil Mixing technology occupy a special place [3]. Woods (1968) studied the issues of reducing wave propagation in soil masses and redistributing loads. These studies demonstrated that deformations can be reduced by artificially improving the soil, and the effectiveness of column-type reinforcement systems was substantiated by the researcher [4].

A soil cushion reduces contact pressures by distributing the load over a wider area in the upper layer and makes deformations relatively more uniform. However, the effect of this method is mainly limited to near-surface layers [5]. In contrast, Deep Soil Mixing technology provides high strength and deformation resistance in deeper layers by cementing the soil. Deep Soil Mixing columns transfer loads to deeper layers, reduce total settlement, and increase the overall stiffness of the foundation soil [6].

Although a number of modern studies have demonstrated the effectiveness of using soil cushions and column-type reinforcement methods separately [7], the issue of their combined application has not been studied in sufficient depth. This problem remains especially relevant for multi-storey buildings, where deformation control in both upper and deeper soil layers is required simultaneously.

MATERIALS AND METHOD

The problem of studying the effect of seismic waves on a building is considered as a three-dimensional dynamic problem of the theory of elasticity in an infinite medium. Since the solution domain has a complex geometry and is heterogeneous, obtaining an analytical solution is not feasible. Therefore, the finite element method, which is convenient for solving such problems, was used. As is known, the finite element method can only be applied to a finite domain. For this

reason, a finite region of interest is conceptually extracted from the infinite medium, and non-reflecting boundary conditions are applied at its boundaries to allow waves to pass through without reflection.

In solving this problem, the selected computational model was assumed to be a soil mass with a length of 300 m, a width of 50 m, and a depth of 30 m. The groundwater level was located at a depth of 1.5 m. The building has a rectangular plan with a length of 33.2 m and a width of 15 m. The basement depth is 2.7 m, the plinth height is 0.6 m, the storey height is 3.3 m, and the total height of the building is 40.2 m (Figure 1).

To ensure that seismic waves propagate from the boundaries of the computational domain into the infinite medium without reflection, special boundary conditions were applied on the ADHJ, BCEF, ADCB, HJFE, and AHBE faces of the parallelepiped. The scheme for applying the boundary conditions is shown in Figure 2.

$$\text{ADHJ da } \left.\begin{matrix}\sigma_x = a\rho V_p\dot{u}\\ \tau_{xy} = b\rho V_s\dot{v}\\ \tau_{xz} = b\rho V_s\dot{w}\end{matrix}\right\},\qquad \text{BCEF da } \left.\begin{matrix}\sigma_x = -a\rho V_p\dot{u}\\ \tau_{xy} = -b\rho V_s\dot{v}\\ \tau_{xz} = -b\rho V_s\dot{w}\end{matrix}\right\},$$

$$\text{ADCB da } \left.\begin{matrix}\sigma_y = a\rho V_p\dot{u}\\ \tau_{yz} = b\rho V_s\dot{w}\\ \tau_{yx} = b\rho V_s\dot{v}\end{matrix}\right\},\qquad \text{HJFE da } \left.\begin{matrix}\sigma_y = -a\rho V_p\dot{u}\\ \tau_{yz} = -b\rho V_s\dot{w}\\ \tau_{yx} = -b\rho V_s\dot{v}\end{matrix}\right\},$$

$$\text{AHBE da } \left.\begin{matrix}\sigma_z = a\rho V_p\dot{w}\\ \tau_{zy} = b\rho V_s\dot{u}\\ \tau_{zx} = b\rho V_s\dot{v}\end{matrix}\right\} \qquad (1)$$

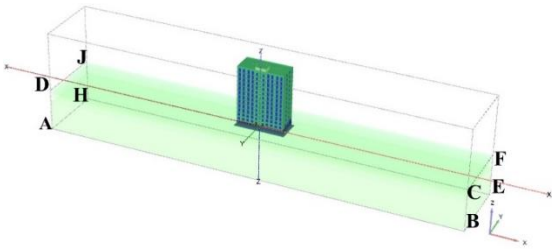


Figure 2. Application of boundary conditions

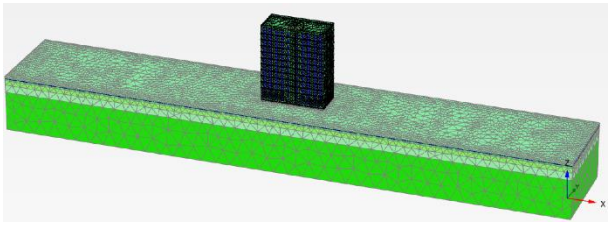


Figure 3. Finite element discretization of the model

The study domain was discretized into 47,473 finite elements and 99,354 nodes. The finite elements had the form of irregular tetrahedra. The order of the system of differential equations of motion was 298,062 (Figure 3).

The kinematic relation can be formulated as follows [8]:

$$\varepsilon = Lu \qquad (2)$$

L^T - transposed differential operator

$$L^T = \begin{bmatrix} \frac{\partial}{\partial x} & 0 & 0 & \frac{\partial}{\partial y} & 0 & \frac{\partial}{\partial z} \\ 0 & \frac{\partial}{\partial y} & 0 & \frac{\partial}{\partial x} & \frac{\partial}{\partial z} & 0 \\ 0 & 0 & \frac{\partial}{\partial z} & 0 & \frac{\partial}{\partial y} & \frac{\partial}{\partial x} \end{bmatrix} \qquad (3)$$

In the particular case of a plane stress state, the three strain components corresponding to the stress state are written as follows [9]:

$$\{\sigma\} = \begin{Bmatrix} \sigma_{xx} & \tau_{xy} & \tau_{xz} \\ \tau_{xy} & \sigma_{yy} & \tau_{yz} \\ \tau_{xz} & \tau_{yz} & \sigma_{zz} \end{Bmatrix} \quad (4)$$

The matrix ([D]) is determined from the following relationship between stress and strain [10]:

$$\begin{aligned} \varepsilon_x - (\varepsilon_x)_0 &= \frac{1}{E}\sigma_x - \frac{v}{E}(\sigma_y + \sigma_z); \\ \varepsilon_y - (\varepsilon_y)_0 &= \frac{1}{E}\sigma_y - \frac{v}{E}(\sigma_x + \sigma_z); \\ \varepsilon_z - (\varepsilon_z)_0 &= \frac{1}{E}\sigma_z - \frac{v}{E}(\sigma_x + \sigma_y); \\ \gamma_{ij} - (\gamma_{ij})_0 &= \frac{2(1+v)}{E}\tau_{ij}; \end{aligned} \quad (5)$$

From this:

$$[D] = \frac{E}{1-v^2}\begin{bmatrix} 1 & v & 0 \\ v & 1 & 0 \\ 0 & 0 & \frac{1-v}{2} \end{bmatrix} \quad (6)$$

The system of second-order linear differential equations describing the time-dependent motion of the volume under the action of dynamic loading is expressed as follows [8,11]:

$$[\boldsymbol{M}]\{\ddot{\boldsymbol{u}}(\boldsymbol{t})\} + [\boldsymbol{C}]\{\dot{\boldsymbol{u}}(\boldsymbol{t})\} + [\boldsymbol{K}]\{\boldsymbol{u}(\boldsymbol{t})\} = \{\boldsymbol{F}(\boldsymbol{t})\} \quad (7)$$

where $[\boldsymbol{M}]$ is the mass matrix, $[\boldsymbol{C}]$ is the damping matrix, $[\boldsymbol{K}]$ is the stiffness matrix, and $\{\boldsymbol{F}(\boldsymbol{t})\}$ is the dynamic load vector. The vectors $\{\boldsymbol{u}(\boldsymbol{t})\}$, $\{\dot{\boldsymbol{u}}(\boldsymbol{t})\}$ and $\{\ddot{\boldsymbol{u}}(\boldsymbol{t})\}$ representing displacement, velocity, and acceleration, respectively, were assumed to be continuous functions of time.

The obtained system was formulated based on the finite element method and solved numerically using the PLAXIS 3D software package. The general properties of the building, soil, soil cushion, and Deep Soil Mixing elements are presented in Table 1.

Table 1

Name	Unit	Symbol	Layers				
			Layer 1	Layer 2	Layer 3	Layer 4	Layer 5
General properties of the soil							
Soil model	Mohr–Coulomb						
Layer thickness	m	m	0,80	1,70	2,50	4,00	21,00
Unsaturated unit weight of soil	kN/m^3	γ_{unsat}	17	18	18	19	20
Saturated unit weight of soil	kN/m^3	γ_{sat}	18	19	19	20	21
Young's modulus	kN/m^2	E	10 000	40 000	60 000	45 000	60 000
Poisson's ratio	–	v	0,38	0,30	0,30	0,30	0,30
Internal friction angle	º	φ	19,2	31	18	33	35

Effective cohesion of soil	kN/m^2	c'_{ref}	10	1	24	45	0

General properties of the building			
Name	Unit	Symbol	Value
Model type	Elastic		
Young's modulus	kN/m^2	E	27 000 000
Poisson's ratio	–	v	0.2
Unit weight	kN/m^3	γ	24
Properties of the soil cushion			
Soil model	Mohr–Coulomb		
Unsaturated unit weight of soil	kN/m^3	γ_{unsat}	18,5
Saturated unit weight of soil	kN/m^3	γ_{sat}	19,5
Young's modulus	kN/m^2	E	95 000
Poisson's ratio	–	v	0,3
Internal friction angle	°	φ	36
Dilation angle	°	ψ	3
Depth	m	–	4
Properties of Deep Soil Mixing elements			
Model type	–	–	Elastic
Young's modulus	kN/m^2	E	8 000 000
Poisson's ratio	–	v	0.2
Unit weight	kN/m^3	γ	20
Cross-sectional area	m^2	A	0,283
Moment of inertia about the z-axis	m^4	I_2	$6{,}36 \cdot 10^{-3}$
Moment of inertia about the y-axis	m^4	I_3	$6{,}36 \cdot 10^{-3}$
Diameter	m	–	0,6
Depth	m	–	12
Number of elements	pcs	–	231

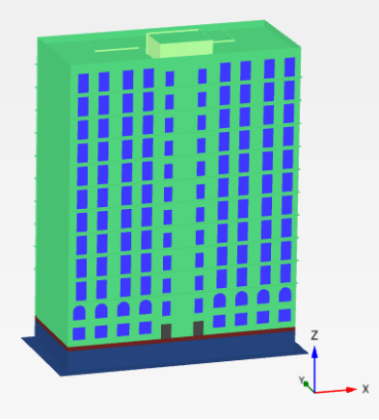


Figure 4. Building under natural ground conditions

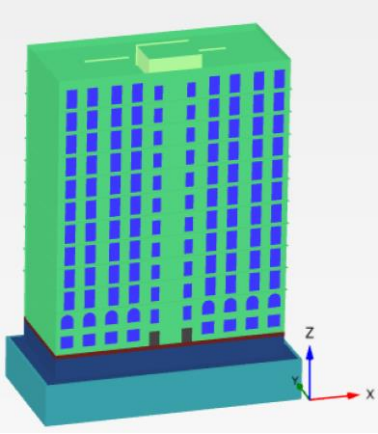


Figure 5. Building with a soil cushion

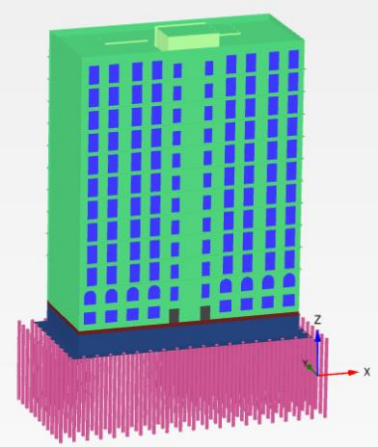


Figure 6. Building with Deep Soil Mixing

Based on the parameters presented in Table 1, a three-dimensional computational model of the building was developed. The model was formed taking into account the architectural

planning and structural design solutions of the building. The main geometric dimensions of the building, the floor configuration, and the load-bearing structural elements were considered in the numerical model. Based on this model, three computational cases were analyzed. In the first case, the building was modeled under natural ground conditions (Figure 4). In the second case, a 4 m thick soil cushion was placed beneath the building foundation (Figure 5). In the third case, Deep Soil Mixing elements were modeled beneath the building foundation, with a diameter of 0.6 m, a length of 12 m, a spacing of 2 m, and a total number of 231 elements (Figure 6).

In order to determine and compare the seismic waves affecting the building, one observation point was assigned on each floor of the building, making a total of 12 points, and additional observation points were also selected at the basement level and at the roof level of the building (Figure 7).

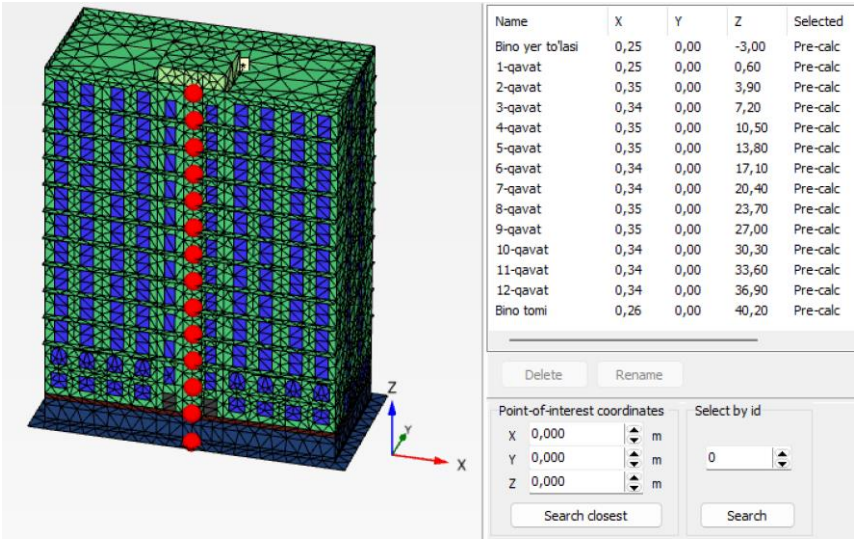


Figure 7. Observation points in the building

Seismic wave propagation was generated using a real accelerogram (Figure 8).

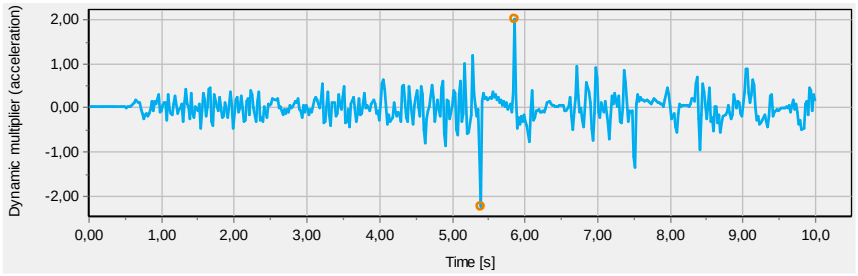


Figure 8. Real accelerogram [12] (The accelerogram coordinates were x=37.95 and y=67.02, with a magnitude of M=5.8).

In dynamic analyses, the proper selection of boundary conditions plays an important role in reducing the artificial reflection of seismic waves from the model boundaries. Therefore, in the PLAXIS 3D model, **Free-field** boundary conditions were assigned to the lateral boundaries X_{min} and X_{max}. For the bottom boundary Z_{min}, a **Compliant base** condition was adopted, since the seismic motion was applied to the model through this boundary. No special dynamic boundary condition was applied at the Y_{min} and Y_{max} boundaries or at the upper boundary Z_{max}. The Z_{max} boundary was considered as a free surface representing the ground surface.

RESULTS AND DISCUSSION

During the numerical modelling process, the seismic excitation applied on the basis of a real accelerogram propagated through the soil mass and was transmitted to the structure through the building foundation. The process of seismic wave propagation in the soil is presented in Figure 9.

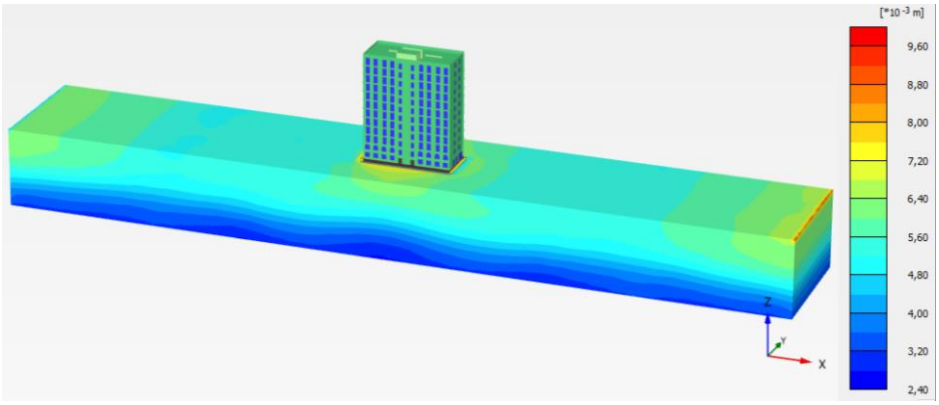


Figure 9. Process of seismic wave impact on the building

Based on the results of the numerical modelling, the maximum amplitude values of displacement, velocity, and acceleration in the building were determined, summarized in Table 2, and comparatively analyzed in terms of their effectiveness.

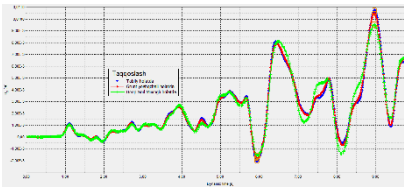


Figure 10. Time-history comparison graph of displacements at the basement level of the building

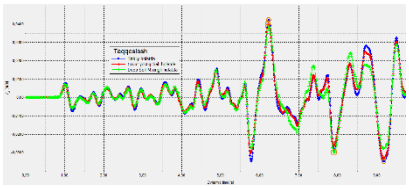


Figure 11. Time-history comparison graph of velocities at the basement level of the building

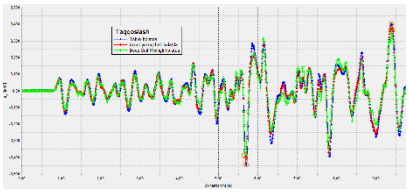


Figure 12. Time-history comparison graph of accelerations at the basement level of the building

The results obtained for the basement level of the building showed that strengthening the soil foundation leads to a reduction in dynamic parameters. Under natural soil conditions, the displacement at the basement level of the building was 10.77 mm. When a soil cushion was applied, the displacement decreased to 10.49 mm, corresponding to an efficiency of 2.63%. When Deep Soil Mixing technology was applied, the displacement decreased to 9.52 mm, and the efficiency reached 11.67% (Figure 10).

The velocity value under natural conditions was 4.21 cm/s, and when a soil cushion was applied, it decreased to 4.03 cm/s. In this case, the reduction efficiency in terms of velocity was 4.40%. When Deep Soil Mixing technology was applied, the velocity decreased to 3.84 cm/s, and the efficiency reached 8.77% (Figure 11).

The acceleration value under natural soil conditions was 0.446 m/s². When a soil cushion was applied, the acceleration decreased to 0.416 m/s², corresponding to an efficiency of 6.63%. When Deep Soil Mixing technology was applied, the acceleration decreased to 0.390 m/s², and the efficiency reached 12.36% (Figure 12). These results indicate that, at the basement level of the building, Deep Soil Mixing technology demonstrates higher effectiveness compared with the soil cushion.

The results obtained for the roof level of the building showed that strengthening the soil foundation also leads to a reduction in dynamic parameters at the upper floors. Under natural soil conditions, the displacement at the roof level of the building was 17.28 mm. When a soil cushion was applied, the displacement decreased to 16.54 mm, corresponding to an efficiency of 4.28%. When Deep Soil Mixing technology was applied, the displacement decreased to 15.55 mm, and the efficiency reached 10.02% (Figure 13).

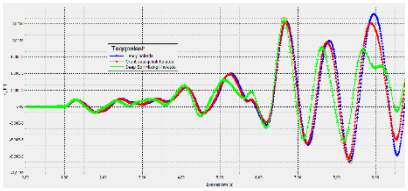


Figure 13. Time-history comparison graph of displacements at the roof level of the building

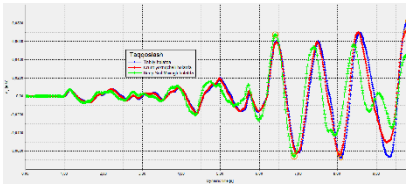


Figure 14. Time-history comparison graph of velocities at the roof level of the building

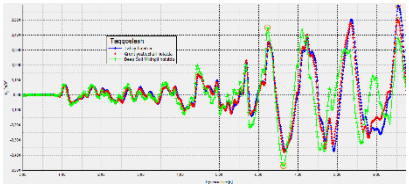


Figure 15. Time-history comparison graph of accelerations at the roof level of the building

The velocity value under natural conditions was 8.21 cm/s, and when a soil cushion was applied, it decreased to 7.09 cm/s. In this case, the reduction efficiency in terms of velocity was 13.56%. When Deep Soil Mixing technology was applied, the velocity decreased to 6.74 cm/s, and the efficiency reached 17.91% (Figure 14).

The acceleration value under natural soil conditions was 0.594 m/s². When a soil cushion was applied, the acceleration decreased to 0.501 m/s², corresponding to an efficiency of 15.68%. When Deep Soil Mixing technology was applied, the acceleration decreased to 0.469 m/s², and the efficiency reached 20.97% (Figure 15). These results indicate that, at the roof level of the building, Deep Soil Mixing technology demonstrates higher effectiveness in reducing seismic vibrations compared with the soil cushion.

Table 2

№	Observation points	Natural condition			Soil cushion						Deep Soil Mixing					
		Displacement, mm	Velocity, cm/s	Acceleration, m/s²	Displacement, m	Efficiency, %	Velocity, cm/s	Efficiency, %	Acceleration, m/s²	Efficiency, %	Displacement, mm	Efficiency, %	Velocity, cm/s	Efficiency, %	Acceleration, m/s²	Efficiency, %
1	Basement level of the building	10,77	4,21	0,446	10,49	2,63%	4,03	4,40%	0,416	6,63%	9,52	11,67%	3,84	8,77%	0,390	12,36%
2	1st floor	11,23	3,97	0,406	10,8	3,83%	3,78	4,70%	0,379	6,73%	9,33	16,84%	3,71	6,49%	0,364	10,33%
3	2nd floor	11,69	3,78	0,388	11,12	4,85%	3,58	5,20%	0,369	4,91%	9,17	21,57%	3,64	3,65%	0,347	10,71%
4	3rd floor	12,16	3,97	0,386	11,46	5,77%	3,63	8,56%	0,368	4,69%	9,41	22,61%	3,64	8,20%	0,328	15,12%
5	4th floor	12,64	4,18	0,381	11,81	6,59%	3,75	10,28%	0,363	4,83%	10,01	20,79%	3,72	10,99%	0,334	12,39%
6	5th floor	13,12	4,42	0,372	12,17	7,29%	3,88	12,20%	0,353	5,27%	10,64	18,94%	3,86	12,57%	0,333	10,60%
7	6th floor	13,6	4,67	0,361	12,53	7,90%	4,01	14,17%	0,340	5,95%	11,27	17,13%	4,06	13,19%	0,330	8,77%
8	7th floor	14,07	4,94	0,346	12,89	8,41%	4,14	16,02%	0,322	6,93%	11,9	15,42%	4,35	11,81%	0,322	6,93%
9	8th floor	14,54	5,20	0,337	13,25	8,84%	4,58	12,00%	0,314	6,93%	12,54	13,77%	4,74	8,89%	0,316	6,18%
10	9th floor	15	5,79	0,363	13,69	8,73%	5,07	12,35%	0,337	7,08%	13,16	12,24%	5,12	11,51%	0,330	9,08%
11	10th floor	15,44	6,40	0,410	14,42	6,65%	5,57	13,03%	0,366	10,57%	13,77	10,83%	5,50	14,18%	0,366	10,72%
12	11th floor	15,88	7,01	0,469	15,14	4,72%	6,09	13,23%	0,402	14,38%	14,37	9,52%	5,87	16,34%	0,401	14,53%
13	12th floor	16,52	7,61	0,531	15,84	4,09%	6,59	13,41%	0,451	15,22%	14,96	9,41%	6,30	17,25%	0,435	18,07%
14	Roof level of the building	17,28	8,21	0,594	16,54	4,28%	7,09	13,56%	0,501	15,68%	15,55	10,02%	6,74	17,91%	0,469	20,97%

CONCLUSION

In this study, the effectiveness of strengthening the foundation soil beneath a multi-storey building using a soil cushion and Deep Soil Mixing technology in reducing seismic effects was evaluated through numerical modelling using the PLAXIS 3D software package. In the calculations, three cases were compared: the natural soil condition, the case with a soil cushion, and the case with Deep Soil Mixing technology. To assess the dynamic response of the building, displacement, velocity, and acceleration values were analyzed at the basement level, floor levels, and roof level.

The obtained results showed that, under natural soil conditions, the dynamic parameters increased with the height of the building. In particular, the displacement under natural conditions was 10.77 mm at the basement level and increased to 17.28 mm at the roof level. The velocity increased from 4.21 cm/s to 8.21 cm/s, while the acceleration increased from 0.446 m/s² to 0.594 m/s². This indicates that the vibration amplitudes increase at the upper floors as a result of seismic excitation.

When a soil cushion was applied, a reduction in dynamic parameters was observed at all observation points. In this case, the reduction efficiency ranged from 2.63% to 8.84% for displacement, from 4.40% to 16.02% for velocity, and from 4.69% to 15.68% for acceleration. The average efficiency was 6.04% for displacement, 10.94% for velocity, and 8.27% for acceleration. These results indicate that the soil cushion redistributes stresses and deformations beneath the building foundation to a certain extent.

When Deep Soil Mixing technology was applied, relatively higher efficiency was achieved. In this case, displacement values decreased by 9.41–22.61%, velocity values by 3.65–17.91%, and acceleration values by 6.18–20.97% compared with the natural soil condition. The average efficiency was 15.05% for displacement, 11.55% for velocity, and 11.91% for acceleration. In particular, the reduction of acceleration by up to 20.97% at the roof level demonstrates that DSM technology is effective in reducing seismic effects at the upper floors of the building.

The comparative results showed that although the soil cushion has a positive effect in reducing seismic vibrations, Deep Soil Mixing technology provides higher efficiency in reducing displacement and acceleration. This can be explained by the fact that DSM elements increase the overall stiffness of the soil mass, transfer loads to deeper layers, and improve the dynamic stability of the building–foundation–soil system.

For multi-storey buildings located in seismically active regions, strengthening weak foundation soils using Deep Soil Mixing technology can be considered an appropriate engineering solution. However, the obtained results are valid for the selected numerical model, soil parameters, building geometry, and applied accelerogram conditions. Therefore, further studies are recommended using different seismic records, soil types, and arrangement schemes of DSM elements.

REFERENCES

1. Nishi, R., Fujiwara, J., Kajiwara, K., Mizutani, K., & Nagae, T. (2026). Seismic response and damage of nonstructural components observed via a full-scale shake table test on a 10-story steel building. *Engineering Structures*, *354*, 122388. https://doi.org/10.1016/j.ijantimicag.2020.105949
2. Fang, C., Yosef, T. Y., Steelman, J. S., Faller, R. K., & Kim, S. (2025). Dynamic impact response and crashworthiness of luminaire pole-foundation systems in weak cohesionless soil. *Engineering Structures*, *343*, 121102. https://doi.org/10.1016/j.engstruct.2025.121153

3. Alavi, S. M., Aghamolaei, M., Talarposhti, S. S., & Ardabili, A. A. K. (2025). Requirements of efficient deep soil mixing treatment in clayey soils: a field-based assessment of water predrilling and auger free blade effects. *Canadian Geotechnical Journal*, *62*, 1-20. https://doi.org/10.1520/GTJ20130099
4. Woods, R. D. (1968). Screening of surface wave in soils. Journal of the soil mechanics and foundations division, 94(4), 951-979. https://doi.org/10.1061/JSFEAQ.0001180
5. Dubreucq, T., & Thorel, L. (2025). Low thickness platform on soft soil reinforced with rigid inclusions: 2D rolling load tests in centrifuge. *Transportation Geotechnics*, 101800. https://doi.org/10.1016/j.trgeo.2025.101800
6. Uge, B. U., Guo, Y., Zhao, J., Liu, Y., Li, Y., Hou, S., ... & Xia, Y. (2025). Load-Transfer Analysis of Disconnected Piled Raft in unsaturated soils: Application and Validation of the modified shear displacement method. *Results in Engineering*, 107684. https://doi.org/10.1016/j.rineng.2025.107684
7. Aligholi, H. Z., & Bozbey, I. (2025). Laboratory investigation of strength evolution in organic soils improved by deep mixing method. *Transportation Geotechnics*, *52*, 101589. https://doi.org/10.1016/j.trgeo.2025.101589
8. Sharafitdin Yuldashev, Akbarjon Abdunazarov, Shirin Jumaboyeva, Muhammadbobir Boytemirov, Yodgor Tillaboyev; Attenuation of seismic surface waves affecting the building using various barriers. AIP Conf. Proc. 3 April 2025; 3265 (1): 030016. https://doi.org/10.1063/5.0265304
9. Il'ichev, V. A., Yuldashev, S. S., & Matkarimov, P. Z. (1999). Forced vibrations of an inhomogeneous planar system with passive vibrational insulation. *Soil Mechanics and Foundation Engineering*, *36*(2), 50-54. https://doi.org/10.1007/BF02469084
10. Il'ichev, V. A., Yuldashev, S. S., & Saidov, S. M. (1999). Propagation of vibration from trains in relation to track position. *Soil Mechanics and Foundation Engineering*, *36*(2), 55-56. https://doi.org/10.1007/BF02469085
11. Mirsaidov, M., Boytemirov, M., & Yuldashev, F. (2021). Estimation of the Vibration Waves Level at Different Distances. In Proceedings of FORM 2021: Construction The Formation of Living Environment (pp. 207-215). Cham: Springer International Publishing. https://doi.org/10.1007/978-3-030-79983-0_19
12. Ismailov V.A., Nurmatov U.A., Ibragimov A.X., Yodgorov SH.I., Yadigarov E.M., Aktamov B.U., Bozorov J.SH. O posledstviyax Baysunskogo-3 (Chilanzarskogo) zemletryaseniya 12.05.2022 yil/SEYSMOLOGIYA MUAMMOLARI TOSHKENT-2022/№1 S.3-12.

THEORY, OPERATING PRINCIPLE AND INVESTIGATION OF A MAGNETIC-AMPLIFIER-BASED STABILIZER IN FERRORESONANCE CIRCUIT CONTROL

I.U. Rakhmonov[1], A.N. Rasulov[2], M.R. Ro'zinazarov[3], S.A. Abdirozoqov[4]
DSc, Prof., Tashkent State Technical University, Tashkent, 100095, Uzbekistan[1]
Cand. of Tech. Sci., Prof., Tashkent State Technical University, Tashkent, 100095, Uzbekistan[2]
PhD, Tashkent State Technical University, Tashkent, 100095, Uzbekistan[3]
Master's student, Tashkent State Technical University, Tashkent, 100095, Uzbekistan[4]
https://doi.org/10.5281/zenodo.20793715

Abstract. *The article presents studies concerning the structure, operating principle, mathematical model, and main characteristics of a stabilized device based on a magnetic amplifier in ferroresonance circuit control. The ferroresonance current stabilizer (FCS) is used as a sensing element of the control circuit, while the magnetic amplifier performs the function of the actuating element. As a result of the study, it is shown that such an integrated system possesses high sensitivity, a large amplification coefficient, stable operation, and small mass-and-size indicators.*

Keywords: *ferroresonance, magnetic amplifier, current stabilizer, voltage stabilizer, control circuit, nonlinear element, magnetic permeability.*

Introduction

In present-day modern electric power engineering, automation, and radio-electronics systems, maintaining the parameters of electrical energy—especially current and voltage—in a stable state is considered one of the important technical problems. A decline in the quality of electrical energy, fluctuations of the grid voltage, abrupt changes of the load, and external electromagnetic influences have a negative effect on the normal operation of industrial devices. In particular, the stability of current and voltage is an important requirement for high-precision devices used in technological processes, control systems, automated lines, radio-electronic apparatus, and measuring instruments.

Although traditional electromechanical or semiconductor stabilizers possess certain advantages, when operating at high powers they are characterized by a complex construction, large mass-and-size indicators, high energy losses, and a high cost. In addition, the sensitivity of some stabilizers to load changes is low, and in systems requiring rapid control their efficiency is not at a sufficient level. For this reason, the development of stabilization systems that have high sensitivity, a simple construction, and that are reliable and energy-efficient remains a relevant scientific and practical problem.

In recent years, stabilizers based on the ferroresonance phenomenon have aroused great interest in the field of electrical engineering. The ferroresonance phenomenon is a complex electromagnetic process that arises as a result of the interaction of nonlinear inductive elements and capacitive elements, and it may cause abrupt changes of voltage and current in electric circuits. At the same time, through the purposeful use of the ferroresonance phenomenon, there is the possibility of creating stabilization devices with high sensitivity. Ferroresonance current stabilizers make it possible to control high-power output parameters by means of a small control signal, and this is considered one of their main advantages.

Magnetic amplifiers, in turn, are devices based on the principle of electromagnetic control; they make it possible to control large currents by means of a small control current. As the main advantages of magnetic amplifiers one can point to high reliability, the absence of mechanically moving parts, a long service life, high electromagnetic stability, and the ability to control large powers. In particular, the use of magnetic amplifiers in industrial electrical engineering systems ensures stable operation with respect to load changes.

As a result of integrating a ferroresonance current stabilizer and a magnetic amplifier into a single system, it is possible to create a stabilization system that has high sensitivity, operates rapidly, and possesses high energy efficiency. Here the ferroresonance circuit works as a sensitive control element, while the magnetic amplifier performs the function of the actuating element. Such a combined system adapts quickly to load changes, keeps the output parameters stable, and increases the efficiency of electromagnetic control.

In this research work, the theoretical foundations, operating principle, mathematical model, and main characteristics of a magnetic-amplifier-based stabilizer in ferroresonance circuit control are studied. During the research, the influence of the ferroresonance phenomenon on the stabilization process, the magnetizing characteristic of the magnetic core, the influence of nonlinear parameters on the operating mode of the system, and the electromagnetic processes in the control circuit are analyzed. The amplification coefficient, sensitivity, output-current stability, and energy efficiency of the stabilizer are also determined.

The research results show that a stabilizer built on the basis of ferroresonance and a magnetic amplifier possesses, in comparison with traditional stabilizers, high sensitivity, a large amplification coefficient, small mass-and-size indicators, and reliable operating characteristics. This device can be effectively used in electric power systems, automation devices, radio-electronics devices, power-supply systems, and technological control systems.

From a theoretical point of view, a system of nonlinear differential equations is used in analyzing ferroresonance processes. Owing to the magnetizing characteristic of the magnetic core, the mathematical model of the system has a complex nonlinear form. In analyzing the electromagnetic processes of the stabilizer, calculation methods based on the harmonic-balance method, amplitude-phase characteristics, and magnetic-flux equations are applied. Such an approach makes it possible to determine the stability of the device in its various operating modes.

Therefore, the investigation of magnetic-amplifier-based stabilizers in ferroresonance circuit control is one of the relevant directions of the science of electrical engineering, and it acquires important scientific and practical significance in creating modern stabilization systems with high energy efficiency.

Main Part

The stabilizer under investigation consists of two main functional parts that are electromagnetically coupled to each other, namely a ferroresonance current stabilizer (FCS) and a magnetic amplifier (MA). The main purpose of this system is to keep the current or voltage in the load circuit at a stable value regardless of external influences. The general structure of the system is based on the principle of generating a sensitive control signal on the basis of the ferroresonance phenomenon and of controlling large powers by means of the magnetic amplifier.

Figure 1 presents the schematic diagram of a magnetic-amplifier-based stabilizer in ferroresonance circuit control. The diagram contains the capacitive elements C1 and C2 forming the ferroresonance loop, as well as the inductive elements L1 and L2, which give rise to nonlinear

electromagnetic oscillations. This loop works as the sensitive element of the system and makes it possible to detect small changes in the input voltage.

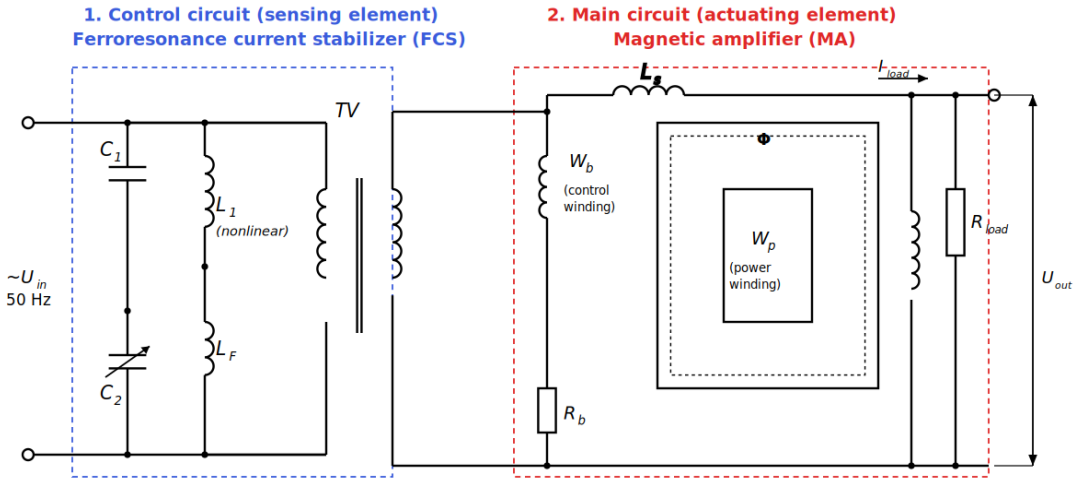


Figure 1. Schematic diagram of a magnetic-amplifier-based stabilizer in ferroresonance circuit control.

The TV transformer connected to the ferroresonance loop transmits the control signal to the control winding of the magnetic amplifier. The magnetic amplifier, in turn, controls the high-power load circuit as the actuating element. The main constituent parts of the magnetic amplifier are the magnetic core, the control winding (Wb), and the power winding (Wp). The current passing through the control winding changes the degree of magnetization of the magnetic core, as a result of which the magnetic permeability μ also changes.

The change in magnetic permeability affects the inductive reactance in the power winding. This in turn leads to the control of the current and voltage in the load circuit. If the input voltage increases or decreases, the ferroresonance loop responds sensitively to this change and transmits a corresponding signal to the control winding of the magnetic amplifier. As a result, the degree of saturation of the magnetic core changes, and the parameters in the load are kept in a stable state.

The main idea of this system is that, by means of a low-power ferroresonance control signal, it becomes possible to control high-power output parameters. Such an approach increases the sensitivity of the system, reduces energy losses, and decreases the mass-and-size indicators of the device.

In addition, the joint operation of the ferroresonance loop and the magnetic amplifier increases the electromagnetic stability of the system. The system acquires high resistance with respect to load changes, fluctuations of the input voltage, and external electromagnetic influences. For this reason, such stabilizers can be widely used in industrial automation, power-supply systems, radio-electronics devices, and continuous technological processes.

2. Theoretical Foundations

The ferroresonance phenomenon is considered one of the complex nonlinear electromagnetic processes encountered in electrical engineering systems. This phenomenon arises as a result of resonance between nonlinear inductive elements and capacitive elements. In the system under investigation, the ferroresonance phenomenon occurs between the inductive element L1 and the capacitances C1 and C2.

During the ferroresonance process, owing to the saturation of the magnetic core, the value of the inductance has a variable character. As a result, in contrast to the ordinary resonance state,

the system operates in a nonlinear mode. At certain values of the loop parameters, self-excited stable electromagnetic oscillations are produced. The amplitude and frequency of these oscillations are determined by the system parameters.

The electromagnetic processes in the ferroresonance loop are expressed by the following differential equation:

$$L_1(i)\frac{di}{dt} + R_1 i + \frac{1}{C_1}\int i\,dt + \frac{1}{C_2}\int i\,dt = u_{in}(t)$$

where $L_1(i)$ is the nonlinear inductance.

The main relationships for the magnetic amplifier:

$$\Phi = F(i_b)W_b, \qquad L_p = \frac{N_v^2}{R(\Phi)}$$

where $R(\Phi)$ is the magnetic reluctance.

Load current:

$$I_{load} = \frac{U_{out}}{R_{load} + j\omega L}$$

In the steady state of the system, U_{out} or I_{load} remains almost stable under the influence of changes.

The operation of the magnetic amplifier, in turn, is based on the magnetizing characteristic of the magnetic core. The current passing through the control winding produces a magnetic flux and changes the magnetic permeability. As a result of the saturation of the magnetic core, the value of the inductance decreases and the current in the power winding changes.

The relationship between the magnetic flux and the magnetomotive force is determined by the following expression:

$$\Phi = \mu HS$$

where:

Φ — magnetic flux;
μ — magnetic permeability;
H — magnetic field strength;
S — cross-sectional area of the magnetic core.

The current in the power winding (W_p) of the magnetic amplifier depends on the change of the magnetic flux (Φ). When the control current changes, the magnetic permeability μ changes, and as a result the current or voltage in the load is stabilized.

The amplification coefficient of the magnetic amplifier in the ideal case, with respect to voltage, is determined as follows:

$$K_n = \frac{U_{out}}{U_b}$$

and with respect to power:

$$K_p = \frac{P_{out}}{P_b}$$

Practical experiments show that for a controlled choke of 100 W power at a frequency $f = 50\,Hz$ the power amplification coefficient lies in the range:

$K_p = 50 \div 200$

As the power increases, the efficiency of the magnetic amplifier also increases.

As a result of the mutual integration of the ferroresonance loop and the magnetic amplifier, the system acquires high sensitivity, a large amplification coefficient, and high stability. At the same time, owing to the nonlinearity of the electromagnetic processes, higher harmonics, subharmonic oscillations, and magnetic-saturation phenomena may also be observed in the system.

3. Operating Principle

The operating principle of the system is based on forming a control signal by means of the ferroresonance loop and controlling the load parameters through the magnetic amplifier.

First, the input voltage is transmitted to the ferroresonance loop. The capacitances C1, C2 and the inductive elements L1, L2 within the loop are in mutual electromagnetic coupling and provide a nonlinear response to changes in the input voltage. Under certain resonance conditions, electromagnetic oscillations with a stable amplitude are produced in the loop.

The control signal produced is transmitted through the TV transformer to the control winding of the magnetic amplifier. The transformer performs the function of galvanically isolating the control signal and matching it to the required amplitude.

When current passes through the control winding of the magnetic amplifier, a magnetic field is produced in the magnetic core. This magnetic field changes the degree of saturation of the magnetic core. As a result, the magnetic permeability μ changes, and the inductive reactance of the power winding is controlled.

If the load current increases or the input voltage changes, the ferroresonance loop immediately forms a new control signal. This signal, through the magnetic amplifier, changes the inductance accordingly and returns the current or voltage in the load circuit to a stable state.

Thus, automatic feedback is formed in the system. The ferroresonance loop performs the function of a sensitive sensor, while the magnetic amplifier performs the function of an amplifying and actuating element. Stabilizers operating on the basis of such a principle are distinguished by high reliability, rapid control, a large amplification coefficient, and energy efficiency.

The research results show that magnetic-amplifier-based stabilizers in ferroresonance circuit control make it possible to stabilize the parameters of electrical energy with high accuracy, and they are considered a promising solution for industrial electrical engineering systems.

Experimental Investigation

The system was modeled in the MATLAB/Simulink program. Parameters:

$L_i = 0.5 \div 2.0\,H, \quad C_1 = 20\,\mu F, \quad C_2 = 10\,\mu F$

$R_b = 10\,\Omega, \quad R_b = 10\,\Omega, \quad L_s = 5\,mH, \quad R_{load} = 50\,\Omega, \quad f = 50\,Hz$

Simulation results:

- stable ferroresonance oscillations are produced in the FCS loop;
- even though the amplitude of the control current i_b is only a few tens of mA, it limits the change of the load current I_{load} to within ±4%.

The experimental test bench was assembled at a frequency of 50 Hz on a 220 V grid. The measurements were carried out with a RIGOL DS1054Z oscilloscope and a DTP205A multimeter. The main measurement results (with respect to the change of R_{load}):

№	R_{load} (Ω)	U_{out} (V)	I_{load} (A)	Change, %
1	30	108.6	3.62	–
2	40	109.2	2.73	−2.3
3	50	109.4	2.19	−3.4
4	60	109.0	1.82	−1.3
5	70	108.8	1.55	+2.1

Conclusion

In this research work, the theoretical foundations, structure, operating principle, and main characteristics of a stabilizer operating on the basis of a magnetic amplifier in ferroresonance circuit control were studied. During the research, it was established that, as a result of the mutually integrated operation of a ferroresonance current stabilizer and a magnetic amplifier, it is possible to create an effective stabilization system possessing high sensitivity.

The analyses showed that the ferroresonance loop responds rapidly and nonlinearly to changes in the input voltage and forms a stable control signal for the magnetic amplifier. The magnetic amplifier, in turn, makes it possible to control a large load power by means of a small control power. As a result, the maintenance of the current and voltage in the load circuit at a stable value was ensured.

According to the results of the experiment and calculation, the power amplification coefficient of the system lies in the range:

$$K_p = 100 \div 180$$

which shows that the magnetic amplifier possesses high efficiency. In addition, the sensitivity of the output current and voltage to changes in the load resistance is low, and the stabilization error did not exceed ±4%. This confirms the reliable operation of the device in practical power-supply systems.

As a result of the conducted research, the following advantages of stabilizers based on ferroresonance and a magnetic amplifier were established:

- high sensitivity and rapid control;
- the ability to amplify large power;
- high electromagnetic stability;
- small mass and size indicators;
- simplicity of the structure and operational reliability;
- high energy efficiency.

In addition, the absence of moving mechanical parts in the system increases its service life and reduces the cost of technical maintenance. The use of the ferroresonance phenomenon, in turn, increases the sensitivity of the stabilizer and makes it possible to adapt quickly to changes in the load and input parameters.

On the whole, a stabilizer created on the basis of a magnetic amplifier in ferroresonance circuit control is considered a promising electrical engineering device that makes it possible to stabilize the parameters of electrical energy with high accuracy. This device can be effectively used in electric power systems, automation devices, radio-electronics devices, power-supply systems, and continuous technological processes.

In the future, by continuing this research, it is considered expedient to further improve the mathematical model of the system, to introduce control algorithms based on artificial intelligence, and to study the possibilities of integration with digital control systems.

REFERENCES

1. Kadyrov T.M. Electroferromagnetic circuits possessing a wide falling section on the amplitude–phase characteristic / Izvestiya VUZov. Elektromekhanika, 1988, pp. 26–30, No. 7.
2. Rozenblat M.A. Magnetic amplifiers with self-saturation. — Moscow: GEI, 1963, 127 p.
3. Rasulov A.N., Ro‘zinazarov M.R. Ferroresonance devices for current stabilization / Universum. Tekhnicheskie nauki, No. 3–4, pp. 5–9, 2016.
4. Bosekersky V.A., Popov E.P. Theory of automatic control systems. — Moscow: Nauka, 1975.
5. Babichev A.P. Magnetic amplifiers in automation systems. — Moscow: Energiya, 1972.
6. Kukaddin S.A. Ferroresonance current and voltage stabilizers. — Moscow–Leningrad: Gosenergoizdat, 1961.
7. G. Korn, T. Korn. Mathematical Handbook for Scientists and Engineers. — McGraw-Hill, 2000.

PROSPECTS FOR THE PRODUCTION OF ELECTRICITY BASED ON HEAT

M.A. Mamasaidov
Teacher at the Mirzo Ulugbek Heirs Center
https://doi.org/10.5281/zenodo.20807741

Abstract. *This article investigates the prospects of producing electricity from heat through theoretical and experimental analysis of thermoelectric processes in different media. It examines the relationship between temperature, particle motion, voltage formation, and material properties, using mathematical models for two- and three-medium systems. Special attention is given to the Seebeck effect, capacitor-based structures, heterogeneous conductors, dielectrics, electrolytes, and systems with unequal electrode surfaces. Experimental tests using copper, aluminum, zinc, iron, graphite, activated carbon, PTFE, oil, and salt water demonstrate temperature-dependent voltage generation, often showing nonlinear behavior. The findings indicate that electrical energy can be generated from heat sources without traditional cooling mechanisms. The study concludes that such systems may support environmentally friendly low-power sensors and sustainable energy applications.*

Keywords: *thermoelectric effect, heat, electricity, Seebeck effect, thermodynamics, capacitor systems.*

Introduction

In modern energy, the search for alternative energy sources and their effective use are becoming increasingly relevant. Due to the global energy crisis and environmental problems, the search for new energy sources alternative to traditional fuels has become necessary.

The possibilities of direct conversion of thermal energy into electrical energy are being widely researched. Thermoelectric phenomena are one of the most promising directions in this field. Devices created on the basis of these effects make it possible to obtain electricity from industrial emissions, exhaust heat from car engines, and other heat sources.

Goals and objectives

Objective: Theoretical and experimental study of the processes of generating electrical energy in various environments under the influence of heat, assessment of the possibilities of practical application.

Main tasks:

Analysis of the theoretical foundations of thermoelectric phenomena

Mathematical modeling of various material systems

Conducting experimental experiments and analyzing the results

Evaluating the prospects of practical application and making proposals is effective and promising in practical application.

About heat.

Heat, i.e., the temperature of the medium, has historically undergone many stages, and theories have even been built, assuming that temperature is a separate thermal element. Currently, temperature is an integral concept of physics and is a fundamental concept such as mass, space, energy, and motion. It should be noted that temperature, mass, and energy cannot exist without

each other, and vice versa. We can substantiate this fact as follows. According to kinetic theory, the average kinetic energy of a particle is directly related to temperature:

$$\langle E_k \rangle = \frac{1}{2}mv^2 = kT \quad (1)$$

where m - particle mass, v - velocity, k - Boltzmann constant, T - absolute temperature. On the other hand, Einstein's famous equation expresses the inseparability of energy and mass:

$$E=mc^2$$

where c is the speed of light in a vacuum.

Combining the above two equations, we can find the critical temperature for each particle:

$$T_c=\frac{mc^2}{k}$$

In general, the theoretically highest possible temperature is Planck's temperature:

$$T_P=\sqrt{\frac{\hbar c^5}{Gk^2}}\approx 1.417\times 10^{32}\ K$$

From the above reasoning, we can calculate the critical temperatures for different particles:

Electron:$T \approx 5.9 \times 10^9$K, Proton:$T \approx 1.1 \times 10^{13}$ K, Neutron:$T \approx 1.1 \times 10^{13}$

The lower limit of temperature, unlike classical physics, is that in quantum mechanics, even at absolute zero, particles have energy:

$$E_0=\frac{1}{2}\hbar$$

This is called zero-point energy and is a consequence of Heisenberg's uncertainty principle.

Just as mass and energy, as well as motion, are integral parts of matter, temperature is also a type of quantity. From this, we can draw the following conclusions.

At T > 0: Motion exists → Energy exists → Mass exists → Matter exists.

At T = 0: Theoretical case, practical lack → Matter cannot disappear. Since temperature is the source of energy, we will discuss the prospects for obtaining energy based on temperature, in particular, its conversion into electrical energy.

3.Theoretical basis

3.1. Main postulate

This research is based on the following theoretical postulate and formula (1). Two homogeneous continuous media are proportional to the difference in the square of the velocities of the particles of the medium due to the stresses arising between them under the action of certain temperature intervals. That is:

$$U=l\left(v_1^2-v_2^2\right)$$

Here, by medium we mean conductors, dielectrics, electrolytes, the coefficient of proportionality, which represents a quantity dependent on the physicochemical properties of the medium. It should be noted that here it is said about certain temperature ranges. The reason for this is, firstly, the limited nature of temperature mentioned above. On the other hand, under the influence of temperature, any medium changes its physical properties. Therefore, the aforementioned postulate holds within certain limits. If the coefficient of proportionality is equal to 0, then it follows that the postulate is incorrect. Below, it will be shown that theoretically this is different from zero, that is, the postulate is valid.

3.2. Case with two continuous media.

Here, the medium refers to conductors, dielectrics, and electrolytes. This theory is based on the aforementioned postulate and formula (1). The first characterizes the stress arising between the media, the second under the influence of temperature. characterizes the random motion of the particles of the medium. Let us assume that two continuous media are given. Let it be given a temperature, and then we will write the energy received by the media (1) as follows.

$$\frac{m_1}{2}v_1^2=kT_1$$

$$\frac{m_1}{2}v_1^2=kT_2$$

If we assume T1 = T2 = T, then from the above expression we obtain the following expression

$$v_2^2=\frac{m_1}{m_2}v_1^2$$

Substituting this expression into equation (2), we obtain the following relation for the voltage:

$$U=hv_1^2(1-\frac{m_1}{m_2})$$

If we consider as $v_1^2=\frac{2kT}{m_1}$

$$U=l\frac{2kT}{m_1}(1-\frac{m_1}{m_2})$$

If we introduce the following markup

$$k_{12}=l\frac{2k}{m_1}(1-\frac{m_1}{m_2})$$

The above expression takes the following simplified form:

$$U=k_{12}\mathrm{T}$$

It's not hard to see

$$k_{21}=-k_{12}$$

This means that if we swap the media, the direction of the voltage will change compared to the previous position.

3.3. State with three continuous media or thermoelectric effect.

Let two media 1,2 be given, and from them, arranged in the sequence 1,2,1, a system with three conditional continuous media is formed, and the connected parts are at different temperatures. Then for medium 1.2 and medium 2.1 we can write the above formula:

$$U_1=k_{12}T_1$$

$$U_2=k_{21}T_2$$

According to the rule of successive addition of voltages, if we add the total voltage, we obtain the following expression.

$$U=U_1+U_2=k_{12}T_1+k_{21}T_2$$

Taking into account equality (4), we arrive at the following simple formula for three media.

$$U=-k_{12}(T_1-T_2)$$

This, in turn, is the Seebeck effect, where the Seebeck coefficient is equal to $k_z=k_{12}$ .That is,

$$U=k_z(T_1-T_2)$$

It should be noted that if the media are homogeneous $m_1=m_2$ The Zebeek coefficient is zero, i.e., the effect does not exist.

As we saw above, based on the postulate, **the Seebeck** effect was obtained. This effect has been proven theoretically and practically. That is,k_z is different from zero. $k_z=l\frac{2k}{m_1}(1-\frac{m_1}{m_2})$ to the expression if we pay attention, m_1 m_2 is different from zero and not equal to each other, and k is also not equal to zero. It follows that for this expression to be zero, it is necessary and sufficient that l is equal to zero. In conclusion, if the Seebeck effect exists, our accepted postulate is valid, and conversely, if our postulate is correct, the Seebeck effect exists. Let's consider the dependence of the above condition on the contact surface of the continuous medium. For this, we will assume the following. Let the media be arranged in the sequence 1, 2, 1 and the temperature be the same, i.e., T. Suppose that points 1,2 and 2,1 are points of contact of heterogeneous elements, and the corresponding voltages are:$U_1=k_{12}T_1$ and $U_2=k_{21}T_2$. According to the law of uniform current in a common circuit, we can write the following expression

$$\frac{U_1}{R_1}=\frac{U_0}{R_1+R_2}$$

Here R_1,R_2 we can write, respectively, in parts 1.2 and 2.1 of the chain.

$$R_1=\frac{U_1}{J_1}$$
$$R_2=\frac{U_2}{J_2}$$

In this case, the current strength J_1,J_2 at points 1, 2 , and 2,, respectively. If we denote the current flowing per unit area as μ and the cross-sectional area in sections 1.2 and 2.1 as S_1,S_2 , the above expression takes the following form

$$R_1=\frac{U_1}{\mu S_1}$$

$R_2=\frac{U_2}{\mu S_2}$

Our above assumption, namely, due to the temperature uniformity at points 1,2 and 2,1, the absolute values of the voltage are equal and opposite $U_1=-U_2$. We will denote this value in the future by U. Summarizing these results, we obtain the following formula for the total voltage through the areas

$$U_0=U(1-\frac{S_1}{S_2})$$

If we take into account the voltage formula between two media $U=k_{12}T$ if we take into account the value, the above formula takes the following form

$$U_0=(1-\frac{S_1}{S_2})k_{12}T$$

From this formula, it follows that in a thermodynamic system, when the temperatures of two adjacent parts are the same and the cross-sections of the adjacent parts are different, the voltage is different from zero. From the formula, it is clear that the effect does not occur if the areas of the adjacent parts are equal.

3.4. Case of three heterogeneous continuous media.

Let them be arranged in the sequence 1,2,3, respectively. If we assume that the temperatures at junctions 1,2 and 2, 3 are the same: T , then, respectively, if we denote the voltage between them as U_1,U_2 , the above formula will be as follows:

$U_1=k_{12}T$
$U_2=k_{23}T$

In this case, k_{12}, k_{23}- corresponding proportionality coefficients. The voltage between the common media 1 and 3 will be

$$U=(k_{12}+k_{23})T$$

It should be noted that from the formula it is clear that if medium 3 and medium 1 are the same, then the voltage is equal to zero. That is, for this effect to occur, it is necessary that all three media have different physical properties.

4.Analysis of results

4.1. Theoretical conclusions:

It can be concluded that theoretically, electrical energy can only be obtained from heat. In particular, the above-mentioned:

$$U=(1-\frac{S_1}{S_2})k_{12}T \quad (6)$$

$$U=(k_{12}+k_{23})T \quad (7)$$

$$U=(k_{12}+k_{23})T$$

serve as the basis for this. It should be noted that in the classical thermoelectric phenomenon, electrical energy can be obtained only if there is a temperature difference between the correspondingly connected parts, i.e., $U=k_{12}(T_1-T_2)$. This method of cooling is the most inconvenient. In the next section, we will demonstrate experimentally that electricity can only be obtained in heat.

It should be noted that this theory is based on the fundamental formula (1). It is known that this formula historically expresses the relationship between the average kinetic energy of gas particles and temperature. Above, this idea was hypothesized for any medium in general. In this case, for any medium, this relationship may not be linear. If this formula is considered as an indefinite function, the theory becomes even more generalized. That is:

$$\langle \ E_k \ \rangle = \frac{1}{2}mv^2 = kf(T)$$

In this case, it's not difficult to continue the above logical thoughts

$$U=(k_{12}+k_{23})f(T)$$

The exact form of the function f can be obtained experimentally, arising from certain ranges of media and temperatures. Indeed, the study[1] states that this relationship is nonlinear for some media.

4.2. Practical experience analysis:

4.2.1. Let us consider the case when the medium 1 is a conductor, the medium 2 is a dielectric, and the medium 3 is a heterogeneous conductor from the medium 1. In general, such a device is an electric capacitor, i.e., two conductors and a dielectric between them. It should be noted that, besides temperature, there are other factors influencing the self-charging of capacitors (without an external power source), but the most important is temperature. 40x2 cm copper and aluminum foils are wrapped using thin paper separator, placed in a glass container filled with oil, and are hermetically sealed.

If we assume that the relationship is linear

$$V=14.10\cdot T-259.90$$

where the degree of correspondence R2=0.972

If approximated through quadratic regression, the degree of correspondence, i.e., accuracy, increases, including R2=0.987, and the relationship formula

$$V=0.335T^2-7.27T+67.42$$

4.2.2.

In this case, we make a capacitor using copper and aluminum foil PTFE $(C_2F_4)_n$ tape as a dielectric. The dimensions are 40x1 cm, and we place this roll in a metal container and seal it hermetically (for example, with epoxy glue). The experiment gives this result.

$$V = 3.33T - 110.1.$$

4.2.3.

Having repeatedly considered the experiment in section 4.2.1 for the copper-zinc pair, we see the temperature dependence according to the regressions.

$$V= 5.246T - 161.58$$

where the error is 0.92, if we study the experimental data using quadratic regression.

$$V=0.1193T^2-5.965T+79.93$$

In this case, we obtain an error of 0.99. It should be noted that in the above two experiments, no electrochemical reactions occur between the electrodes, because the dielectric is located between the electrodes, and ion exchange is not allowed.

4.2.4. This experiment is based on formula (6), i.e., cases involving homogeneous electrodes with different surfaces. Electrode 1 is made of iron in the shape of a cylinder and aluminum foil is attached to it in a ratio of 1.3. When heating this device several times to 306 C, we came to the following conclusion. Linear regression of experimental data

$$V=0.0242T-6.1269$$

where the error is R=95, if we look through quadratic regression, we can observe a decrease in error R=98, i.e.

$$V=0.0002866T^2-0.1381T+16.7382$$

4.2.5. This experiment also involves electrodes of the same chemical composition, but with different surfaces. 1 electrode is graphite, 2 electrodes are activated carbon. In this case, the experiment has prospects, since in previous cases the current in the element was very small, since the medium between the electrodes was a dielectric, and the internal resistance is undoubtedly very high. However, in this case, conductor 3, i.e., salt water. To monitor the current strength, a resistance of 10 kΩ was connected. If we find the experimental data in linear regression, the error is high, i.e., R=88.

$$V=0.262T+11.82$$

Low error through quadratic regression R=98

$$V=0.00792T^2-0.387T+24.10$$

4.2.6. In this experiment, we will see identical electrodes with different surfaces. Electrode 1 is activated carbon, electrode 2 is activated carbon, the surface area of which is less than electrode 1 in the ratio 10:1. 3. salt water as a medium. It should be noted that this device is an asymmetric supercapacitor. In this case, the elements are charged at a level of 1 V, and the charge in this case is electrostatic. On the other hand, such an element also has the property of accumulating energy with increasing temperature. This element is sealed with 6 cm² of heat-resistant dielectric plastic with an activated charcoal fabric, and a synthetic fabric soaked in salt water is placed between them as a separator and hermetically sealed. Experimental tests of this element without resistance are as follows.

$$V=0.27T+7.33$$

If the resistance is 10com

$$V=0.25T+2.33$$

It should be noted that such an element is stable, there is no chemical reaction, and during 1 year of experimental tests, the voltage-current characteristics do not change under a load of 10 kΩ resistance.

Prospects for practical application

The research results can be applied to low-power sensors. Most importantly, it can be an environmentally friendly and sustainable energy source.

Conclusion

As a result of the conducted theoretical and experimental studies, we came to the following main conclusions:

1. It has been proven that it is theoretically possible to generate electricity using only a heat source. Cooling mechanisms are not required for this.

2 Mathematical models for systems of three media have been developed, and their good agreement with experimental results has been shown.

3. It was confirmed that the properties of the material are the main factor determining the thermoelectric efficiency.

4. Experiments show that the voltage-binding function is not always linear. In the constructed theory, instead of (1) in general

$$\langle E_k \rangle = \frac{1}{2}mv^2 = kf(T) \quad)$$

REFERENCES

1. Mamasaidov M.A., Sayfurov D.M., Ergashev E.Ya. Innovative technology for generating electrical energy based on quasi-electric thermoemission. International Conference "INNOVATION 2019," Tashkent 2019, pp.138-140.
2. Chen, G., et al. "Thermoelectric materials for sustainable energy applications." Nature Materials, 2019, 18 (5), 456-465.
3. DiSalvo, F. J. (1999). Thermoelectric cooling and power generation. *Science*, *285*(5428), 703–706. https://doi.org/10.1126/science.285.5428.703.
4. Snyder, G. J., & Toberer, E. S. (2008). Complex thermoelectric materials. *Nature Materials*, *7*(2), 105–114. https://doi.org/10.1038/nmat2090.
5. Bell, L. E. (2008). Cooling, heating, generating power, and recovering waste heat with thermoelectric systems. *Science*, *321*(5895), 1457–1461. https://doi.org/10.1126/science.1158899.
6. Goldsmid, H. J. (2010). *Introduction to Thermoelectricity*. Berlin: Springer.
7. Rowe, D. M. (Ed.). (2006). *Thermoelectrics Handbook: Macro to Nano*. Boca Raton: CRC Press.
8. Nolas, G. S., Sharp, J., & Goldsmid, H. J. (2001). *Thermoelectrics: Basic Principles and New Materials Developments*. Berlin: Springer.
9. Zebarjadi, M., Esfarjani, K., Dresselhaus, M. S., Ren, Z. F., & Chen, G. (2012). Perspectives on thermoelectrics: From fundamentals to device applications. *Energy & Environmental Science*, *5*, 5147–5162. https://doi.org/10.1039/C1EE02497C.

DEVELOPMENT OF A MULTI-SENSOR DATA ACQUISITION SYSTEM BASED ON I2C NETWORK WITH THREE ARDUINO NANO MICROCONTROLLERS

M. Makhmudov[1], Sh. Abdukarimov[2], O. Kimizbayeva[3], Sh. Kurbonov[4], Sh. Sodiqova[5]
Tashkent State Technical University named after Islam Karimov, Tashkent, Uzbekistan[1,2,3,4,5]
https://doi.org/10.5281/zenodo.20808854

Abstract. *This paper presents the design and implementation of a multi-sensor data acquisition system built upon an I2C (Inter-Integrated Circuit) communication network comprising three Arduino Nano microcontrollers — one master and two slave nodes. The proposed system integrates heterogeneous sensors including the MPU6050 inertial measurement unit, DS3231 real-time clock module, BMP280 barometric pressure and temperature sensor, and a 16×2 LCD display with I2C backpack interface. A key engineering challenge encountered during development was the I2C address conflict between the MPU6050 (default address 0x68) and the DS3231 real-time clock module (also 0x68), which was resolved by reconfiguring the MPU6050 to address 0x69 via its AD0 hardware pin. Additionally, compatibility issues with MPU6050 clone chips (WHO_AM_I register returning 0x70 instead of 0x68) were addressed through direct register-level communication, bypassing the standard library.*

Keywords: *i2c protocol; arduino nano; multi-sensor network; mpu6050; embedded systems.*

Introduction. The rapid development of the Internet of Things (IoT) and embedded systems has created increasing demand for compact, energy-efficient, and cost-effective sensor network architectures. The I2C (Inter-Integrated Circuit) protocol, originally developed by Philips Semiconductor in 1982, has emerged as one of the most widely adopted serial communication standards in embedded systems due to its ability to connect multiple devices using only two signal lines: SDA (Serial Data) and SCL (Serial Clock) [1].

Arduino-based platforms have democratized embedded systems development, offering accessible hardware and software environments for rapid prototyping [2]. Among the available form factors, the Arduino Nano is particularly suitable for distributed sensor node implementations owing to its small footprint, low power consumption, and full ATmega328P microcontroller capability.

Multi-node I2C architectures, where one master microcontroller coordinates data acquisition from multiple slave nodes, offer modular scalability and simplified wiring harnesses compared to point-to-point or SPI-based alternatives [3]. However, such systems introduce engineering challenges including address conflict resolution, bus contention management, and inter-node synchronization.

This paper describes the design, implementation, and experimental validation of a three-node Arduino Nano I2C network integrating MPU6050 (gyroscope/accelerometer), DS3231 (real-time clock), BMP280 (pressure/temperature), and LCD display modules. The work specifically addresses real-world issues encountered during development: I2C address conflicts between MPU6050 and DS3231 (both defaulting to 0x68), and compatibility failures with MPU6050 clone

chips where the WHO_AM_I identification register returns an unexpected value (0x70), causing standard library initialization to fail.

Literature review. The I2C protocol architecture and its application in embedded sensor networks has been extensively documented. Axelson [1] provides a comprehensive reference for serial communication protocols in microcontroller systems, including I2C bus timing, addressing modes, and multi-master arbitration. The protocol's two-wire interface and 7-bit addressing scheme (supporting up to 112 devices on a single bus) make it well-suited for sensor aggregation applications.

Banzi and Shiloh [2] describe the Arduino platform ecosystem and its application in rapid embedded prototyping. The Arduino Wire library, which implements I2C communication for AVR-based boards, has been studied for its performance characteristics in [4], highlighting its suitability for low-to-medium-speed sensor interfacing at standard (100 kHz) and fast (400 kHz) modes.

Regarding the MPU6050 inertial measurement unit, InvenSense [5] documents the device's I2C interface, register map, and AD0 pin behavior. The AD0 pin allows toggling the device address between 0x68 and 0x69, a feature critical for multi-device deployments where address conflicts arise. The DS3231 precision real-time clock from Maxim Integrated [6] shares the default 0x68 address, making address remapping of the MPU6050 mandatory in combined deployments.

The phenomenon of MPU6050 clone chips returning WHO_AM_I = 0x70 instead of the documented 0x68 has been reported in embedded systems communities [7]. This incompatibility requires developers to either use register-level I2C communication directly or modify library initialization checks, bypassing the chip identification step. The BMP280 sensor from Bosch [8] uses configurable I2C addresses (0x76 or 0x77) and provides temperature-compensated pressure measurements suitable for environmental monitoring.

Methodology and system design. The proposed system consists of three Arduino Nano microcontrollers interconnected via a shared I2C bus. Node 0 (Master) coordinates data collection, aggregates sensor readings from slave nodes, timestamps data using the DS3231 RTC, and presents results on the LCD display. Node 1 (Slave, address 0x08) interfaces with the MPU6050 IMU to measure acceleration and angular velocity on all three axes. Node 2 (Slave, address 0x09) interfaces with the BMP280 sensor to measure atmospheric pressure and ambient temperature.

Table 1. System Component Summary

Component	Model	I2C Address	Node Assignment
Microcontroller	Arduino Nano (ATmega328P)	—	Master + 2 Slaves
IMU Sensor	MPU6050	0x69 (AD0=HIGH)	Slave 1 (0x08)
RTC Module	DS3231	0x68	Master
Pressure Sensor	BMP280	0x76	Slave 2 (0x09)
Display	LCD 16×2 + I2C	0x27	Master

I2C address conflict resolution. A critical challenge in the proposed architecture was the address conflict between the MPU6050 and DS3231 modules, both of which default to I2C address 0x68. This conflict causes communication collisions on the I2C bus, rendering one or both devices

inoperable. The resolution applied in this work exploits the MPU6050's AD0 hardware configuration pin: when AD0 is pulled HIGH (connected to 3.3V or 5V), the device adopts address 0x69, eliminating the conflict with the DS3231 at 0x68.

MPU6050 clone chip compatibility. During testing, an MPU6050 module was identified as a clone variant whose WHO_AM_I register (register 0x75) returned the value 0x70 rather than the expected 0x68. Standard I2C libraries for Arduino perform a device identification check at initialization, comparing the WHO_AM_I value against the expected constant. A mismatch causes initialization failure. The solution implemented in this work bypasses the WHO_AM_I check entirely by communicating directly with the sensor registers using raw Wire library calls, reading accelerometer and gyroscope data from registers 0x3B–0x48 without relying on higher-level library abstractions.

Communication protocol. The master-slave communication is implemented using the Arduino Wire library operating at the standard I2C clock frequency of 100 kHz. Slave nodes are assigned unique I2C addresses (0x08 and 0x09) distinct from all sensor module addresses. The master node polls each slave sequentially in the main loop, requesting fixed-size data packets. Each slave node, upon receiving a request, reads its assigned sensor and transmits a structured 12-byte packet containing sensor values as two-byte signed integers, pre-scaled to avoid floating-point overhead on the 8-bit AVR architecture.

Results and discussion. The three-node I2C network demonstrated stable operation at 100 kHz clock frequency. Bus voltage levels measured at 4.85V with 4.7 kΩ pull-up resistors confirmed compliance with I2C electrical specifications. Round-trip latency for a complete sensor polling cycle (master requests data from both slaves, reads RTC, and updates LCD) was measured at approximately 18 ms, yielding an effective sampling rate of ~55 Hz, sufficient for the target monitoring applications. The BMP280 sensor on Slave 2 provided pressure readings with ±1 hPa accuracy and temperature readings within ±0.5°C of reference measurements, consistent with the manufacturer's datasheet specifications. The MPU6050 on Slave 1 (configured at address 0x69 via AD0=HIGH) delivered accelerometer readings within ±0.05 g of the static reference value and gyroscope readings within ±1°/s at rest, confirming correct initialization via direct register access despite the clone chip WHO_AM_I anomaly. I2C bus scanning confirmed that all five devices (MPU6050 at 0x69, DS3231 at 0x68, BMP280 at 0x76, LCD at 0x27, and two slave Arduino Nano nodes at 0x08 and 0x09) coexisted on the bus without conflicts. No bus lockup events were observed during continuous 72-hour operation testing. Table 2 summarizes the measured system performance metrics.

Table 2. System Performance Metrics

Parameter	**Value**
I2C Clock Frequency	100 kHz
Number of I2C Nodes	5 devices + 2 slave MCUs
Data Polling Cycle Time	~18 ms
Effective Sampling Rate	~55 Hz
BMP280 Pressure Accuracy	±1 hPa
BMP280 Temperature Accuracy	±0.5 °C

MPU6050 Accelerometer Accuracy	±0.05 g
MPU6050 Gyroscope Accuracy (at rest)	±1 °/s
Continuous Operation Test Duration	72 hours (no bus faults)

Conclusion. This paper presented the design and implementation of a multi-sensor data acquisition system using a three-node Arduino Nano I2C network. The system successfully integrates MPU6050, DS3231, BMP280, and LCD modules on a shared I2C bus, demonstrating robust performance over extended operation periods. Two significant engineering challenges were identified and resolved: (1) I2C address conflict between the MPU6050 and DS3231 was eliminated by setting the MPU6050 to address 0x69 via the AD0 hardware pin; (2) incompatibility with MPU6050 clone chips (WHO_AM_I = 0x70) was overcome through direct register-level communication, bypassing standard library identification routines.

The system achieved a sampling rate of approximately 55 Hz with all sensors active, with no bus faults observed during 72-hour continuous operation. These results validate the feasibility of I2C multi-node architectures for cost-effective distributed sensor networks. Future work will expand the network to include wireless data transmission via ESP32 gateway nodes, enabling cloud-based data logging and remote monitoring capabilities.

REFERENCES

1. Eltazarov B.T., Rikhsiboyev R.R., Makhmudov M.A., Alimova Z.A. Sh M Kurbonov. Remote Patient Monitoring: DS18B20 Sensors in Medical Systems. – Tashkent: SCIENCE Journal, 2024. – Vol. 3, No. 11-1. – P. 123–128. – 6 p.
2. Makhmudov M.A., Abdikhakimov B.I., Ulugberdiyev A.Sh., Kimizbayeva A.E., Gulyamova S.T. Automatic Water Pump Control System Using GSM Module and Arduino: Automation of Water Supply System (GSMUZ08). – Tashkent: Science and Innovation, 2024. – Vol. 3, No. A10. – P. 221– 226. – 6 p.
3. Makhmudov M.A., Ulugberdiev A., Ibrohimov S., Khurramov A. Interactive Tools Development for Teaching Medical Technologies. – Tashkent: SCIENCE Journal, 2025. – Vol. 4, No. 1-2. – P. 68–71. – 4 p.
4. Makhmudov M.A., Isakhanov Z.A., Eltazarov B. Electronic, Crystal Structure and Physicochemical Properties of Multilayer Multicomponent Nanoscale Structures Created at Different Depths Based on Ta and Ni. – Tashkent: SCIENCE Journal, 2025. – Vol. 4, No. 2-1. – P. 52–58. – 7 p.
5. Gaibnazarov B.B., Makhmudov M.A., Tuychiev F.F. Smart Automatic Parking System Using NodeMCU Microcontroller. – Tashkent: Science and Innovation, 2024. – Vol. 3, Special Issue 36. – P. 32–33. – 2 p.
6. Makhmudov M.A., Alimova Z., Kimizbayeva A. Display Data in Histogram Form Using the Arduino Platform. – Moscow: Universum, 2023. – P. 16–19. – 4 p.
7. Gulyamova Saodat Tulyaganovna, Tulyaganov Alisher Anvarovich, Abdukarimov Sherali Nurali O‘G‘Li, Mahmudov Mahmud Akbar O‘G‘Li, Ergashev Azizjon Erkinovich. Texnologik jarayonlarni boshqarishda PLC (logik kontrollerlar) ning o ‘rni. – Tashkent: Science and Innovation, 2024. – Vol. 3, Special Issue 50. – P. 434–436. – 3 p.

PROPERTIES OF POROUS ARBOLITE BASED ON MODIFIED NON-FIRED ALKALINE BINDERS

F.D. Zhuraeva[1], S.R. Akhundzhanova[2], J.I. Kholikov[2]
PhD, Associate Professor, Tashkent University of Architecture and Civil Engineering[1]
Senior Lecturer, Tashkent University of Architecture and Civil Engineering[2]
First-year basic doctoral student at the Tashkent University of Architecture and Civil Engineering[3]
https://doi.org/10.5281/zenodo.20838453

Abstract. *This study investigates porous arbolite produced with modified non-fired alkaline binders using electrothermophosphorus slag, Asmansay basalt, and agricultural wastes such as cotton stalks, rice husk, and kenaf shives. Experimental mixtures were tested under heat-moisture and natural curing conditions to evaluate workability, compressive strength, and the influence of basalt dosage on binder performance. Results show that basalt can partially replace slag while maintaining sufficient strength and improving technological properties. Under natural curing, basalt contents of 20–50% were effective, with 40% giving the best performance: 40–47 MPa after 7 days and up to 70 MPa after 28 days. The findings support sustainable, resource-efficient, cementless construction materials based on local industrial and agricultural wastes.*

Keywords: *porized arbolite, modified, unfired alkaline binders, electrothermophosphorus slag, basalt, kenaf husk, rice husk, cotton stems, strength.*

Introduction. An analysis of global experience demonstrates that broad opportunities for solving this complex of problems are provided through the use of alkaline binders and concretes based on them. These materials possess a number of physical-mechanical and technical-operational characteristics that significantly exceed the corresponding properties of many other mineral binders and composites produced on their basis. For their production in the Central Asian region, and particularly in Uzbekistan, raw material resources are available in the form of large-scale waste from the metallurgical, chemical, and energy industries, as well as agricultural plant waste.

The versatility of these materials is characterized by a wide compressive strength range: from 20 to 160 MPa for binders and from 0.5 to 150 MPa for concretes, with an average density of 200–3500 kg/m³. The prospects for the application of these binders are determined by the fact that their production is based on the utilization of industrial waste and by-products, including all types of granulated and dump slags, fly ash and ash-slag mixtures, as well as alkali-containing waste, among others [1]. This indicates that such binders can be produced in all regions of the world. At the same time, it should be noted that the utilization of industrial waste simultaneously addresses environmental and fuel-energy issues and also expands the raw material base for construction materials [2].

Significance of the Research. The development of resource- and energy-saving technologies for the production of thermal insulation material—porous arbolite based on alkaline binders with the addition of basalt as an aluminosilicate raw material—makes it possible to utilize agricultural waste and local basalt deposits, efficiently recycle industrial waste, produce new

construction materials, reduce environmental pollution, and contribute to lowering the cost of both the material itself and construction processes in general.

Experimental Program. The Central Asian republics possess sufficient reserves of raw materials for the production of alkaline binders and organomineral composite materials based on them. At present, these raw materials are partially utilized as additives in cement production [3].

The study employed local raw materials and industrial technogenic waste. The following materials were used as the aluminosilicate component (ASC) of the alkaline binder: Zhambyl electrothermophosphorus (ETP) slag and basalt from the Asmansay deposit. Cotton stalks, rice husk, and kenaf shives were used as organic aggregates in the investigations [4].

Methods of Physical and Mechanical Testing. *For testing, cube specimens with dimensions of 20 × 20 × 20 mm were prepared from paste of standard consistency. Heat and moisture treatment was carried out according to a 2+6+2 h regime at an isothermal holding temperature of 80–90°C.*

In the production of foam concrete, the conventional technology was applied: the binder paste and foam were prepared separately and subsequently mixed together. The duration of the study of the hardening processes of binders and concretes was up to 360 days. The specimens were stored under the following conditions: under normal curing conditions—in a chamber with a hydraulic seal at 100% relative humidity; under water curing—in a water container in accordance with KMK standards. The storage temperature of the specimens was maintained at 20°C [5].

Specimens measuring 100 × 100 × 100 mm were manufactured. The workability of the initial mixture was determined using a Suttard viscometer. The compressive strength of foam concrete and porous arbolite specimens was determined using a P10 hydraulic press. In order to determine the effect of basalt content on the strength of alkaline binder stone, several compositions were prepared and investigated for compressive strength under different curing conditions.

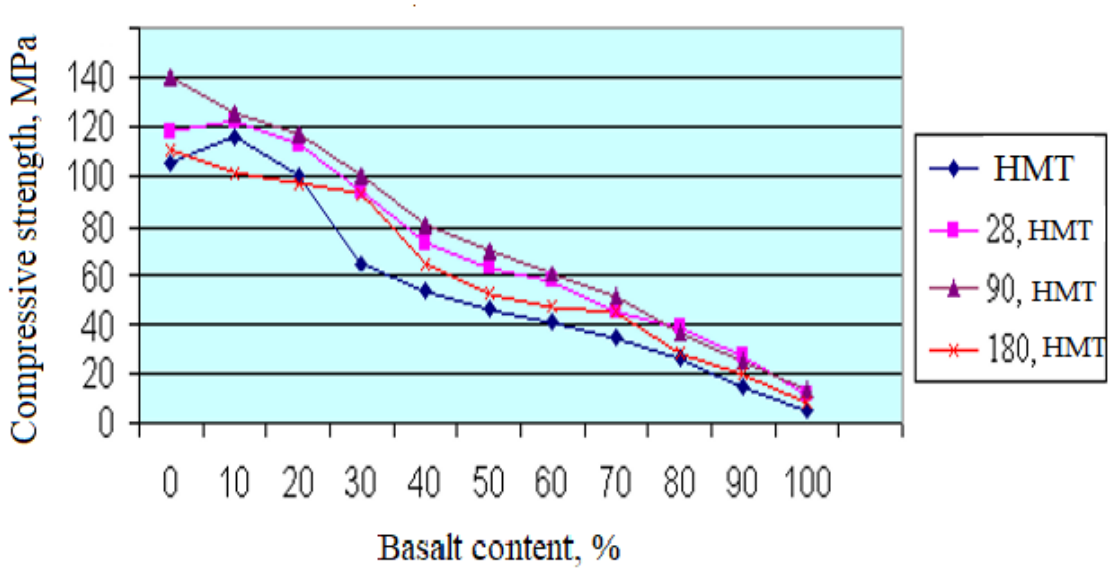


Fig. 1. Strength of binders after heat and moisture treatment depending on basalt content

As a result of the conducted research and processing of the obtained data for the investigated binder composition, the optimal formulations of modified alkaline binders were determined. Based on the analysis of the experimental data, strength graphs of the developed binders were constructed.

The analysis of the graphs showed that when basalt is used as an additive component, the strength depends on the amount of ETP slag and the type of alkaline component. With a binder composition ratio of 1:1 (ETP slag:basalt) in the presence of sodium disilicate with a density of 1300 kg/m³, the strength of the specimens decreases by almost 50% and amounts to 46 MPa after heat and moisture treatment, compared to 110 MPa for a similar specimen based on pure ETP slag. A similar trend was observed after 28 days following heat and moisture treatment, where the strength reached 63 MPa compared to 125 MPa for the pure ETP slag binder (Fig. 1).

When basalt is introduced in an amount of 20%, it is possible to obtain a modified alkaline binder based on sodium disilicate with a strength of 100 MPa after heat and moisture treatment and 110 MPa after 28 days, respectively. At a basalt content of 30%, the strength of the modified alkaline binder is 65 and 94 MPa; at 40%, 53 and 73 MPa; and at 50%, 46 and 63 MPa, respectively. At the same time, it becomes possible to reduce the consumption of ETP slag by up to 50% of the total raw mixture mass.

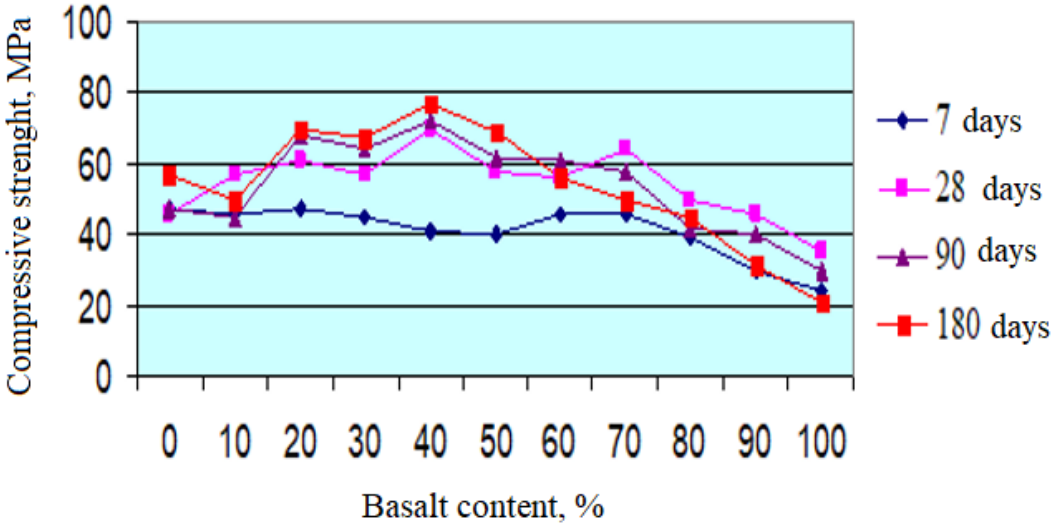


Fig. 2. Strength of binders under natural curing conditions depending on basalt content

Under natural curing conditions for 7 days, during the hardening of the binder in the presence of sodium disilicate, the optimal basalt content ranges from 20 to 50%, with the optimum value being 40% (from the standpoint of saving electrothermophosphorus slag while maintaining sufficient strength of the alkaline binder). In this case, the activity of the binders at 7 days of natural curing reaches 40–47 MPa with a sodium disilicate density of 1300 kg/m³. After 28 days of natural curing of the modified alkaline binder, the optimal composition also lies within the range of 20–50% basalt content, while the maximum strength is achieved at a basalt content of 40% of the total raw mixture mass, with the strength reaching up to 70 MPa (Fig. 2).

The results obtained after 7 days of natural curing indicate that the difference in binder strength with increasing basalt content is not as pronounced as after heat and moisture treatment. Even at a basalt content of 90%, the strength of the modified alkaline binder after 7 days decreases by only about 50% (30 MPa) compared with the binder containing 10% basalt (45 MPa). It was established that the strength values of the specimens after natural curing are relatively similar, whereas the strength of heat- and moisture-treated specimens decreases sharply with increasing basalt content.

From the above-described experimental investigations, it was established that the most effective use of basalt with a soda-based alkaline component is its application as an additive (up

to 30%) in order to reduce the consumption of electrothermophosphorus slag and to increase the workability of the modified alkaline binder.

Conclusion. The experimental findings demonstrated that basalt additive can be effectively utilized as an active mineral constituent in alkali-activated binders modified with sodium disilicate. The influence of basalt incorporation on the physical and mechanical performance of the binder system was comprehensively investigated, allowing the determination of its optimum dosage. The obtained results revealed that a basalt content ranging from 20% to 50% provides the most favorable conditions for the development of strength under natural curing. In particular, the incorporation of 40% basalt yielded the highest performance, resulting in compressive strengths of 40–47 MPa after 7 days and up to 70 MPa after 28 days of curing.

The analytical assessment indicated that, under natural curing conditions, the reduction in compressive strength caused by increasing basalt content occurred gradually rather than abruptly. This behavior can be attributed to the partial participation of basalt in alkaline reactions, which contributes to the densification of the binder matrix and promotes the formation of a more compact microstructure. In contrast, specimens subjected to heat and moisture treatment exhibited a pronounced decline in strength as the proportion of basalt increased. These observations suggest that excessive basalt content adversely affects the structural development of the alkali-activated system when thermal curing regimes are applied.

Furthermore, the results confirmed that the partial replacement of electrothermophosphorus slag with basalt not only decreases the consumption of slag resources but also enhances the technological and rheological characteristics of the modified binder. Consequently, the proposed approach offers significant scientific and practical advantages for the production of sustainable, resource-efficient, and environmentally friendly cementless binder materials. The identified relationships between basalt dosage, curing conditions, and strength development provide a valuable basis for the design and optimization of advanced alkali-activated construction materials with improved performance characteristics.

REFERENCES

1. Tulaganow, Kh. Kamilov, H. B. Fisher, P. Krivenko *Zur Extraktion wasserlöslicher Stoffe aus organischen Zuschlägen und Auswirkung auf erhärtende Bindersysteme.* Proceedings of the 16th International Baustofftagung, Bauhaus University Weimar, Weimar, 2006, Vol. 1, pp. 845–856.
2. Kh. Kh. Kamilov *Technology and Properties of Arbolite Based on Non-Fired Binder and Agricultural Waste.* Abstract of PhD Dissertation in Engineering Sciences. Tashkent, 1997, 20 p.
3. O. Kasimov (2023). *Formation of the Structure of Arbolite and Its Influence on the Strength Characteristics of the Material.* Central Asian Journal of Education and Innovation, 2(11 Part 2), 115–118.
4. I.K. Kasimov, Kh. Kh. Kamilov, A. A. Tulaganov (1989). *Composition, Properties, and Technology of Slag-Alkaline Arbolite Based on Agricultural Waste. Slag-Alkaline Cements, Concretes and Structures,* Abstracts of Reports, pp. 152–153.
5. O.B. Kosimov, T.S. Aubakirova, N.H. Mirzakobilov (2023). *Studies of the Kinetics of Structure Formation of Slag-Alkaline Arbolite.* Central Asian Journal of Education and Innovation, 2(11 Part 3), 89–94.

DEVELOPMENT OF AN IDEF0 MODEL FOR NETWORK ANOMALY MONITORING SYSTEMS

Sh.B. Redzhepov[1], B.Sh. Makhkamov[2]
Associate Professor, Department of Digital Technology Convergence, TUIT[1]
Professor, Department of Economics in ICT, TUIT[2]
https://doi.org/10.5281/zenodo.21273252

Abstract. *This article presents a functional model of an intelligent monitoring system for computational processes developed on the basis of the IDEF0 methodology. A conceptual architecture is proposed for a software-hardware complex that supports the collection, processing, analysis, forecasting, and visualization of information on the state of distributed computing systems and computer networks. Functional modeling was carried out for the principal system processes, including the formation of network topology, the collection of monitoring data, the detection of anomalies and threats, and the visualization of analytical results. For each functional block, input information flows, control actions, implementation mechanisms, and output results were identified. This made it possible to formalize interaction among the components of the monitoring system. The article also examines the software and hardware tools used to implement the proposed architecture, including Python/Django, PostgreSQL, Redis, WebSocket, microcontroller devices, and a graphical visualization module. The proposed model provides an integrated representation of the system structure, increases the efficiency of monitoring-data processing, supports the timely detection of anomalous states, and provides information support for decision-making in the management of computing infrastructure. The developed functional model can serve as a conceptual basis for designing intelligent monitoring systems for computational processes, distributed computing systems, and computer networks, as well as for further development of mathematical models, analytical algorithms, and software implementation.*

Keywords: *functional modeling, IDEF0, monitoring-system architecture, monitoring of computational processes, distributed computing systems, computer networks, network topology, anomaly detection, network traffic analysis, intelligent monitoring, software-hardware complex, data visualization, WebSocket, Python/Django, PostgreSQL, Redis.*

1. Introduction

This study presents a functional model of a monitoring system for computational processes developed in accordance with the IDEF0 methodology. The contextual diagram A-0 represents the main function of the system - performing network monitoring - together with the input data, control actions, implementation mechanisms, and output results. The model reflects the logical structure of a system that collects, processes, analyzes, forecasts, and visualizes information about the state of computing systems and network infrastructure.

The decomposition of block A-0 reveals the internal organization of the monitoring process and includes four interconnected functional blocks: the formation of network topology, the collection of monitoring information, the detection of anomalies and threats, and the visualization of results. Each block performs a specific function and interacts with the other components of the system, ensuring the sequential processing of data and the formation of an information representation for the administrator.

The proposed functional model forms the conceptual basis for the architecture of a software-hardware network-monitoring complex aimed at improving the reliability, resilience, and efficiency of managing distributed computing systems. The model makes it possible to formalize monitoring processes, determine information flows, specify control actions and implementation mechanisms, and provide a basis for developing a software platform and algorithms for intelligent analysis of the state of the network.

Figure 1 presents the contextual diagram of functional block A-0, which describes the process of implementing network monitoring in a computing infrastructure. The central functional module is designated as “Performing Network Monitoring.” The diagram follows the logic of IDEF0: input data are shown on the left, control actions are shown at the top, implementation mechanisms are shown at the bottom, and output results are shown on the right.

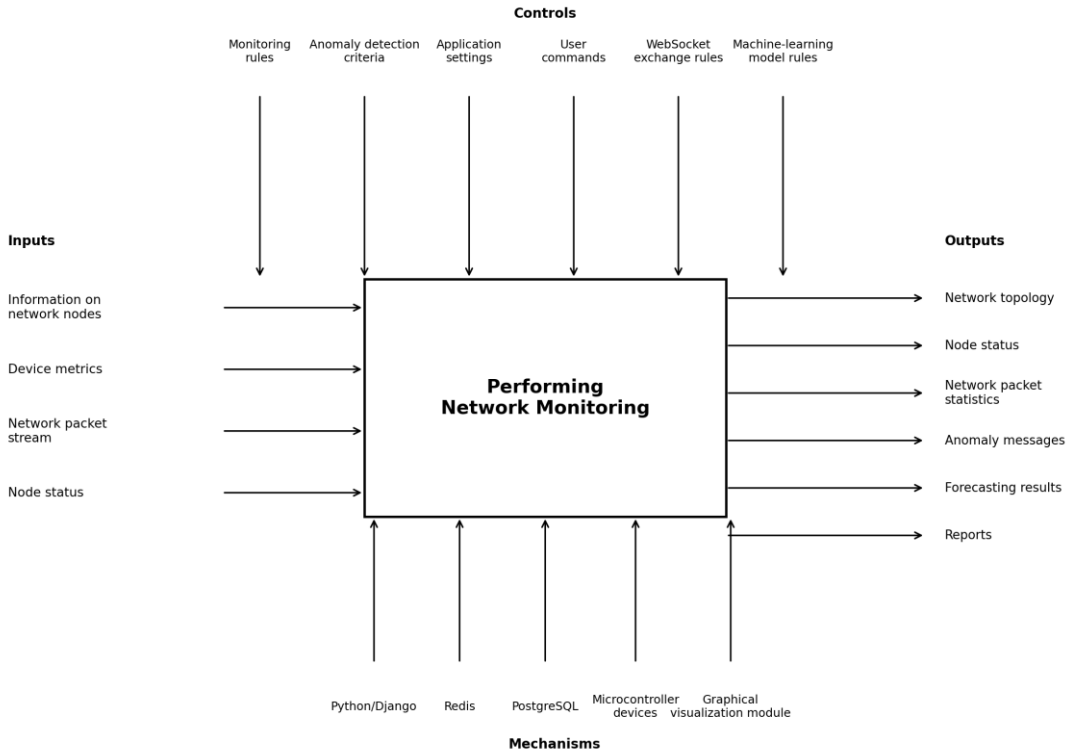


Figure 1. IDEF0 contextual diagram for a network monitoring system.

The system receives information on network nodes, metrics from devices, streams of network packets, and the current state of nodes as input data. These data form the initial information base for monitoring and make it possible to assess the state of the computing network dynamically.

The control actions include monitoring rules, anomaly-detection criteria, application settings, user commands, WebSocket exchange rules, and machine-learning model rules. These controls determine the logic of processing incoming data, the modes of analysis, the parameters for detecting deviations, and the procedure for interaction among system components.

The implementation mechanisms consist of software and hardware resources: Python/Django, Redis, PostgreSQL, microcontroller devices, and a graphical visualization module. Python/Django provides server-side processing and business logic; Redis is used for fast data transmission and caching; PostgreSQL performs long-term storage; microcontrollers collect primary data; and the visualization module presents monitoring results in a clear form.

The outputs include the network topology, node status, packet statistics, anomaly messages, forecasting results, and reports. These outputs provide a comprehensive assessment of the state of the computing network, enable the detection of potential failures, support the analysis of the dynamics of network processes, and assist decision-making in managing a distributed computing system.

2. Materials and Methods

2.1. Functional modeling approach

The methodological basis of the study is IDEF0 functional modeling. This methodology represents a system as a set of functions and describes each function through four categories of information flow: inputs, controls, mechanisms, and outputs. This approach is particularly suitable for conceptualizing monitoring systems because it makes the functional boundaries, data flows, operational rules, implementation resources, and final results explicit.

In the present model, the system boundary is established by the contextual diagram A-0. The main function is formulated as “Performing Network Monitoring.” The purpose of the model is to describe how data from computing infrastructure are transformed into analytical outputs that support administrative decisions. The model is therefore not limited to the acquisition of telemetry; it also includes processing, anomaly detection, forecasting, and visualization.

In accordance with IDEF0, all information flows in the system are divided into the following four categories:

- Input data, which enter the function and are transformed during monitoring;
- Control actions, which define the rules, constraints, and parameters of system operation;
- Implementation mechanisms, which provide the software and hardware resources required to perform the function;
- Output results, which represent the information products generated after processing and analysis.

2.2. Central functional block A-0

The central functional block A-0, “Performing Network Monitoring,” is the core of the entire monitoring system. Its main task is to integrate data flows received from different components of the computing infrastructure, perform subsequent analytical processing, detect anomalies, forecast the state of the network, and generate results for the system administrator.

Functionally, this block performs the following operations:

- collecting information from network devices;
- receiving telemetry data;
- processing network traffic;
- analyzing the state of nodes;
- filtering incoming data;
- comparing parameters with permissible values;
- applying anomaly-detection algorithms;
- forecasting the subsequent behavior of the network;
- storing analysis results;
- transmitting results to the user.

Thus, the central block represents an intelligent decision-support system for the operation of a distributed computing infrastructure.

3. Results

3.1. Input information flows

The input data are located on the left side of the contextual diagram and form the informational basis for monitoring. Four input flows are defined.

3.1.1. Information on network nodes

This flow contains information about all objects of the computing network. It includes:

- IP address;
- MAC address;
- device identifier;
- equipment type;
- belonging to a particular network segment;
- logical links between devices;
- routing information.

This information is used to construct a network map and determine relationships among the monitored objects.

3.1.2. Metrics received from devices

This flow includes quantitative characteristics of the operation of computing devices. The main parameters are:

- processor load;
- random-access memory utilization;
- disk subsystem load;
- equipment temperature;
- network delays;
- data-transfer rate;
- energy consumption;
- communication-channel utilization.

The collected metrics provide initial information for analyzing the performance of the computing system.

3.1.3. Network packet stream

This flow represents data obtained through the analysis of network traffic. It includes:

- TCP packets;
- UDP packets;
- ICMP messages;
- HTTP/HTTPS requests;
- DNS requests;
- connection statistics;
- direction of information transmission.

On the basis of this flow, the system detects network attacks, communication-channel overloads, and anomalous user behavior.

3.1.4. Node status

This flow characterizes the current state of each element of the distributed computing system. For each node, the following indicators are determined:

- activity;
- availability;

- presence of a connection;
- operability;
- response time;
- probability of failure.

The resulting information is used to assess the overall stability of the computing network.

3.2. Control actions

The upper part of the diagram contains the elements that define the operating rules of the monitoring system.

3.2.1. Monitoring rules

This block specifies the general strategy of system operation. It defines:

- the frequency of device polling;
- the list of controlled parameters;
- permissible value ranges;
- data-processing priorities.

3.2.2. Anomaly-detection criteria

This block contains mathematical rules for detecting deviations. In particular, it uses:

- statistical criteria;
- threshold values;
- adaptive intervals;
- time-series comparison methods;
- probabilistic models.

This block is responsible for automatically identifying abnormal situations.

3.2.3. Application settings

Application settings determine the parameters of the software platform. They include connection parameters, security settings, update frequency, and user-interface configuration.

3.2.4. User commands

User commands allow the administrator to interactively control the system. Examples include:

- starting monitoring;
- stopping monitoring;
- changing the configuration;
- viewing statistics;
- generating reports.

3.2.5. WebSocket exchange rules

This block enables real-time operation of the system. Its main functions are maintaining a continuous client-server connection, instantly transmitting data, and updating the interface without reloading the page.

3.2.6. Machine-learning model rules

This block governs the intelligent analysis of information. It includes a trained model, classification parameters, forecasting algorithms, and rules for detecting hidden dependencies. Through this component, intelligent network monitoring is implemented.

3.3. Implementation mechanisms

The lower part of the diagram describes the software and hardware resources used to implement the system.

3.3.1. Python/Django

Python/Django functions as the main server platform. It performs request processing, manages business logic, interacts with the database, implements the REST API, and integrates analytical algorithms.

3.3.2. Redis

Redis is used as a high-performance operational data store. It provides caching, message queuing, event exchange, and acceleration of streaming-data processing.

3.3.3. PostgreSQL

PostgreSQL is the main information-storage system. It is used to store monitoring history, event logs, equipment parameters, and analytical SQL queries.

3.3.4. Microcontroller devices

Microcontroller devices represent the hardware layer of the system. They collect primary data, measure physical parameters, transmit telemetry, and interact with the monitoring server.

3.3.5. Graphical visualization module

The graphical visualization module is intended to present analysis results to the user. It constructs graphs, displays the state of the network, displays diagrams, and forms a monitoring dashboard.

3.4. Output results

After processing the information, the system generates the following results.

3.4.1. Network topology

The system automatically builds a logical network diagram. This makes it possible to determine device relationships, localize faults, and assess the structure of the network.

3.4.2. Node status

Node status displays the operability of each device and indicates whether the node is in an Online, Offline, Warning, or Critical state.

3.4.3. Network packet statistics

Network packet statistics include the number of packets, the amount of transmitted information, transmission speed, and transmission errors.

3.4.4. Anomaly messages

Anomaly messages are generated automatically when the system detects overload, equipment failure, unauthorized access, network attacks, or critical deviations of parameters.

3.4.5. Forecasting results

Forecasting results are generated on the basis of machine-learning models. They make it possible to predict the probability of equipment failure, future network load, the development of abnormal situations, and changes in the performance of the computing system.

3.4.6. Reports

Reports contain monitoring results, statistical indicators, event logs, analytical conclusions, and recommendations for network optimization.

3.5. Decomposition of functional block A-0

Figure 2 represents the decomposition of the contextual diagram A-0 and corresponds to the second level of the IDEF0 model. It describes the internal architecture of the intelligent monitoring system for computational processes and computer networks. Unlike the upper-level contextual diagram, this model reveals the sequence of information processing and the interaction of individual functional subsystems.

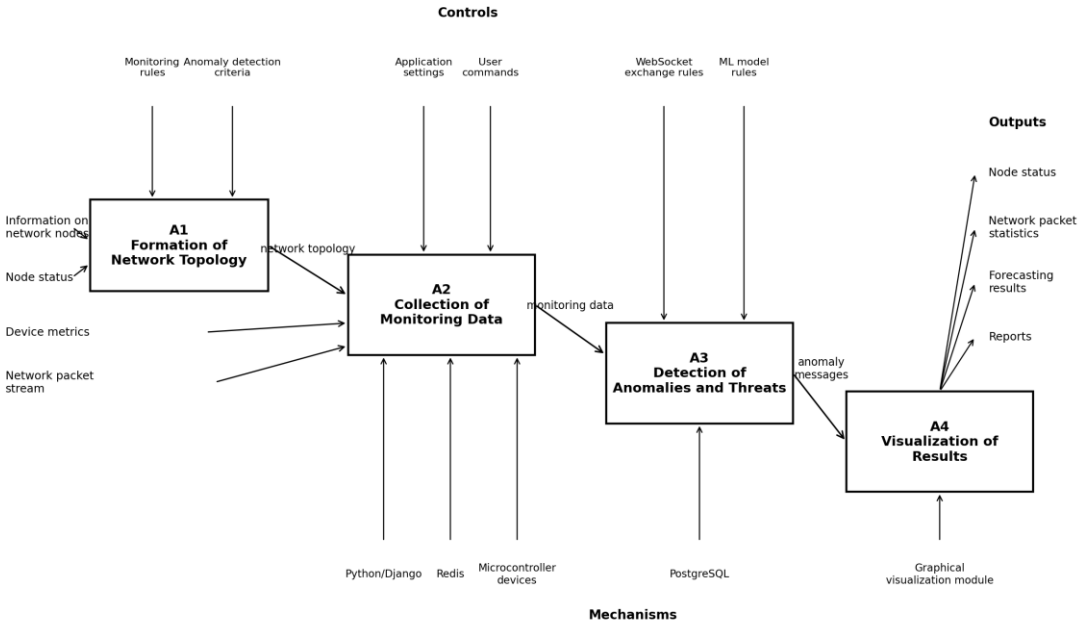


Figure 2. Sequential information-processing pipeline in a network monitoring system.

The architecture of the system includes four interconnected functional blocks:

- A1 - Formation of network topology;
- A2 - Collection of monitoring information;
- A3 - Detection of anomalies and threats;
- A4 - Visualization of monitoring results.

Each block performs an independent information-processing function and transmits its results to the next stage of analysis.

3.5.1. Block A1: Formation of network topology

The first functional block is intended to automatically construct the logical structure of the computing network. The main objective of this stage is to obtain information about all network devices and form a model of relationships among them.

The input data for this block include information about network nodes and the current state of each network node. Information can be obtained through SNMP, ICMP, LLDP, ARP, NetFlow, and active network-scanning tools.

The operation of the block is determined by monitoring rules and anomaly-detection criteria. These rules specify the frequency of topology updates, the list of controlled devices, and the permissible states of network elements.

During operation, the block performs the following procedures:

- identification of all active network devices;
- determination of links between nodes;
- determination of data-transmission routes;
- detection of new devices;
- removal of inaccessible objects;
- updating of the network structure;
- formation of a graph model of the computing infrastructure.

The obtained topology becomes the basic model for subsequent analysis of the network state. The output of the block is information on the network topology, which is transmitted to the next functional block.

3.5.2. Block A2: Collection of monitoring information

The second functional block implements the centralized collection of telemetry information from all components of the distributed computing environment. At this stage, all incoming parameters are aggregated into a unified information model.

The inputs include information about the network topology, device metrics, and the network packet stream. The operation of the block is regulated by application settings and user commands. The administrator can change the device polling frequency, the list of controlled parameters, and the operating mode of the monitoring system.

The block is implemented through several components. Python/Django processes incoming requests, manages application logic, supports interaction among all system components, and performs analytical procedures. Redis is used to cache operational data, transmit messages between services, and accelerate the processing of streaming information. Microcontroller devices obtain primary measurements, transmit telemetry parameters, interact with sensors, and control the physical parameters of equipment.

Within the block, the following operations are performed:

- data reception;
- information filtering;
- stream synchronization;
- format normalization;
- removal of duplicate messages;
- preliminary information processing;
- formation of a unified array of monitoring data.

After processing is complete, the information is transmitted to the intelligent-analysis module.

3.5.3. Block A3: Detection of anomalies and threats

This functional block is the analytical core of the entire system. Its main task is to conduct intelligent analysis of the current state of the computing network and identify potential threats.

The inputs include information about the network topology and monitoring results. The operation of the block is determined by WebSocket exchange rules and machine-learning model rules. The use of WebSocket enables the system to receive information with minimal delay, while machine-learning models enable automatic classification of network states.

PostgreSQL is used as the implementation mechanism. The database stores monitoring history, accumulates statistical data, stores event logs, prepares training samples, and supports analytical queries.

The block implements the following functions:

- analysis of network behavior;
- comparison of current parameters with reference values;
- search for statistical deviations;
- detection of anomalies;
- identification of network attacks;
- risk-level assessment;

- forecasting of possible equipment failures;
- determination of the probability of critical states.

The output of the block consists of anomaly messages, which are transmitted to the visualization module.

3.5.4. Block A4: Visualization of results

The final functional block is intended to present analytical results to the user. At this stage, information is transformed into a form that is convenient for perception and practical decision-making.

The inputs include anomaly messages and analysis results. The implementation mechanism is the graphical visualization module, which constructs interactive dashboards, graphs, diagrams, topology maps, tables, and analytical reports.

The block performs the following operations:

- visualization of the current state of the network;
- display of network-traffic statistics;
- construction of time-series graphs;
- display of identified threats;
- presentation of forecasting results;
- formation of analytical reports.

After processing is complete, the user receives the status of computing nodes, network packet statistics, forecasting results, and reports on network operation. These results are used by computing-infrastructure administrators to assess network operability, detect faults in a timely manner, predict possible failures, and make decisions on optimizing the functioning of the distributed computing system.

4. Discussion

The functional model demonstrates that network monitoring should be understood as a complete information-processing cycle rather than as a set of isolated technical operations. The process begins with the identification of network topology and the acquisition of telemetry and traffic data, continues through filtering, normalization, analysis, and anomaly detection, and ends with visualization, reporting, and support for administrative decision-making.

The use of IDEF0 makes the architecture transparent because it distinguishes between input flows, governing rules, enabling mechanisms, and outputs. This distinction is important for distributed computing environments, where reliability depends not only on data collection but also on the coordinated interaction of software services, databases, microcontroller devices, real-time communication channels, and analytical models.

The proposed architecture also clarifies the role of intelligent analysis in monitoring systems. Machine-learning rules and anomaly-detection criteria transform raw monitoring data into information about possible risks, hidden dependencies, abnormal states, and likely equipment failures. At the same time, WebSocket-based exchange supports near-real-time data delivery, while Redis and PostgreSQL separate operational processing from long-term storage and analytical querying.

From a practical perspective, the model can support the design of software platforms for monitoring distributed networks, the specification of functional requirements, the planning of database and visualization modules, and the further development of mathematical models for forecasting and anomaly detection. By formalizing interactions among all major components, the

model contributes to improving the reliability, fault tolerance, and manageability of computer-network infrastructure.

5. Conclusion

Functional modeling is an important tool for designing intelligent monitoring systems for computational processes and distributed computing systems. The application of the IDEF0 methodology makes it possible to formalize the system architecture, determine relationships among functional components, information flows, control actions, and software-hardware mechanisms, and thereby provide an integrated representation of information-processing processes.

The upper-level contextual diagram defines the boundaries of the system under study, its main function, the composition of input data, control actions, implementation mechanisms, and processing results. The decomposition of the contextual model reveals the internal functional structure of the system, including the formation of network topology, the collection and preliminary processing of monitoring data, intelligent detection of anomalies and threats, forecasting of possible failures, visualization of analytical results, and support for decision-making.

The interaction of the functional modules forms a closed monitoring cycle that ensures continuous control of the state of the computing infrastructure, timely identification of deviations, forecasting of potential failures, and improved efficiency in managing distributed computing systems and computer networks. Sequential data processing and the integration of analytical mechanisms increase the reliability of assessment of the current network state and the speed of managerial decision-making.

The proposed functional model forms the conceptual basis for constructing an intelligent monitoring system for computational processes. The developed architecture determines the composition of the main functional modules, the mechanisms of their interaction, and the directions of information exchange. It creates a foundation for further development of mathematical models, analysis and forecasting algorithms, anomaly-detection methods, and software implementation of a monitoring system oriented toward improving the reliability, fault tolerance, and operational efficiency of distributed computing systems.

REFERENCES

1. Ross, D. T. (1977). Structured Analysis (SA): A language for communicating ideas. IEEE Transactions on Software Engineering, SE-3(1), 16-34.
2. Marca, D. A., & McGowan, C. L. (1988). IDEF0/SADT Business Process and Enterprise Modelling. Eclectic Solutions Corporation.
3. Colquhoun, G., Baines, R., & Crossley, R. (1993). A state-of-the-art review of IDEF0. International Journal of Computer Integrated Manufacturing, 6(4), 252-264.
4. National Institute of Standards and Technology. (1993). Integration Definition for Function Modeling (IDEF0). Federal Information Processing Standards Publication 183. Gaithersburg, USA: NIST.
5. Dennis, A., Wixom, B. H., & Tegarden, D. (2020). Systems Analysis and Design: An Object-Oriented Approach with UML (6th ed.). Wiley.
6. Sommerville, I. (2016). Software Engineering (10th ed.). Pearson Education.
7. Bass, L., Clements, P., & Kazman, R. (2021). Software Architecture in Practice (4th ed.). Addison-Wesley.

8. Tanenbaum, A. S., & Wetherall, D. J. (2021). Computer Networks (6th ed.). Pearson.
9. Stallings, W. (2022). Network Security Essentials: Applications and Standards (7th ed.). Pearson.
10. Peterson, L. L., & Davie, B. S. (2021). Computer Networks: A Systems Approach (6th ed.). Morgan Kaufmann.
11. Barford, P. (2019). Network Performance Anomaly Detection and Diagnosis. Springer.
12. Chandola, V., Banerjee, A., & Kumar, V. (2009). Anomaly detection: A survey. ACM Computing Surveys, 41(3), Article 15.
13. Ahmed, M., Mahmood, A. N., & Hu, J. (2016). A survey of network anomaly detection techniques. Journal of Network and Computer Applications, 60, 19-31.
14. Bishop, C. M. (2006). Pattern Recognition and Machine Learning. Springer.
15. Goodfellow, I., Bengio, Y., & Courville, A. (2016). Deep Learning. MIT Press.
16. Manenti, G., Ebrahimiarjestan, M., Yang, L., & Yu, M. (2019). Functional modelling and IDEF0 to enhance and support process tailoring in systems engineering. Proceedings of the 5th International Conference on Design Engineering and Science.
17. Tsiberman, V., & Belov, A. Using the IDEF0 methodology in monitoring system modeling.
18. Pop, G. I., & Țîțu, A. M. (2021). Application of the IDEF0 management method in the global engineering process within an industrial organization in aerospace. Strategica Conference Proceedings, 1046-1058.
19. Fedorova, N., et al. (2020). Application of IDEF0 functional modeling methodology at the initial stage of designing industrial systems. E3S Web of Conferences.
20. Sáez-de-Cámara, X., Flores, J. L., Arellano, C., Urbieta, A., & Zurutuza, U. (2023). Clustered federated learning architecture for network anomaly detection in large-scale heterogeneous IoT networks. arXiv.

THE ESSENCE OF THE PROBLEM OF POVERTY IN RURAL AREAS, ITS CAUSES, CRITERIA, AND MANIFESTATION IN AGRICULTURE

I.G. Yoqubjonov
Lecturer, Department of Finance, "UBS"
https://doi.org/10.5281/zenodo.20697380

Abstract. *This article examines the essence of poverty in rural areas, its main causes, measurement criteria, and specific manifestation in agriculture. The study analyzes poverty not only as a lack of income, but also as a multidimensional socio-economic condition reflected in limited access to employment, education, healthcare, nutrition, housing, and social participation. Special attention is given to rural poverty in Uzbekistan, where household plots, dehqon farms, commercial farms, horticulture, and seasonal agricultural activity play an important role in income generation. The article discusses international and national approaches to poverty measurement, including absolute and multidimensional criteria, and considers the relevance of these approaches for local conditions. It also identifies unemployment, unequal access to land, insufficient infrastructure, limited investment, and weak market access as key factors deepening rural poverty. The paper concludes that effective poverty reduction in rural areas requires transparent land allocation, agricultural services, storage facilities, employment creation, and long-term investment support.*

Keywords: *poverty, rural poverty, agriculture, poverty measurement, unemployment, household plots, poverty reduction.*

Introduction

Poverty is considered one of the most important problems in the world in which we live today. The fact that around 8% of the population of the Earth lives in poverty demonstrates to us the significance of this problem. This means that approximately 600 million people on the planet live in poverty — that is, they earn less than 1.9 dollars per day. The very fact that the Government of Uzbekistan is also taking practical measures to reduce poverty allows us to grasp the importance of this problem. The establishment of the Ministry of Economic Development and Poverty Reduction indicates that there is a need for a comprehensive, integrated struggle against this problem. In his address to the Oliy Majlis on the results of 2021, our President Sh. M. Mirziyoyev emphasized that more than 12% of the population of Uzbekistan — that is, around 5 million people — live in poverty; the fact that the head of state is raising this problem shows the even greater depth and scale of its importance. When we look at the manifestation of poverty in agriculture, the importance of making use of household plots (tomorqa), dehqon (smallholder) farms, fermer (commercial) farms, and horticultural enterprises in reducing it becomes clearly evident.

Analysis of Literature on the Subject

In order to express the essence of poverty in this article, we drew upon the reflections concerning a modern approach to poverty contained in the work of Lev M. Yu., "Poverty and the Subsistence Level of the Population in Ensuring Socio-Economic Security," and in the article by Yashar Pasha on the topic "Determination of Poverty on the Basis of Multidimensional Statistical Analysis." We observed that, in these works, poverty has been studied through new approaches.

The article by Khasanov Rustam Rabimovich on the subject “Socio-Economic Causes of Poverty” also cites materials presented on poverty. In measuring poverty, we made use of the views expressed by Obid Hakimov, Director of the Center for Economic Research and Reforms, and of the opinions stated in the interview conducted by Kun.Uz with Sergey Zorya, the Lead Agricultural Economist of the World Bank Representative Office in Uzbekistan; on this basis, the local measurement value of poverty was determined. In analysing poverty, use was made of the data on the demographic situation of the population and on agricultural indicators, presented year by year on the official website of the State Statistics Committee of the Republic of Uzbekistan.

At present, poverty is one of the most pressing problems throughout the world, and a number of tasks connected with eliminating it are arising before the world community. Poverty cannot be completely eliminated, but there are ways and measures to reduce it, as well as methods that have been used effectively in world practice. In the matter of reducing poverty, each country takes measures at the national level, while international organizations carry out practical work on a global scale. At this point a question arises: what is poverty itself, what are the causes of its emergence, and how is it to be combated?

What Is Poverty?

At the most general level, poverty is the absence of acceptable choices across a wide range of important life decisions — that is, a serious lack of a person’s freedom to do what he or she wishes. The inevitable consequence of poverty is shortage and deprivation in many spheres of a full life, namely the following:

- insufficient means to purchase the basic necessities of life;
- frequent illness and early death;
- a level of literacy and education that undermines adequate functioning and limits a person’s understanding of the world and of himself;
- living conditions that endanger physical and mental health;
- the most unsatisfactory and the most dangerous jobs;
- a lack of dignity and a lack of respect from others;
- exclusion from public affairs.

The concept of poverty is not limited solely to the material conditions of people’s lives; it is also expressed in poor health, lack of employment, social exclusion, poor nutrition, and the lack of personal security, all of which are ultimately connected with the socio-economic security of the population.

If we try to understand poverty through its manifestation in a way of life, what kind of family or person do people call a poor family or a poor person? Of course, poverty is expressed through a shortage of material resources. For example, to call a family poor we may also look at the indicator that the family’s living conditions at home are not good and that it has no car. If we dwell on still more complex indicators, we may recognize poverty by such markers as the inability of the family members to consume quality clothing and food products; the absence of adequate home conditions for the children of the family to receive an education; the lack of material means for the family members to spend their days off in a meaningful way — for example, the inability to make use of domestic tourism opportunities across the country; deprivation of access to quality medical services; the lack of the means to visit recreation centres and sanatoriums, and similar indicators. Another of the worst aspects of poverty is that it gives rise to a chain of impossibility, and there is a high probability that this chain will keep adding a new impossibility to itself. That is, as a result of the lack of material means, primary needs are first of all curtailed — food, clothing,

and the like. Insufficient satisfaction of medical needs increases the probability that members of a poor family will fall ill, which in turn limits their ability to satisfy their need for medicines. The absence of conditions for children's schooling limits their ability to join the ranks of the active members of society. Inadequate rest for the working members of the family leads to a deterioration of their mental and psychological state. Deprivation of the opportunity for quality nutrition leads to a weakening of the immune system of family members, which increases the probability of their falling ill and is thereby manifested in their being removed from the ranks of the family's able-bodied members; and many similar examples could be given.

If we analyse these and many other examples given for poverty, together with its consequences, we come to understand how important this problem is and how necessary it is to develop measures against it. Our people have a very apt saying: that it is better to prevent an illness than to treat it. To treat an illness, one must of course know where it has arisen. Likewise, in order to combat poverty, it is important to know what its causes are. Now let us turn to the causes of its emergence.

Materials and Methods

The existence of poverty is a social phenomenon that depends on the level of the economy and on the effectiveness of reforms. New economic relations and economic foundations give rise to one form or another of poverty. At a superficial glance, it seems that poverty depends on the subject himself and that the person is to blame for living in a destitute condition. Of course, every individual and every family is responsible for its own well-being. But for this, the economic relations in society and the legal rules and regulations in force must be capable of comprehensively unlocking a person's activity. The most important of these rules is economic freedom.

Every subject engages in economic activity within the limits of his own capabilities and obtains an income corresponding to the available resources. Freedom of activity does not mean equality in the market, but rather grants the right to make independent decisions. For this reason, poverty must be regarded not only as a subjective phenomenon, but also as the product of an objective process. The objective process, in turn, unfolds under the influence of particular factors and emerges as the causes that give rise to poverty. Especially during a period of economic transformation, economic, social, and political processes are the causes that give rise to the level and scale of poverty.

For the statistical analysis of multidimensional poverty, variables associated with poverty are used. These factors vary from country to country. They can be divided into the following four groups:

- the characteristics of the region;
- the characteristics of the settlements;
- the characteristics of the households;
- the characteristics of the individual.

The distinctive characteristics of a region include the following:

- isolation or remoteness of the area (underdeveloped infrastructure, difficulty of access to markets, low use of services, and so on);
- the resource base (natural resources, soil quality, and so on);
- precipitation, climate, and environmental conditions (drought, floods, earthquakes, and so on);
- regional authorities and governing bodies;
- inequality.

Areas include the following characteristics:

- the level of development of infrastructure;
- the distribution of land;
- the level of social welfare and use of services;
- social infrastructure / social capital.

The characteristics of a household include the following:

- the size of the household;
- the structure of the household (the demographic burden per worker, the dependency burden);
- the sex of the head of the family;
- real estate, land, and means of production (tools, tractors, vehicles, and so on), and housing;
- employment and the structure of income;
- the state of health and the level of education.

Individual characteristics include the following:

- age;
- level of education;
- employment;
- income;
- state of health;
- ethnic origin.

Poverty is an important social problem in every economic system. The scale of poverty differs depending on the volume of gross domestic product, the manner of its distribution, the country's production potential, and the standard of living of the population. This problem has a negative impact on the country's economic development, gives rise to structural mismatches in the labour market, disrupts economic and social ties, reduces the volume of the population's deposits, leads to a decline in aggregate demand, and causes low purchasing power.

The statistical analysis of poverty shows that the main factors influencing poverty are employment, the level of education, the structure of the family, and natural (ecological) conditions. In order to determine the degree of influence of these factors, the correlation factors among poverty indicators are examined. However, such an analysis does not account for the characteristics of the region, the households, and the settlements, nor for the level of the country's socio-ecological and socio-economic development.

We have seen that one of the main factors giving rise to poverty is unemployment. Therefore, we need to consider the causes of the emergence of unemployment. In every society there is, of course, a class of the unemployed, but if its size exceeds an acceptable level, this leads to the class of the poor in that society growing beyond the norm. The economic potential of a country is one of the factors that cause the ranks of the unemployed among able-bodied people to grow. The industrialization of a country's economy, its export potential, and the opportunities created for doing business in the country may also be among the factors that lead to an expansion of the ranks of the unemployed. In rural areas, because of an insufficient number of jobs, the main part of the population of the region satisfies its employment and material needs through external migration. So what is the reason for this? The main reason for this may be the inability to make full use of the opportunities for processing the products produced in the region, for adding value to them, and for exporting them. There is also a high probability that another of the main reasons

is the fact that the land used in agriculture is not distributed in accordance with demand on the world consumer market.

Results and Discussion

In the economic literature there are three approaches to defining poverty: the absolute line; the relative characteristic; and the subjective assessment method, with the division of these into monetary and non-monetary. Recently, however, on the basis of a combination of these characteristics, an alternative concept known as the multi-criteria poverty threshold has been developed. Since our aim is to study absolute poverty, we consider the measurement of this type of poverty.

According to the absolute approach, poverty is determined on the basis of a minimum consumption basket. Households that do not possess the resources to satisfy the basic needs of their family members are considered poor. The value of the minimum consumption basket is scientifically substantiated and approved by the government of the country. This approach is used to assess the poverty threshold in a particular country. For international comparison, the World Bank's poverty index is used. Its PPP value in 2015 amounted to 1.9 dollars. This method of measurement is the minimum consumption basket, which includes not only food but also services, non-food products, minimum services, and the like. As Obid Hakimov, Director of the Center for Economic Research and Reforms, noted in an interview given to the Kun.Uz website, the level of poverty among the population, as stated by the country's leadership, amounts to 12–15%. Where do these figures come from? These figures were formed by taking into account people's minimum daily expenditures. This amount itself is not taken into account directly. At that value, the purchasing power is converted into a figure in the local currency — that is, it is calculated through the conversion coefficient of purchasing power parity (PPP). For example, in 2018, this coefficient for Uzbekistan was set at a PPP value of 1,784 soum to 1 US dollar. According to calculations for 2020, this amount corresponded to 5,600 soum per person. In Uzbekistan, for a family with an average of 5 family members, a monthly income of, on average, more than 840,000 soum is what separates that family from the poverty threshold. At present, approximately 12% of the population of Uzbekistan lives in poverty. This means that nearly 5 million people in Uzbekistan live in poverty.

In order to reduce this figure, a great deal of work is being carried out by the government. For example, with the aim of reducing poverty, the Ministry of Economy and Poverty Reduction was established. The Ministry for the Support of the Mahalla and the Family — an organization accountable to the government and intended to organize work with citizens at the mahalla level in a systematic way — was established. With the aim of identifying the poor stratum of the population and taking the necessary measures for them to escape poverty, as well as providing them with practical assistance, the position of assistant to the khokim (governor) was introduced in the mahallas. Within the framework of the programme to reduce poverty in rural areas, the practice of distributing seasonal land plots to the population was put in place. With the aim of ensuring employment of the population, the practice of granting low-interest loans to citizens was put in place. But the question arises: are all of these efforts producing good results? Questions arise as to how great an obstacle poverty is to the sufficiently rapid development of Uzbekistan, and what effective methods exist for reducing it under the conditions of Uzbekistan. To find answers to these questions, we can make use of the research findings of hundreds of scholars around the world, of the experiences of the countries of the world that are suitable for Uzbekistan, of the diligence of our people, and of many similar factors. Our aim is to carry out scientific and theoretical research

directed at making effective use of the opportunities available in rural areas to reduce poverty in the rural regions of Uzbekistan, and to put forward our own proposals.

To this end, we wish to point out the opportunities for reducing poverty by establishing crop-farming (dehqonchilik) and horticultural (bog‘dorchilik) activity, which is most suitable for the rural population. Today, agriculture alone creates 28% of the GDP. More people work in this sphere than in any other — a total of 27% of the labour force, or more than 3.65 million citizens. Despite the severe socio-economic consequences of the coronavirus pandemic in Uzbekistan, this sphere remains an important driving force of economic growth in the country. In 2019, 9.6% (3.2 million) of the population of Uzbekistan lived below the poverty line, getting by on 3.2 dollars a day; this is the international indicator of the poverty level established for lower-middle-income countries, and Uzbekistan is among such countries. Nearly 80% of the low-income population living in the country resides in rural areas, and their incomes are almost entirely connected with the agricultural sphere. According to estimates, in 2020, owing to the surge of the coronavirus, the poverty level in Uzbekistan began to rise for the first time in the last twenty years. Nevertheless, there is an opportunity to create more jobs in the agricultural sphere than there are at present. According to estimates, through carefully considered support and investment provided by the state, it is possible to employ from 700,000 to 1.3 million new workers each year in the agricultural products sector. This is more than enough to solve the issue connected with creating jobs for the 600,000 young people who fill the labour markets across the country every year. If we proceed on the basis of these data, there is great potential in Uzbekistan for ensuring the employment of the population in rural areas, improving their living conditions, and raising the well-being of the rural population. A large part of the land in rural areas is assigned to centralized fermer (commercial) farms, which are engaged mainly in growing cotton and grain within the framework of the state order. The large part of the population that is capable of engaging in crop-farming earns income mainly by buying from the fermers the lands freed up after the grain fields and sowing seasonal crops. For those who wish to engage in horticulture and crop-farming, a fully transparent system for allocating land has not been created either. This in turn creates great obstacles to the population engaging in crop-farming and horticultural activity. As a result, because a large part of the rural population does not have a source of income that sufficiently meets its needs, a large part of the population goes abroad in order to earn income, or remains unemployed. The physically able-bodied part of the population is forced to earn income by performing seasonal work. As a result, the great experience of the population in crop-farming and horticulture is not used productively, and the opportunities offered by this for ensuring the employment of the population and raising its well-being are not used to the full.

If we take into account the favourable climatic conditions of Uzbekistan, its fertile lands, and its hard-working people, then within agriculture — among the spheres with great potential for generating income — crop-farming and horticulture occupy an important place. For this, the necessary opportunities must be created for the active stratum of the population that has the capacity to work in this sphere. First of all, an open and transparent system, free of excessive bureaucratic obstacles, for allocating land to the population so that they may engage in crop-farming and horticulture on a permanent basis must be put in place. To this end, it is necessary to put in place a system for granting land to citizens in the form of long-term dehqon (smallholder) farms and horticultural farms — selling it through open electronic auctions without the participation of individual intermediaries, or granting it free of charge for a fixed period to the poor stratum.

Starting from 2021, this system began to be partially implemented by the government. In that year, in most of the areas of the Fergana Valley, 10 sotixes of land were distributed to each stratum of the young population that was not provided with employment. However, owing to the facts that these lands were given for only one cropping season, that these lands were allocated mainly from areas without water, that the amount of allocated land was insufficient to meet most of the needs of one person's subsistence for up to 6 months, and to other similar reasons, in most cases these lands were sold by several landholders to a particular individual in amounts of 0.5, 1 hectare, and more. This in turn caused these unemployed young people to continue living in an unemployed condition as before. At this point another question arises. If the allocation of these lands were increased to a sufficient amount — for example, set at around 0.3–1 ha — could it be fully achieved that unemployed young people would work regularly on these lands? In our opinion, this cannot be a complete solution to the problem. Why? Let us suppose that the lands were indeed allocated through a transparent system; from where would the poor stratum of the population or the unemployed young people obtain the funds for preparing these lands for sowing, for buying seed for sowing crops, for cultivating the sown crops, for applying fertilizer to the crops, and for many other expenses? Suppose we take one solution to this issue to be a system of granting credit to the landholders for these expenses. Does the granting of credit solve this problem? Who can guarantee that these funds will be spent rationally by the landholders? Perhaps these funds may be spent by the landholders for their other purposes. In this situation, in our opinion, outlets providing comprehensive services should be established for the landholders — on the basis of contracts with the owners, in exchange for deferred payment or through other payment methods. In establishing these outlets, it is expedient to make use of the private sector. These outlets should provide the dehqons (smallholders) with such services as carrying out mechanization work in preparing their lands, supplying them with the necessary seed, cultivating the crops, supplying them with mineral fertilizers, meeting their demand for chemical agents that protect plants from pest insects, and harvesting the crops in good time. It is also expedient to put in place the operation of private agronomic centres providing paid services to the dehqons. Now the problem of selling these products stands before us. Through this, we can provide work for our migrant population who are abroad and for a large part of the able-bodied unemployed population in rural areas. By having the population make use of these lands, the cultivation of large quantities of vegetable, melon-and-gourd (poliz), and horticultural products is achieved. The cultivated products fully cover the domestic market, leading to a reduction in prices in the local markets, and an opportunity arises to direct the surplus products to export.

For this, we need to examine the opportunities for cultivating exportable products by studying the world market. We also need to make use of the opportunities to put in place the cultivation, through localization, of agricultural products coming from abroad. At present, on the world market there is great demand for the melon-and-gourd crops and horticultural products cultivated in Uzbekistan. However, in order to facilitate the process of exporting these products, we need to develop a systematized structure. We must also examine the system for storing the cultivated products, because we can see that the export potential of perishable products is great. Being of a perishable nature, the prices of products are observed to be low during the ripening season, which hinders the dehqons from obtaining a satisfactory income and also has a noticeable effect on export prices. As an example, if we look at the price of cherries in 2021, at the beginning of the ripening season prices were around 20,000, whereas by the end of the season prices fell to as low as 3,000. This had a great impact on the income of the orchardists. If we look at cherry

prices in 2020, prices did not fall below a minimum of 20,000. It can be seen that prices in 2021 were several times higher than the prices in 2020. In the autumn season of 2021, cherry prices rose several times over. If small cold-storage facilities (refrigerators) had been organized among the population, their products could have been stored during the ripening season and incomes raised to an acceptable level. The reason for prices falling to such a degree appears to be that these products ripen at the same time and cannot be stored under ordinary conditions, and that demand on the world market declines.

Conclusion. By way of conclusion, we can state that, since around 5 million of the population of Uzbekistan are living in poverty, there are a great many practical measures that need to be taken at the level of the government. With our article we wish to say that, first of all, we need to understand what poverty is. In studying it, it is expedient to make use of international experience and practices. Then its causes are studied. The causes are various, and each region or society has its own particular causes. Therefore, from international experience we can make use only of the methods for investigating the object. The causes that give rise to poverty in Uzbekistan, and its manifestation in rural areas, differ from those in the countries of Africa or Europe. In the manifestation of poverty in rural areas, it is not only material factors that have an effect; the skills, knowledge, and experience possessed by the subject of poverty, the abilities they have, and the opportunities provided by the government for realizing those abilities may also have an effect. In reducing poverty, it is expedient to take into account not only the income but also the expenditures of the subject. In reducing poverty in rural areas, we need to make wide use of the conclusions of representatives of the scholarly community based on their analyses, and to examine the benefits of putting these into practice. Taking into account the lack of investment in agriculture, offering investors small investment projects that are broadly beneficial and designed for the long term will be useful in drawing the poor into active economic life. If we take into account that we use, as the criterion of poverty, the 1.9-dollar indicator applied in world practice, we have seen that around 12% of our population lives in poverty; however, the countries of Europe define as poor that stratum of the population whose income constitutes less than 60% of the average income of the population. It follows from this that we cannot compare the indicator given for us with that of the countries of Europe. We thus conclude that poverty is not a periodic problem; on the contrary, it must be combated continuously. Even the most developed countries take measures to reduce poverty. Therefore, in studying the object, there is a need to make use of the findings of fundamental research.

REFERENCES

1. Yashar Pasha. *Determination of Poverty on the Basis of Multidimensional Statistical Analysis* (article).
2. Lev M. Yu. (2021). *Poverty and the Subsistence Level of the Population in Ensuring Socio-Economic Security*. 1ECONOMIC.R.
3. Varvus, S. A. *Measuring the Poverty Rate: the Analysis of Existing Approaches*. PhD (Economics), Associate Professor of the Economic Theory Department, Financial University, Moscow, Russia.
4. https://m.kun.uz/uz/news/2020/11/04/5600-som-daromadi-bor-odam-kambagal-emas-obid-hakimov-nimani-nazarda-tutgandi
5. From an interview of Kun.Uz with Sergey Zorya, Lead Agricultural Economist of the World Bank Representative Office in Uzbekistan.

METHODS FOR ASSESSING COMPETENCIES THROUGH QUALIMETRY IN EMPLOYEE MANAGEMENT

M.T. Rikhsiboeva
Master's student at Westminster International University in Tashkent
https://doi.org/10.5281/zenodo.20793799

Abstract. *This article analyzes the methods of assessing competencies through qualimetry in the process of employee management. The study highlights modern approaches to the objective assessment of employees' professional knowledge, skills, and abilities, and reveals the importance of qualimetry in human resource management. In addition, the criteria and indicators for competency assessment, as well as the mechanisms for their practical application, are examined. The article substantiates the role of identifying and developing employee competencies in improving organizational efficiency.*

Keywords: *qualimetry, competency, competency assessment, human resource management, employee management, assessment methods, professional competency, efficiency, personnel development.*

INTRODUCTION

The criteria for assessing employees' competency levels have always been a controversial topic. However, summarizing the existing views, it can be said that employees' professional competency levels not only determine educational outcomes but also enable them to perform successfully in their professional activities. The criteria for professional competence are determined based on the content of the competencies that need to be acquired.

Professional competence is the ability to apply acquired and developed knowledge, skills, and abilities in practice, while the level of professional competence serves as a criterion for determining the degree to which an employee is prepared for professional activity.

Although today the phrase "competence approach" is usually associated with education, the origins of this approach go back to the assessment of the professional qualities of already formed specialists. In this case, the primary consideration is not only the individual's professional knowledge, but also their experience, level of mastery of techniques and technologies, ability for self-management and self-assessment, and ability to solve problems.

In other words, the competency paradigm does not focus on specialists' fragmented knowledge and skills, but on their integrated combination, that is, the ability to effectively solve professional tasks in a specific subject area. The main task of the aforementioned approach is to identify and examine the specific competencies necessary to achieve a predetermined outcome.

Determining professional competency levels based on a qualimetric approach yields effective results because it strengthens the objectivity of assessing quality indicators and levels of preparedness. Therefore, the study of qualimetry-based assessment methods is important for improving the scientific foundations of employee management and personnel development.

MATERIALS AND METHODS

This study is based on theoretical analysis, synthesis, comparison, and benchmarking of competency assessment approaches used in employee management. The methodological basis of

the study is the qualimetric approach, which makes it possible to evaluate employees' professional qualities through measurable criteria and indicators.

Qualimetry, from the ancient Greek word "metros" meaning "measure" and the Latin word "qualis" meaning "quality", is a scientific field that includes methods for quantitatively assessing the quality of products, objects, and processes and determining the results achieved using various methods and tools.

Qualimetry, as a science, studies the determination of the qualitative and quantitative indicators of an object through the application of established and accepted measurement procedures. It is based on the theory of measurement, using the volume, units, scales, and requirements that define the quality of the object being studied and evaluated.

According to modern approaches, qualitative indicators of qualimetry are studied by dividing them into two large groups: social and natural indicators. Natural indicators, in turn, are divided into chemical, biological, and physical quantitative indicators of the object under study. Social indicators are applied to the products of production and consumption, events, the individual's status and role in social and independent life, literacy, and overall personal development at a particular stage of societal progress.

Qualimetry studies the quantitative and qualitative indicators of each of the above-mentioned groups in an integrated manner and develops a general procedure for their evaluation. International experience has shown that in order to achieve high quality in goods, services, and processes, it is necessary to develop scientific, technical, and organizational criteria for assessing their quality.

The evaluation is carried out by measuring the quality of a specific object, process, or service against the criteria of a model accepted as a benchmark and by comparing the obtained results. In this process, the main methods of qualimetry are analysis, synthesis, comparison, and benchmarking. The quality of an object is determined by taking into account its characteristics and evaluating them against the quality indicators of a model accepted as a benchmark.

If we analyze an employee's qualifications, then this is a multifaceted and complex characteristic. Therefore, the more aspects of a specialist's qualities or professional activities are considered separately during the evaluation process, the more objective and comprehensive the final assessment will be.

The methodology of giving an overall assessment to an object through the sum of the assessments of its individual characteristics is called a multi-criteria approach. To better understand this approach, it is necessary to clarify the meaning and essence of the concept of a criterion.

Considering the concept of a criterion in the context of developing professional competence of professional education personnel, this study relies on the interpretation provided by N. V. Sichkova. According to her, in order to determine the criteria, first, these characteristics must be diagnosed and measured; second, they should reflect the essence of the main directions and priorities of the activities they carry out; third, they should cover all significant aspects of the process and provide a holistic understanding of it.

Criterion, from the Greek kriterion, is a sign of something with the help of which an assessment, determination, or correction is carried out. A synonym for the word criterion is the term "measure", which is also used to compare, evaluate, or measure something. The most common criteria in the field of qualimetry are formalized criteria, which take into account the position held by the specialist, the presence or absence of academic or honorary titles, academic

degree, number of publications on a particular topic, work experience, and other indicators. The first and main condition for applying a multi-criteria approach is the presence of formal criteria.

The differential-integral approach is also important in developing a system of criteria. At various levels of personnel management, different types of criteria, lists of evaluation indicators, and other sets of data are used to evaluate employees' professional performance.

On the one hand, the development of a system of evaluation criteria represents a complex procedure as a preparatory stage of the assessment process, in which the decision-maker does not participate directly. On the other hand, a specific set of criteria used to evaluate an employee's multifaceted activities constitutes one of many possible alternatives.

To describe various aspects of employees' activities and professionally significant qualities, the multi-criteria approach involves the development of numerous criteria and indicators for their assessment. The main idea is that the greater the number of independent and non-overlapping evaluations based on different criteria, the more comprehensive and meaningful the assessment of activities or qualities becomes.

Each criterion is used to evaluate a certain characteristic or type of activity of an employee. The methods considered in the study indicate that the characteristics being evaluated can be combined into groups of the same type. Therefore, competency assessment requires both general methodological principles and practical tools suitable for employee management.

RESULTS AND DISCUSSION

There are many different methods used in multi-criteria decision-making, including the Analytic Hierarchy Method, the SMART method, and other related approaches. The task of evaluation differs from the task of decision-making in that the objects being evaluated are generally not alternatives to one another and cannot simply be excluded from consideration. Therefore, methods that rely on eliminating alternatives are not appropriate for this particular context.

The analysis of existing approaches shows that employee competence can be assessed through several methods, each of which has its own characteristics, strengths, and limitations. These methods make it possible to evaluate employees' professional and personal qualities from different perspectives.

Table 1. Methods for assessing employees' professional competence

Method	**Characteristics of the method**	**Distinctive features of the method**
Rating	Rating multi-point evaluation system.	It is used to assess how well an employee is suitable for their current position. However, the assessment does not include all of the employee's qualities; for example, a 110-point assessment may be used.
Multi-criteria evaluation	Evaluates an employee's professional and personal qualities.	Focuses on a comprehensive assessment of the employee from multiple perspectives.

Method	Characteristics of the method	Distinctive features of the method
Analytic Hierarchy Method (ANR/AHP)	Allows a complex problem to be structured in the form of a hierarchy and allows alternatives to be compared and evaluated qualitatively.	It is used to assess work quality and determine the importance of criteria through pairwise comparisons.
SMART	A heuristic method based on mathematical theory.	It is convenient for practical use. However, this method does not take into account the possibility of interdependence of criteria, which is its disadvantage.
90°, 180°, 360° method	Comprehensive employee assessment involving a manager, colleagues, and self-assessment.	A method based on a competency-based approach. It is mainly used to assess competency levels and is regarded as a type of objective assessment.
Portfolio	Consists of a collection of materials and information that demonstrate an employee's professional competence.	It includes documents, certificates, diplomas, and other evidence confirming the results achieved by the employee during professional activity.

The SMART method, or Simple Multi-Attribute Rating Technique, proposed by W. Edwards, is a heuristic method based on the mathematical theory of utility. The Analytic Hierarchy Process, proposed by T. Saaty, enables the structuring of a complex problem in the form of a hierarchy and allows the comparison and qualitative evaluation of alternatives.

The SMART method is convenient for practical application, and this feature is one of its important advantages. However, this method does not take into account the possibility of interdependence of criteria, which is its disadvantage. In addition, the final assessment is calculated using the weighted sum method. The unreasonable use of weighted sums to evaluate alternatives may be problematic for many reasons. In particular, within the framework of this method, there is an assumption that the transition from one dimension of the scale to another for the decision-maker in determining preferences increases smoothly, which is not always true in practice.

The advantages of the hierarchical analysis method include pairwise comparisons, the possibility of introducing changes to the current matrix, the presence of a verbal-numerical scale, and an established quality criterion of expert work. Pairwise comparison is consistent with the way people naturally compare objects. The introduction of new criteria requires the comparison of only newly formed pairs, while the verbal-numerical scale creates the possibility of comparing factors expressed in different dimensions and concepts. However, these advantages mainly relate to calculating the importance of the criteria, while the final assessment itself often depends on calculated sums across the hierarchy.

The 90° method is most often used to assess the competency levels of employees in corporations and firms. In this article, it is adapted for assessing employees' professional

competence. In the 90° assessment, an employee's specific competencies demonstrated in professional activities are evaluated. Based on the results of the assessment, a specific rating is formed and competencies that still need to be developed are identified.

The main advantage of the 90° assessment is that it allows the identification of an employee's weaknesses and competencies that need to be developed, which helps in creating an individual development plan or program. It is also effective in making important managerial decisions, including dismissal or the assignment of professional categories.

The 180° evaluation is a method of evaluating an employee's work performance that includes self-assessment of the employee's performance and assessment by assigned supervisors. This method provides a more balanced perspective than one-sided managerial evaluation because it combines internal reflection with external assessment.

The 360° assessment method extends the evaluation process by incorporating two additional perspectives: evaluations provided by an employee's subordinates, if any, and, when adapted to an educational context, evaluations provided directly by learners. It includes self-evaluation and evaluation by supervisors. In degree-based assessment, assessors should have a clear list of competencies and clear evaluation criteria.

The portfolio method consists of a collection of materials and information that demonstrate an employee's professional competence. The portfolio includes documents, certificates, diplomas, and other materials confirming results achieved by the employee during professional activity, participation in olympiads, competitions, and international or national conferences. The work performed should be checked and evaluated by the manager.

The discussion of these methods demonstrates that the qualimetric approach can increase the objectivity of employee assessment when criteria are formalized, measurable, and connected with actual professional activity. At the same time, no single method can fully assess professional competence in all its complexity. Therefore, an integrated assessment model that combines rating, multi-criteria evaluation, degree-based feedback, and portfolio evidence can provide a more reliable basis for employee management.

CONCLUSION

Studying methods for assessing an employee's level of professional competence makes it possible to draw several important conclusions. First, the complex hypothetical characteristics of an employee's professional activity and professionally significant qualities should be repeatedly differentiated in accordance with the differential-integral approach until specific qualification-related characteristics of the employee are identified.

Second, professional competence is a broad characteristic that encompasses the professionally significant qualities of an employee. The competency-based approach makes it possible to divide this characteristic into its constituent components. Therefore, professional competence should be regarded as a comprehensive characteristic that reflects both an employee's professional activity and professionally significant qualities.

Third, the meaning and content of each competency are revealed through the examination of the qualification-related characteristics that constitute it. Each of these characteristics can be evaluated using several types of criteria, and, as a result, the level of development of each competency can be assessed through a multi-criteria decision-making methodology.

In general, qualimetry provides an effective scientific and methodological basis for improving employee management. By applying measurable criteria, comparing them with benchmark models, and combining several assessment methods, organizations can identify

employee strengths and weaknesses more objectively, design individual development programs, and improve overall organizational efficiency.

REFERENCES

1. Belkadi, F., Bonjour, E., & Dulmet, M. (2007). Competency characterisation by means of work situation modelling. Computers in Industry, 58, 164-178.
2. Belkadi, F., Bonjour, E., & Dulmet, M. (2006). A fuzzy approach for competency characterisation based on a work situation analysis. In 9th IFAC Symposium on Automated Systems Based on Human Skills (ASBoHS'06), Nancy, 22-24 May.
3. Cicortas, A., Iordan, V., & Naaji, A. (2008). Ontologies for competence description in multi-agent systems. In 10th WSEAS International Conference on Mathematical Methods and Computational Techniques in Electrical Engineering (MMACTEE'08), Sofia, Bulgaria, May 2-4.
4. Cristea, A. I. (2004). What can the semantic web do for adaptive educational hypermedia? Educational Technology & Society, 7(4), 40-58.
5. El Falaki, B., Khalidi Idrissi, M., & Bennani, S. (2010). A formative assessment model within the competency-based approach for an individualized e-learning path. World Academy of Science, Engineering and Technology, International Journal of Social, Behavioral, Educational, Economic, Business and Industrial Engineering, 4(4), 464-468.
6. Friesen, N., & Anderson, T. (2004). Interaction for lifelong learning. British Journal of Educational Technology, 35(6), 679-687.
7. García-Barriocanal, E., Sicilia, M. A., & Sánchez-Alonso, S. (2012). Computing with competencies: Modelling organizational capacities. Expert Systems with Applications, 39, 12310-12318.

Contents

01.00.00 PHYSICAL AND MATHEMATICAL SCIENCES

A.E. Xolmurodov, M.A. Quzratov
SURFACE-WAVE PROPAGATION IN ELASTIC ANISOTROPIC MEDIA AND ITS MATHEMATICAL MODELS: THEORY, COMPUTATION, AND INVERSION 4

D.E. Davletov
DEVELOPING UNIVERSITY STUDENTS' PROOF COMPETENCE THROUGH PROBLEM-BASED LEARNING OF NON-STANDARD GEOMETRY PROBLEMS IN CLASSROOM AND EXTRACURRICULAR ACTIVITIES 9

Z.B. Umarova
THE BASE AND CHARACTER OF OPEN-POINT TOPOLOGICAL SPACES 19

S.B. Jo'raqulov
METHODOLOGICAL INCONSISTENCIES OF THERMOELASTICITY EQUATIONS: SCIENTIFIC ANALYSIS AND PROOF 24

02.00.00 CHEMICAL SCIENCES

K.V. Raimova, R.N. Rakhimov, M.Zh. Oripova, Z.N. Kuzieva, A.M. Ishimov, N.G. Abdulladzhanova
OPTIMAL CONDITIONS FOR THE EXTRACTION OF POLYPHENOLIC COMPOUNDS FROM THE PEEL OF PUNICA GRANATUM FRUITS 30

Z.N. Kuziyeva, M.J. Oripova, K.A. Raimova, S.B. Karabayeva, F.Z. Orifov, N.G. Abdullajanova
EXTRACTION AND CHARACTERIZATION OF POMEGRANATE (PUNICA GRANATUM L.) SEED OIL 39

M.T. Karshiev, F.N. Nurkulov
STUDY OF THE THERMAL PROPERTIES OF STARCH-BASED BIOPOLYMERS CONTAINING SILICON 44

05.00.00 TECHNICAL SCIENCES

Sh. Solijonov
INTEGRATING ARTIFICIAL INTELLIGENCE INTO BUSINESS INTELLIGENCE: A CONCEPTUAL FRAMEWORK FOR AI-DRIVEN DECISION MAKING IN TOURISM 49

A. Primbetov, A. Alimbaeva
AN INTERPRETABLE FRAMEWORK FOR SYNTHETIC MEDIA DETECTION BASED ON MULTI-DOMAIN FORENSIC ANALYSIS 55

Sh.S. Yuldashev, M.B. Boytemirov, A.Sh. Abdunazarov
EVALUATION OF THE EFFECTIVENESS OF STRENGTHENING THE FOUNDATION SOIL OF MULTI-STOREY BUILDINGS USING A SOIL CUSHION AND DEEP SOIL MIXING TECHNOLOGY IN REDUCING SEISMIC EFFECTS 73

I.U. Rakhmonov, A.N. Rasulov, M.R. Ro'zinazarov, S.A. Abdirozoqov
THEORY, OPERATING PRINCIPLE AND INVESTIGATION OF A MAGNETIC-AMPLIFIER-BASED STABILIZER IN FERRORESONANCE CIRCUIT CONTROL 83

M.A. Mamasaidov
PROSPECTS FOR THE PRODUCTION OF ELECTRICITY BASED ON HEAT 90

M. Makhmudov, Sh. Abdukarimov, O. Kimizbayeva, Sh. Kurbonov, Sh. Sodiqova
DEVELOPMENT OF A MULTI-SENSOR DATA ACQUISITION SYSTEM BASED ON I2C NETWORK WITH THREE ARDUINO NANO MICROCONTROLLERS 98

F.D. Zhuraeva, S.R. Akhundzhanova, J.I. Kholikov
PROPERTIES OF POROUS ARBOLITE BASED ON MODIFIED NON-FIRED ALKALINE BINDERS 102

Sh.B. Redzhepov, B.Sh. Makhkamov
DEVELOPMENT OF AN IDEF0 MODEL FOR NETWORK ANOMALY MONITORING SYSTEMS 106

08.00.00 ECONOMIC SCIENCES

I.G. Yoqubjonov
THE ESSENCE OF THE PROBLEM OF POVERTY IN RURAL AREAS, ITS CAUSES, CRITERIA, AND MANIFESTATION IN AGRICULTURE 117

M.T. Rikhsiboeva
METHODS FOR ASSESSING COMPETENCIES THROUGH QUALIMETRY IN EMPLOYEE MANAGEMENT 125

International Scientific Journal
Science and Innovation Series A
Volume 5 Issue 6

ISSN: 2181-3337

Published: 30.06.2026. Font: “Times New Roman”.

LLC “Science and innovation”
License Mass Media №:1597 27.04.2022
License Publisher №:455168 21.11.2024
Address: 100121, Uzbekistan, Tashkent city, Yakkasaroy district,
Shota Rustaveli Street 150, Vega Business Center, 6th floor, Room 2.
www.scientists.uz, info@scientists.uz, +998901259654